

MITOCHONDRIAL REACTIVE OXYGEN SPECIES MEDIATE
LYSOPHOSPHATIDYLCHOLINE-INDUCED ENDOTHELIAL CELL ACTIVATION

A Dissertation
Submitted to the
Temple University Graduate Board

In Partial Fulfillment of the
Requirement for the
Degree of Doctor of Philosophy

By
Xinyuan Li
May 2015

Examining Committee Members:

Dr. Xiao-Feng Yang (Advisor), Department of Pharmacology, Temple University
Dr. Hong Wang (Co-Advisor), Department of Pharmacology, Temple University
Dr. Barrie Ashby, Department of Pharmacology, Temple University
Dr. Douglas G. Tilley, Department of Pharmacology, Temple University
Dr. Muniswamy Madesh, Department of Biochemistry, Temple University
Dr. Shey-Shing Sheu (External Examiner), Department of Medicine, Thomas Jefferson University

Copyright © 2015
By Xinyuan Li
All Rights Reserved

ABSTRACT

Mitochondrial Reactive Oxygen Species Mediate Lysophosphatidylcholine-induced

Endothelial Cell Activation

Xinyuan Li

Doctor of Philosophy

Temple University, 2015

Doctoral Advisory Committee Chair: Xiao-Feng Yang, MD, PhD

Lysophosphatidylcholines (LPCs) are a class of pro-inflammatory lipids that play important roles in atherogenesis. LPC activates endothelial cells (ECs) to upregulate adhesion molecules, cytokines and chemokines, which is the initiation step of atherogenesis. However, the mechanisms underlying LPC-triggered EC activation are not fully understood. Previously considered as the toxic by-products of cellular metabolism, mitochondrial reactive oxygen species (mtROS) are recently found to directly contribute to both the innate and adaptive immune responses. Here we tested a novel hypothesis that mtROS serve as signaling mediators for LPC-induced EC activation.

Using electron spin resonance and flow cytometry, we found that several LPC species including LPC 16:0, 18:0, and 18:1 induced mtROS in human primary aortic ECs (HAECs). Mechanistically, our analysis using confocal microscopy and Seahorse XF96 mitochondrial function analyzer showed that LPC induced mtROS via increasing mitochondrial calcium-mediated increase of mitochondrial respiration. In addition, we

found that mtROS scavenger MitoTEMPO abolished LPC-induced EC activation by downregulating Intercellular adhesion molecule 1 (ICAM-1) in HAECs. Moreover, our analysis with mass spectrometer analysis of histone H3 lysine acetylation and electrophoretic mobility shift assay (EMSA) showed that MitoTEMPO acts by blocking LPC-induced histone H3 lysine 14 acetylation (H3K14ac) and nuclear translocation of pro-inflammatory transcription factor activator protein-1 (AP-1). Remarkably, all the above effects can be inhibited by anti-inflammatory cytokines interleukin (IL-35) and IL-10.

Our results indicate that mtROS are responsible for LPC-induced EC activation, which can be inhibited by anti-inflammatory cytokines. MtROS targeting therapies and anti-inflammatory cytokines such as IL-35 may serve as novel therapeutic targets for vascular inflammation and cardiovascular diseases.

The studies in this dissertation were supported by grants from the National Institutes of Health (NIH) funded to Dr. Xiao-Feng Yang.

ACKNOWLEDGEMENTS

First, it is my great honor to be a PhD student in Dr. Yang's lab. When I first joined the lab in 2010 as a BS of Pharmacy with little experience in research, Dr. Yang was very patient and gave me freedom to learn from my trials and errors. He is extremely busy, but I can always feel free to knock his door whenever I need his input for the discussion of my research project. My training not only includes how to design and perform experiments, but also how to think critically and logically, how to write manuscript and grant application. His enthusiasms for science influence me a great deal as well. Therefore, I would like to express my gratitude to Dr. Yang for this comprehensive training.

It is also my great honor to be co-supervised by Dr. Wang. Wang and Yang labs share joining lab meeting and journal club every week, when I have the chance to learn from others from Wang/Yang labs and also receive precious suggestions from Dr. Wang for my own experiments. In addition, our two labs share many biochemical equipment and highly sophisticated high-end techniques such as electron spin resonance (ESR) and flow cytometer, which allow me to learn fundamental biochemical assays and state-of-art novel techniques. She also teaches me a great deal about critical thinking and how to develop a research project. Furthermore, I learned a lot from Dr. Wang about how to prepare figure slides and how to give a scientific talk in public. Thus, I am grateful for Dr. Wang's co-supervision and support.

I am also very grateful to my other committee members. I sincerely appreciate the critical judging from Dr. Barrie Ashby, Dr. Douglas G. Tilley, and Dr. Muniswamy Madesh throughout my preliminary exam, thesis proposal, committee meeting, and thesis defense, which all together compose an extraordinary important part of my PhD training. I would also like to thank Dr. Shey-Shing Sheu for his agreement to become my external committee member and his precious time and effort for editing my thesis and attending my defense.

I would also like to express gratitude sincerely to our lab manager, Ms. Xiaohua Jiang. She taught me the good practice of cell culture and animal work, from Western blot to the isolations of aortas from mice. She also helps me to order every reagent and supplies which are used in this study.

People from Yang lab and Wang lab are all very supportive for my study. To the former Yang and Wang lab graduate students, Dr. Pu Fang, Dr. Shu Meng, Dr. Xinyu Xiong, Dr. Ying Yin, Dr. Meghanaben Pansuria, Dr. Jietang Mai, and Dr. Anthony Virtue who are all my role models during the PhD training, they taught me the principles of cell culture, animal procedure, and experiment techniques. I am also sincerely thankful to everyone else from Yang and Wang labs, especially Dr. Xiaojin Sha for our collaboration in the IL-35 project, Dr. Ya-Feng Li for his help of microarray and metabolomics data analysis, Dr. Fuyong Du for his metabolomics experiments, Dr. Ramon Cueto, for his help when performing the EPR, Dr. Huimin Shan, for supplying

Western blot and PCR reagents, and Drs. Ying Shao and Ai Song, who helped me to collect samples in large batch of experiments.

I would love to express my sincere appreciations to those who helped me out of the lab, especially Dr. Nicholas E. Hoffman from Dr. Muniswamy Madesh's lab in the Center for Translational Medicine (CTM) who taught me how to measure cytosolic and mitochondrial calcium by confocal microscope, Dr. Walter J. Koch in CTM for sharing the seahorse XF96 analyzer in his lab, Dr. Xiaoxuan Fan in the Temple University Flow Cytometry Core Facility for his help of flow cytometry experiments, Dr. Yin-Ming Kuo from Dr. Andrew J. Andrews's lab in the Fox Chase Cancer Center who taught me how to measure histone acetylation by mass spectrometer, and Dr. Ji-Youn Youn and Dr. Kin Lung Siu from Dr. Cai's lab in University of California at Los Angeles who taught me how to measure ROS with electron spin resonance.

The whole thesis is supported by the training fund from Temple University School of Medicine, and the research funding awarded to Dr. Xiao-Feng Yang from NIH.

Last but not least, I deeply appreciate the strong support from my family: my wife Dr. Pu Fang, my parents Liping Dong and Ying Li. With their love and support, I am able to finish the PhD training within 5 years. The coming of my son, Ryan Li, gave me strength and his curiosity of this world reminds me that one is born a great scientist.

Xinyuan Li

January 2015

DEDICATION

To my parents and my wife, for their love and support

TABLE OF CONTENTS

ABSTRACT.....	iii
ACKNOWLEDGEMENTS.....	v
DEDICATION.....	viii
LIST OF FIGURES.....	xiii
LIST OF TABLES.....	xiv
LIST OF ABBREVIATIONS.....	xv
CHAPTER 1 - GENERAL INTRODUCTION.....	1
Atherosclerosis.....	1
Atherosclerosis is the Usual Cause of Cardiovascular Diseases.....	1
Atherosclerosis is a Chronic Inflammatory Disease.....	2
Atherosclerosis is Initiated by Endothelial Activation.....	4
Lysophosphatidylcholine (LPC).....	6
LPC are a Group of Bioactive Lipids.....	6
LPC is a Key Atherogenic Component of OxLDL.....	8
LPC Induces EC Activation.....	9
Mitochondrial Reactive Oxygen Species (MtROS).....	10
ROS in the Cell.....	10
Production of MtROS.....	11
Disposal of MtROS.....	14
Regulation of MtROS.....	17
MtROS and EC Functions.....	24

MtROS and Cardiovascular Diseases	30
Histone Acetylation	32
Histone Acetylation Favors Gene Transcription.....	32
Histone Acetylation and Atherosclerosis.....	34
Histone Acetylation and EC Activation.....	35
IL-35	36
Anti-inflammatory Cytokines Suppress Atherosclerosis Development	36
Anti-inflammatory Cytokines Suppress EC Activation.....	37
IL-35 is a Novel Responsive Anti-inflammatory Cytokine	38
Rationale and Hypothesis of Dissertation.....	40
CHAPTER 2 - MATERIAL AND METHODS	42
Chemicals and Antibodies	42
Animals.....	43
Mouse Genotype	43
Metabolomics Analysis.....	44
Cell Culture.....	44
Fluorescence Activated Cell Sorting (FACS).....	45
Fluorescence Microscopy	45
Electron Spin Resonance (ESR)	45
Toxicology Assay	46
Seahorse XF96 Analyzer	46
Confocal Microscopy.....	47

Western Blot Analysis	47
Real-Time PCR.....	48
Human EC Biology PCR Array.....	48
Site-Specific Histone Acetylation Screening.....	49
Genome-wide Analysis of H3K14ac	49
Preparation of Nuclear Extracts	51
Electrophoretic Mobility Shift Assay	51
Microarray Analysis.....	52
Statistical Analysis.....	52
CHAPTER 3 - RESULTS.....	53
Aortic LPC species are induced during early atherogenesis in mice.....	53
LPC induces mtROS in human aortic endothelial cells (HAECs).....	58
LPC increases mitochondrial respiration in HAEC	62
Mitochondrial Ca ²⁺ entry mediates LPC-induced respiration and mtROS.....	65
LPC-induced mtROS mediate ICAM-1 upregulation in HAEC.....	68
LPC-induced mtROS contribute to EC activation	70
LPC induced-mtROS contribute to histone H3 lysine 14 (H3K14) acetylation.....	72
LPC-induced H3K14ac contribute to ICAM-1 upregulation.....	74
LPC-induced H3K14ac contribute to EC biology changes	76
LPC-induced mtROS and histone acetylation contribute to AP-1 nuclear translocation.....	81

Anti-inflammatory cytokines IL-35 and IL-10 suppress LPC-induced ICAM-1 upregulation by inhibiting mtROS-H3K14ac-AP-1 pathway	83
IL-35 suppresses LPC-induced EC activation	85
CHAPTER 4 - DISCUSSION	87
Major LPC species are induced in the aortas of mice during early atherogenesis.....	90
LPC induces mtROS in HAEC	91
LPC-induced mtROS is mediated by Ca ²⁺ -regulated respiration increase	94
LPC-induced mtROS leads to ICAM-1 upregulation by H3K14ac-AP-1 pathway	97
IL-35 and IL-10 suppress LPC-induced ICAM-1 by inhibiting mtROS ..	99
Summary and Future Directions	101
REFERENCES CITED.....	103

LIST OF FIGURES

Figure 1. Atherosclerosis is initiated by endothelial activation.....	5
Figure 2. Production of mtROS	13
Figure 3. Regulation of mtROS production.....	23
Figure 4. IL-35 is a novel responsive anti-inflammatory cytokine.....	39
Figure 5. Aortic LPC species are induced during early atherogenesis in mice	55
Figure 6. LPC level changes in plasma, heart, and liver between WT and ApoE ^{-/-} mice.....	57
Figure 7. LPC induces mtROS in human aortic endothelial cells (HAECs).	59
Figure 8. Higher concentration of LPC (40µM) does not further increase mtROS but induces cell death in HAECs.	60
Figure 9. ESR detection of cytosolic and mitochondrial ROS in HAECs.....	61
Figure 10. LPC increases mitochondrial respiration in HAEC.....	63
Figure 11. Ca ²⁺ mediates LPC-induced respiration and mtROS in HAEC.	66
Figure 12. LPC-induced mtROS mediate ICAM-1 upregulation in HAEC.	69
Figure 13. LPC-induced mtROS contribute to EC activation.....	71
Figure 14. LPC-induced mtROS contribute to H3K14 acetylation.	73
Figure 15. LPC-induced H3K14ac contribute to ICAM-1 upregulation.	75
Figure 16. LPC increases H3K14ac peak lengths and shifts H3K14ac binding locations in the genome.....	78
Figure 17. LPC-induced H3K14ac contribute to EC biology changes.....	79
Figure 18. LPC-induced mtROS and histone acetylation contribute to AP-1 binding....	82
Figure 19. Anti-inflammatory cytokines IL-35 and IL-10 suppress LPC-induced ICAM-1 upregulation by inhibiting mtROS-H3K14ac-AP-1 pathway.....	84
Figure 20. IL-35 suppresses LPC-induced EC activation.....	86
Figure 21. Working Model	102

LIST OF TABLES

Table 1. Candidate receptors for LPC and the associated effects.....	7
Table 2. Identified pathologic stressors that induce mtROS in EC.	29
Table 3. Expression differences of LPC species in aorta, heart, liver and plasma between ApoE ^{-/-} mice and WT mice.	56
Table 4. Summary of H3K14ac Chip-Seq in HAEC.	77

LIST OF ABBREVIATIONS

ADP	adenosine diphosphate
AMPK	AMP-activated protein kinase
AMPK	AMP-activated protein kinase
Ang II	angiotensin II
AP-1	activator protein-1
ApoE	apolipoprotein E
ATP	adenosine triphosphate
CHIP	chromatin immunoprecipitation
CHIP-Seq	CHIP-sequencing
CVDs	cardiovascular diseases
EBI3	Epstein-Barr virus induced 3
ECs	endothelial cells
EMSA	electrophoretic mobility shift assay
ETC	electron transport chain
FADH2	flavin adenine dinucleotide
GPx	glutathione peroxidase
GSH	glutathione
H3K14ac	histone H3 lysine 14 acetylation
HAEC	human primary aortic EC
HAT	histone acetyltransferase
HDAC	histone deacetylase

HUVEC	human umbilical vein endothelial cells
ICAM-1	Intercellular adhesion molecule 1
IL-35	interleukin 35
LDH	lactic dehydrogenase
LDL	low-density lipoprotein
LPA	lysophosphatidic acid
LPC	lysophosphatidylcholines
mtDNA	mitochondrial DNA
mtROS	mitochondrial ROS
NADH	nicotine adenine dinucleotide
NADPH	nicotinamide adenine dinucleotide phosphate
NFAT	nuclear factor of activated T cells
NFκB	nuclear factor-κB
NO	nitric oxide
NOS	endothelial NOS
NOS	nitric oxide synthase
OCR	oxygen consumption rate
oxLDL	oxidized LDL
PLA2	phospholipase A2
PPAR α	peroxisome proliferator activated receptor α
ROS	Reactive oxygen species
SMCs	smooth muscle cells

SOD2	superoxide dismutase 2
STAT	signal transducer and activator of transcription
TCA	tricarboxylic acid
TGF- β	transforming growth factor beta
Th	T helper cells
TNF- α	tumor necrosis factor alpha
Treg	regulatory T cells
Trx2	thioredoxin-2
TSA	trichostatin A
UCPs	uncoupling proteins
VEGF	vascular endothelial growth factor
WT	wild-type
$\Delta\psi_m$	mitochondrial membrane potential

CHAPTER 1 - GENERAL INTRODUCTION

Atherosclerosis

Atherosclerosis is the Usual Cause of Cardiovascular Diseases

CVDs including coronary heart disease and stroke are the number one cause of deaths in the US¹ and worldwide². The underlying pathological mechanism of CVDs is atherosclerosis, which is a general term describing the pathogenic processes of the thickening (Athero-) and hardening (-sclerosis) of arteries.

Atherosclerosis begins in childhood, with early atherosclerotic lesions as a thin layer of white-yellowish streaks detectable in youths as young as 7 years of age^{3,4}. It remains asymptomatic for decades until the adverse effects may appear. The clinical consequences of atherosclerosis only occur after severe narrowing or closure of an artery impedes blood flow in different organs⁵. Atherosclerosis in the coronary arteries leads to myocardial infarction, which is usually manifested as the chest pain of angina and may cause sudden death. In the brain, atherosclerosis can cause ischemic stroke, which could lead to progressive brain damage. In the peripheral arteries, it can cause peripheral artery disease, which may lead to gangrene and leg amputation. In the kidneys, atherosclerosis can lead to renal impairment and hypertension.

Atherosclerosis is a Chronic Inflammatory Disease

Historically considered as merely a lipid deposition dysfunction disease with aging, recent studies established atherosclerosis as a chronic inflammatory disease^{6,7}. Animal studies, epidemiological studies and clinical investigations have established that hyperlipidemia, characterized as high circulating concentrations of cholesterol, promote atherogenesis. Cholesterol is transported by low-density lipoprotein (LDL) in the blood, which contain esterified cholesterol and triglycerides surrounded by a shell of phospholipids and unesterified cholesterol, as well as Apo B-100. When hyperlipidemia occurs, sub-endothelial migration and oxidation of LDL will accumulate oxidized LDL (oxLDL) in the tunica intima (the innermost layer of the artery). The oxidized lipids derived from oxLDL such as LPC can then initiate innate inflammatory response. LPC activates EC to upregulate adhesion molecules, cytokines and chemokines, which mediate the adhesion and trans-EC migration of blood leukocytes into the intima⁸. Once reside in the artery wall, monocytes (the most abundant leukocytes in plaques) differentiate into tissue macrophages, which is necessary for the development of atherosclerosis⁹. Subsequently, macrophages uptake cholesterols and become foam cells, which is a hall marker of atherosclerotic lesion⁵. Besides monocytes, other immune cell including T cells also participate in this process, although different subtypes of T cells play different roles, either promoting or suppressing roles, in atherogenesis^{10,11}. As the disease progresses, vascular smooth muscle cells (VSMCs) are recruited from the tunica media (the middle layer of the artery wall) into the intima, where VSMCs proliferate and produce extracellular matrix molecules to form a fibrous cap, which covers the plaque⁵.

This cap typically overlies a collection of apoptotic as well as necrotic cells, cell debris, and cholesterol crystals, forming a complex advanced lesion⁷. This can result in stenosis (narrowing of the lumen) that impedes blood flow to the surrounding tissue. Rupture of the fibrous cap further leads to thrombosis, when thrombogenic materials including collagen from the lesion are released to the lumen and elicit ischemia, with myocardial infarction and ischemic stroke as life-threatening consequences.

Atherosclerosis is Initiated by Endothelial Activation

As mentioned in the previous section, atherosclerosis is initiated by the activation of endothelial cells (ECs) that line the inner surface of the blood vessel wall (Figure 1) ⁵. Normally, ECs are quiescent and resist the adhesion of circulating leukocytes. However, when hyperlipidemia occurs, the peroxidation of the phospholipids component of oxLDL generates modified phospholipids including LPC and oxidized 1-palmitoyl-2-arachidonoyl-sn-glycero-3-phosphocholine (ox-PAPC)⁷. These proinflammatory lipids can activate ECs to produce adhesion molecules such as intercellular adhesion molecules 1 (ICAM-1) and vascular cell adhesion molecule 1 (VCAM-1) as well as cytokines and chemokines^{8, 12}. The mechanisms that mediate EC activation by LPC and ox-PAPC are not fully understood. The downstream effects of ox-PAPC seems to involve the transcription factor peroxisome proliferator activated receptor α (PPAR α)¹³, the Janus kinase (JAK)/signal transducer and activator of transcription (STAT) pathway¹⁴, and the unfolded protein response¹⁵; while Ca²⁺ and ROS are involved in LPC-induced EC activation¹⁶. In addition, it has also been recently reported the LPC derivative lysophosphatidic acid (LPA) also promotes atherosclerosis by releasing endothelial chemokine CXCL1, which mediates LPA-induced monocyte adhesion and atherogenesis¹⁷. As a result of EC activation induced by these proinflammatory lipids, leukocytes (mainly monocytes) can migrate from the blood stream into the intima where they differentiate into macrophages. Macrophages can further take up lipids to become foam cells and produce proinflammatory cytokines and pro-coagulants that amplify

inflammation responses and promote thrombotic events⁵. Thus, ECs serve as the gate-keeper of atherogenesis by controlling the leukocyte entry in the lesion¹⁸.

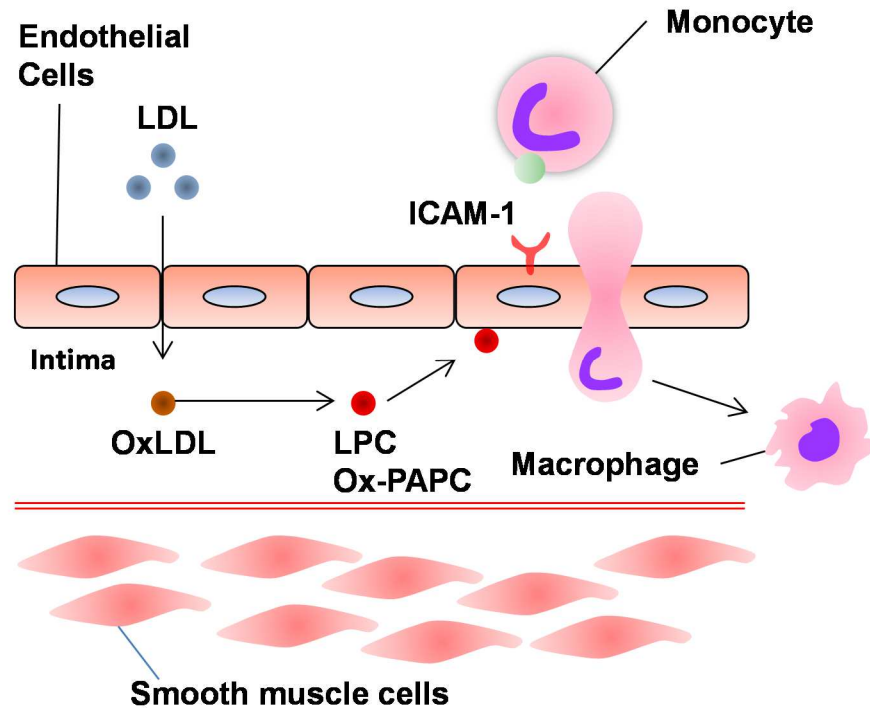


Figure 1. Atherosclerosis is initiated by endothelial activation.

ECs line in the innermost layer of the arteries. Normally, ECs are quiescent. When hyperlipidemia occurs, however, retention and oxidation of LDL will generate oxLDL. The modified phospholipid components of oxLDL including LPC and ox-PAPC can activate EC to produce adhesion molecules such as ICAM-1 and chemokines which mediate the adhesion and migration of monocytes into the intima. Once inside the blood vessel wall, monocytes differentiate into tissue macrophages and further become foam cells.

Lysophosphatidylcholine (LPC)

LPC are a Group of Bioactive Lipids

LPC is produced in the cell by the superfamily of phospholipase A₂ (PLA₂) enzymes, which catalyze the hydrolysis of the sn-2 position fatty acid of membrane phosphatidylcholine to generate LPC. There are four categories in the PLA₂ superfamily enzymes: secreted sPLA₂, cytosolic cPLA₂, calcium-independent iPLA₂, and lipoprotein associated Lp-PLA₂¹⁹. Recent studies have established central roles of sPLA₂ and Lp-PLA₂ in atherogenesis²⁰. sPLA₂ is Ca²⁺-dependent and hydrolyzes glycerophospholipids to generate LPC and free fatty acids. Various sPLA₂ enzymes are highly expressed in human atherosclerotic lesions, and experimental and clinical studies suggest their involvement in atherosclerosis and CVDs^{21, 22}. By contrast, Lp-PLA₂ is Ca²⁺-independent and hydrolyzes oxidized phospholipids to generate LPC and oxidized fatty acids²³. In preclinical animal studies, inhibition of Lp-PLA₂ attenuates the development of atherosclerosis, suggesting that it is not only a biomarker but also a candidate risk factor mediator for atherogenesis²⁴.

Several receptors have been reported to be LPC's receptor in the cells, which include GPR4, GPR132 (also known as G2A), GPR119, and PAFR. The different candidate LPC receptors engage with different G proteins and elicit distinct cellular responses (Table 1). However, with the two major papers that investigated LPC receptors retracted^{25, 26}, the real receptor(s) for LPC remains to be identified.

Numerous publications study LPC-induced responses in different cell types after the observation that LPC is upregulated at the sites of inflammation²⁷. One major signaling effect that is shared by different studies is the induction of cytosolic Ca²⁺. LPC also inhibits or activates MAPK and affects adenylate cyclase (AC) signaling to produce cAMP (Table 1).

Table 1. Candidate receptors for LPC and the associated effects

Receptor	G-protein	Cell signalling	Cellular effects	PMID
GPR4	G _{i/o}	[Ca ²⁺] _i ↑, ERK, ↑↓, MAPK ↑, AC↑	Endothelial barrier dysfunction	16461426
GPR132 (G2A)	G _{i/o} , G _q , G _{12/13} , G _s	[Ca ²⁺] _i ↑, ERK, ↑, MAPK ↑, AC↓, PLC ↑, Rho ↑, Rac ↑, Ras ↑	T cell chemotaxis Macrophage chemotaxis Macrophage apoptosis	14681556 15383458 15834123
GPR119	G _s	cAMP ↑, AC↑	Induction of insulin from β-cells	15607732
PAFR	G _{i/o} , G _q , G _s	[Ca ²⁺] _i ↑	Monocyte production of IFN-γ	10337026

LPC is a Key Atherogenic Component of OxLDL

More than 30 years ago, it was discovered by Dr. Steinberg's group that when LDL is incubated with cultured ECs, LDL is oxidized and 40% of the phosphatidylcholine (PC) of LDL is degraded to LPC²⁸. The same group reported later that LPC generated in this process is a potent chemoattractant for monocytes, which may contribute to atherogenic process²⁹. This hypothesis is supported by the finding that both human and rabbit atherosclerotic lesions contain LPC-enriched oxLDL³⁰ and LPC induces the expression of adhesion molecules and leukocyte adhesion in rat using intravital microscopy *in vivo*³¹. In addition, plasma LPC levels are also higher in mild coronary atherosclerosis patients and correlate with coronary endothelial dysfunction, suggesting a role of LPC as a participant in early atherosclerosis in humans³². Furthermore, LPC positively correlated with proinflammatory cytokine production, macrophage content, and lesion size while negatively correlated with VSMC content in human atherosclerotic plaques, suggesting that LPC play a key role in plaque inflammation and vulnerability as well³³. Oral administration of a potent inhibitor of Lp-PLA₂, the enzyme that produces LPC during LDL oxidation, reduces lesion LPC content and inhibits complex coronary atherosclerosis development in the pigs²⁴, indicating that targeting LPC could be a plausible approach for the treatment of CVDs.

Mechanistically, LPC exerts its proatherogenic effects by altering various functions in a number of cell types^{20,23}. These effects include chemotaxis of immune cells, induction of EC adhesion molecules, cytokines and chemokines; stimulation of

VSMC migration, proliferation, and cell death; and induction of macrophage inflammation.

LPC Induces EC Activation

LPC induces monocyte adhesion in cultured human ECs by inducing the expression of EC adhesion molecules intercellular adhesion molecule-1 (ICAM-1) in human umbilical vein endothelial cells (HUVECs)⁸. The induction of ICAM-1 by LPC can be blocked by general ROS inhibitor diphenyleneiodonium³⁴ and intracellular calcium inhibitor BAPTA¹⁶. There are also controversial reports on whether protein kinase C (PKC) is involved^{35,36}. In addition, LPC also activates proinflammatory transcription factors nuclear factor- κ B (NF κ B), activator protein-1 (AP-1), and cAMP response element-binding protein in ECs^{37,38}. However, the intracellular sources of ROS induced by LPC remain poorly characterized and the mechanisms underlying those cellular signaling events and the mechanistic links between them remain unclear.

Mitochondrial Reactive Oxygen Species (MtROS) *

ROS in the Cell

There are multiple sources of reactive oxygen species (ROS) in the cell including nicotinamide adenine dinucleotide phosphate (NADPH) oxidase, xanthine oxidase, uncoupling of nitric oxide synthase, cytochrome P450, and mitochondrial electron transport chain (ETC). As a major site of ROS production, mitochondria have drawn considerable interest because it was recently discovered that mitochondrial ROS (mtROS) directly contribute to inflammatory cytokine production by activation of inflammasomes (IL-1 β production)³⁹, mitogen-activated protein kinases pathway (MAPK) (IL-6 production)⁴⁰ and nuclear factor of activated T cells (NFAT) (IL-2 production)⁴¹. In addition, pathological conditions as diverse as malignancies, autoimmune diseases, and cardiovascular diseases all share common phenotype of increased mtROS production above basal levels⁴².

* This part of introduction is modified and updated from the article “Targeting Mitochondrial Reactive Oxygen Species as Novel Therapy for Inflammatory Diseases and Cancers” *J Hematol Oncol*, 2013. The first author of this article is the author of this thesis.

Production of MtROS

Mitochondria have a four-layer structure, including outer mitochondrial membrane, intermembrane space, inner mitochondrial membrane and matrix. Generation of mtROS mainly takes place at the electron transport chain (ETC) located on the inner mitochondrial membrane during the process of oxidative phosphorylation (Figure 2). Oxidative phosphorylation is an essential cellular process that uses oxygen and simple sugars to create adenosine triphosphate (ATP), which is the cell's main energy source. Four big protein complexes and ATP synthase are involved in this process. These ETC complexes are named complex I (NADH dehydrogenase (ubiquinone), 45 protein subunits), complex II (succinate dehydrogenase, 4 protein subunits), complex III (ubiquinol-cytochrome c reductase, 10 protein subunits), complex IV (cytochrome c oxidase, 19 protein subunits), and ATP synthase (19 protein subunits). Electrons donated from nicotine adenine dinucleotide (NADH) at complex I and flavin adenine dinucleotide (FADH₂) at complex II pass through ETC and ultimately reduce O₂ to water at complex IV. Meanwhile, positively charged protons (H⁺) are actively being pumped from the mitochondrial matrix into the intermembrane space, resulting in the increased negative charges in the mitochondrial matrix and the upregulated positive charges in the intermembrane space, and thus creating a mitochondrial membrane potential ($\Delta\psi_m$) across the inner mitochondrial membrane. This proton-motive force allows complex V - ATP synthase (ATP-ase) to generate ATP from adenosine diphosphate (ADP) and inorganic phosphate when protons re-enter the mitochondrial matrix through the complex V enzyme. However, either by accident or by design, the process of ETC is not perfect.

Leakage of electrons at complex I and complex III leads to partial reduction of oxygen to form superoxide ($O_2^{\cdot-}$). It has been estimated that 0.2% to 2.0% of O_2 consumed by mitochondria generates $O_2^{\cdot-}$ ⁴³. There are three leak events: complex I leaks $O_2^{\cdot-}$ towards the mitochondrial matrix, while complex III leaks $O_2^{\cdot-}$ towards both the intermembrane space and mitochondrial matrix^{43, 44}. Subsequently, $O_2^{\cdot-}$ is quickly dismutated to hydrogen peroxide (H_2O_2) by two dismutases including superoxide dismutase 2 (SOD2) in mitochondrial matrix and superoxide dismutase 1 (SOD1) in mitochondrial intermembrane space. Collectively, both $O_2^{\cdot-}$ and H_2O_2 generated in this process are considered as mtROS. These two mtROS have different fates however. Given its electrophilic property and short half-life, $O_2^{\cdot-}$ can hardly pass through mitochondrial outer membrane and unlikely to become the candidate of signaling transduction molecule in the cells. Instead, $O_2^{\cdot-}$ can undergo radical-radical reaction with nitric oxide (NO) to form peroxynitrite within mitochondria, a detrimental oxidant capable of induction of DNA damage, disruption of mitochondrial integrity, and irreversible modification of proteins⁴³. In contrast, H_2O_2 is electrophobic and more stable than $O_2^{\cdot-}$. Indeed, the concentrations of H_2O_2 in mitochondria are 100 times greater than that of $O_2^{\cdot-}$ ⁴⁵. These properties render mitochondrial H_2O_2 an ideal signaling molecule in the cells.

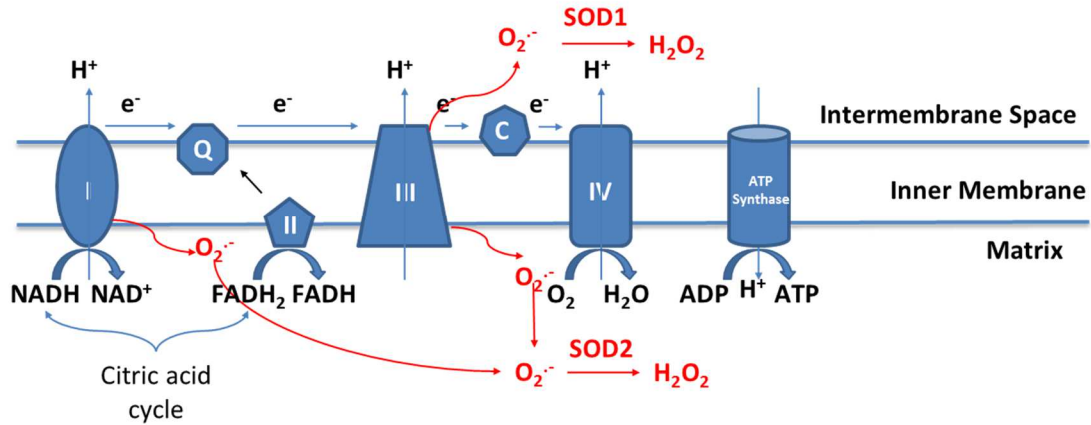


Figure 2. Production of mtROS

Electrons (e^-) donated from NADH and FADH₂ pass through the electron transport chain and ultimately reduce O_2 to form H_2O at complex IV. MtROS are produced from the leakage of e^- to form superoxide ($O_2^{\cdot -}$) at complex I and complex III. $O_2^{\cdot -}$ is produced within matrix at complex I, whereas at complex III $O_2^{\cdot -}$ is released towards both the matrix and the intermembrane space. Once generated, $O_2^{\cdot -}$ is dismutated to H_2O_2 by superoxide dismutase 1 (SOD1) in the intermembrane space and by SOD2 in the matrix. Afterwards, H_2O_2 is fully reduced to water by enzymes including glutathione peroxidase (GPX). Both $O_2^{\cdot -}$ and H_2O_2 produced in this process are considered as mtROS. OM: outer membrane; IM: inner membrane.

Disposal of MtROS

Owing to the high reactivity and toxicity of mtROS, mammalian cells have evolved a number of antioxidant enzyme systems to scavenge mtROS as soon as they are generated. As mentioned in the previous section, the SOD family of antioxidant enzymes catalyze the dismutation of O_2^- to H_2O_2 . Subsequently, H_2O_2 is quickly reduced to water by other enzymes such as catalase and glutathione peroxidase (GPx).

SODs

Three isoforms of SOD have been identified, including SOD1/copper-zinc SOD (CuZn-SOD), SOD2/ manganese SOD (Mn-SOD), and extracellular SOD3 (EC-SOD). SOD1 is widely distributed throughout the cell cytoplasm, nucleus, and intermembrane space of mitochondria⁴⁶. SOD2 is expressed only in the mitochondrial matrix⁴⁶, and SOD3 is found in the extracellular space. The physiological importance of SOD2 is highlighted by the finding that in contrast to other SOD isoforms, the deficiency of SOD2 causes early neonatal death in gene knockout mice⁴⁷ and endothelial dysfunction in carotid artery of proatherogenic mouse model apolipoprotein E (ApoE)-deficient mice^{43, 48}.

Catalase

Catalase is a heme-containing tetramer of four polypeptide chains that reduces H_2O_2 to water. Although catalase is highly efficient at reducing hydrogen peroxide, it may not play a central role in scavenging ROS in the mitochondria since it is localized

mainly in peroxisomes except that rat heart mitochondria does partially depend on catalase to scavenge ROS⁴⁹. Nevertheless, overexpression of catalase in ApoE^{-/-} mice results in the retardation of atherosclerotic process⁵⁰. In addition, overexpression of catalase in the mitochondria decreased oxidative damage, inhibited cardiac pathology, and extended the lifespan of mice⁵¹. These results suggest the importance of catalase in suppressing cardiovascular inflammation and damage and atherosclerosis.

Glutathione peroxidase (GPx)

GPx catalyzes the reductive inactivation of H₂O₂ using reduced glutathione (GSH) as a cofactor. GSH is a tripeptide containing of three amino acid residues including glutamate, cysteine, and glycine. During the process of reducing H₂O₂, GSH is oxidized to oxidized glutathione (GSSG). GSSG is then recycled back to GSH by the enzyme glutathione reductase using NADPH as a substrate⁵². Thus, the maintenance of GSH for optimal scavenging capacity is dependent on the bioavailability of NADPH stores. Deficiency of GPx results in acceleration of atherogenesis in ApoE^{-/-} mice, highlighting the importance of glutathione peroxidase in suppressing vascular inflammation and atherosclerosis⁵³.

Peroxiredoxin

Peroxiredoxins are a family of antioxidant enzymes that regulate cytokine-induced peroxide levels and mediate signal pathways⁵⁴. There are six peroxiredoxins in this family. Importantly, H₂O₂ has the highest affinity to peroxiredoxin 2 (100%), then to

GSH (<0.01%), demonstrating the importance of peroxiredoxins⁵⁵. Overexpression of mitochondrial matrix peroxiredoxin (peroxiredoxin-3) prevents left ventricular remodeling and failure after myocardial infarction in mice⁵⁶.

Thioredoxins

Thioredoxins are small proteins that play a variety of roles depending upon binding interactions and oxidoreductase activity. Mammalian thioredoxin-2 (Trx2) is a mitochondrial protein. Trx2 deficiency results in embryonic lethality at gestational day 10.5 and embryos show massive apoptosis. The timing coincides with the maturation of mitochondrial function. In addition, Trx2 protects against vascular pathology in the ApoE-knockout mouse model for CVD⁵⁷. Furthermore, the accumulated data strongly support a role for Trx2 in protecting against oxidant-induced apoptosis via regulating mitochondrial permeability transition⁵⁸.

Regulation of MtROS

ROS production in mitochondria is determined by the rates of both mtROS production and disposal, which is regulated by a number of factors, such as metabolic state of mitochondria, mitochondrial membrane potential (Fig. 2).

Mitochondrial Membrane Potential ($\Delta\psi_m$)

As described above, $\Delta\psi_m$ is created when protons are pumped from the mitochondrial matrix to the intermembrane space as electrons pass through the ETC. The concept that higher (more polarized) $\Delta\psi_m$ is associated with greater mtROS generation is widespread in literature, and this is thought to be due to the slowed electron transport⁴³. This idea is supported by the observation of decreased ROS generation when $\Delta\psi_m$ is dissipated by either chemical uncouplers⁵⁹, such as FCCP⁶⁰, or overexpression of mitochondrial uncoupling proteins (UCPs)⁶¹. However, it has also been shown that uncoupling of the mitochondrial ETC in cardiomyocytes using chemical uncouplers in fact increased ROS accumulation⁶². To reconcile this obvious discrepancy, a redox-optimized ROS balance hypothesis is proposed, stating that physiological ROS signaling occurs within an optimized $\Delta\psi_m$, and oxidative stress can happen at either the extreme of high $\Delta\psi_m$ or low $\Delta\psi_m$ ⁶². This hypothesis is based on the fact that the redox couples involved in substrate oxidation (NADH) are closely linked to the redox couples involved in antioxidant defenses (NADPH). Hence, it is vital to balance an adequate level of $\Delta\psi_m$ to maintain matrix NADPH rather than NADP⁺, which is necessary for mitochondrial antioxidant enzyme systems. In other word, an increase in mitochondrial uncoupling of

the ETC can increase ROS production, which is primarily due to the fact that the antioxidant system of the cell is compromised.

Respiration rate

Endogenous modulators such as nitric oxide (NO) and Ca^{2+} can regulate the production of mtROS by regulating the respiration rate of mitochondria. NO is a diffusible gas synthesized by three nitric oxide synthase (NOS) enzymes including endothelial NOS (eNOS), inducible NOS and neuronal NOS. These three enzymes share 50–60% homology at the amino acid sequence and have an N-terminal oxygenase domain with heme-, L-arginine-, tetrahydrobiopterin-binding domains, a central calmodulin-binding region, and a C-terminal reductase domain with NADPH, FAD, and FMN binding sites⁶³. The identification of NOS in the mitochondria⁶⁴ and the fact that the ETC has several NO· reactive-redox metal centers⁴³ strongly argue NO's role as an important modulator of mtROS production. NO can modulate mitochondrial respiration and oxygen consumption through reversible binding and inhibition at complex IV, leading to the accumulation of NADH and increases in ROS production⁶⁵. Mitochondria also participate in Ca^{2+} homeostasis by serving as a high-capacity, low-affinity transient Ca^{2+} store. In contrast to NO, mitochondrial Ca^{2+} stimulates the rate of electron flow in the ETC⁶⁶. By allosteric activation of key enzymes in the tricarboxylic acid (TCA) cycle and ATP synthase, Ca^{2+} stimulates oxidative phosphorylation and mtROS production⁶⁷.

O₂ concentration

MtROS production also depends on O₂ concentration. As cellular O₂ concentration increases, the rate of mtROS production increases linearly⁶⁸. However, during hypoxia, a paradoxical increase in mtROS release was reported⁶⁹. This mtROS release appears to come from complex III and functions as a regulator of hypoxia-inducible factor 1 α (HIF-1 α). Nevertheless, the precise molecular basis underlying the seemingly controversial relationship between ambient oxygen levels and mtROS production remains obscure. The redox-optimized ROS balance hypothesis mentioned previously can be used to account for this discrepancy. It is postulated that hypoxic cells would exhibit high $\Delta\psi_m$ and augmented mtROS production due to the low electron flow⁶². In this setting, the increased generation of mtROS could then be relieved by overexpressing mitochondrial UCPs⁷⁰.

Transcription factors

Several nuclear transcription factors with well-characterized functions in the nucleus are also present in the mitochondria and become mitochondrial transcription factors. Mitochondrial transcription factors include those of the nuclear hormone receptor family as well as transcription factors such as p53, NF- κ B and STATs that are activated downstream of the binding of growth hormones and cytokines to cell-surface receptors⁷¹. These TFs have several different mechanisms in regulating mitochondrial function and ROS levels. P53 can bind to the Bcl-2 family members and induces apoptosis. Also, p53 can inhibit SOD2. In addition, interferon regulatory transcription

factor family 3 can interact with proapoptotic protein Bax. Moreover, TFs including cAMP-responsive transcription factor, NF- κ B, myocyte enhancer factor-2D and STAT3 all can regulate gene expression.

STAT3, initially identified as a transcription factor that regulates gene expression in response to cytokines such as IL-6 and IL-10, has recently been found to modulate mtROS through mechanisms independent of its nuclear factor activity, but dependent on its ability to directly modulate the activity of the ETC^{52, 72}. It has been shown that STAT3 is present in the mitochondrial matrix, and deficiency of STAT3 in murine hearts leads to decreased activities of complexes I and II while increasing mtROS at complex I⁵². However, the molecular mechanism by which STAT3 modulates ETC activity is not well understood and it remains to be determined whether STAT3 is unique among STAT proteins in localizing to mitochondrial matrix and regulating mtROS. Since STAT3 responds to cytokines of the IL-6 and IL-10 families, which themselves regulate cellular metabolism process, it is tempting to speculate that by modulating mitochondrial ETC activity and mtROS generation, STAT3 links cytokine signaling pathways to cellular metabolism.

HIF-1 mediates adaptive responses to chronic hypoxia with reduced oxygen availability by regulating gene expression. HIF-1 reduces mtROS production under hypoxic conditions through multiple mechanisms including: *i*) a subunit switch in cytochrome c oxidase that increases the efficiency of mitochondrial complex IV; *ii*) induction of pyruvate dehydrogenase kinase 1, which shunts pyruvate away from the

mitochondria; *iii*) induction of BCL2/adenovirus E1B 19 kDa protein-interacting protein 3, which triggers mitochondrial selective autophagy; and *iv*) induction of microRNA-210, which blocks assembly of Fe/S clusters that are required for oxidative phosphorylation⁷³.

Non-mitochondrial ROS sources

Under certain conditions, non-mitochondrial generated ROS can augment mtROS production, a process known as “ROS-induced ROS”. It has been demonstrated that many other ROS-producing enzymes, including NADPH oxidase⁷⁴, xanthine oxidase⁷⁵, and uncoupled eNOS⁷⁶, can stimulate mtROS production. The “ROS-induced ROS” system downstream of angiotensin II (Ang II) signaling pathway is well characterized. Ang II is a well-known stimulator of NADPH-oxidase-derived ROS⁷⁷, but a role of mtROS downstream of Ang II-mediated cellular signaling has also emerged only recently⁷⁴. However, “ROS-induced ROS” can be a two-way street, which suggests that cytosolic ROS induce mtROS and mtROS also promotes cytosolic ROS. In fact, it has been suggested that by activating NADPH oxidase, Ang II induces mtROS, which in turn leads to further activation of NADPH oxidase. Moreover, scavenging of mtROS using mitochondria-targeted antioxidant can interrupt this vicious cycle and significantly decrease blood pressure after the onset of Ang II-induced hypertension⁷⁸.

The question of how other sources of ROS induce mtROS remains. However, the importance of p66^{shc} in this process is highlighted by the fact that p66^{shc} is localized within the mitochondrial intermembrane space and can directly transfer electrons from *cytochrome c* to O₂ to generate mtROS⁷⁹. Importantly, intracellular antioxidants such as

GSH are thought to maintain the mitochondrial form of p66^{shc} in an inactive state⁸⁰. Thus, p66^{shc} may serve as a thiol-based redox sensor that signals to mitochondria to induce mtROS when the ROS level in cytoplasm becomes high. As such, the atherosclerotic risk factor mediator, oxidized LDL, activates p66^{shc} through NADPH oxidase⁸¹. Furthermore, deficiency of p66^{shc} gene renders mice resistant to complications of atherosclerosis⁸².

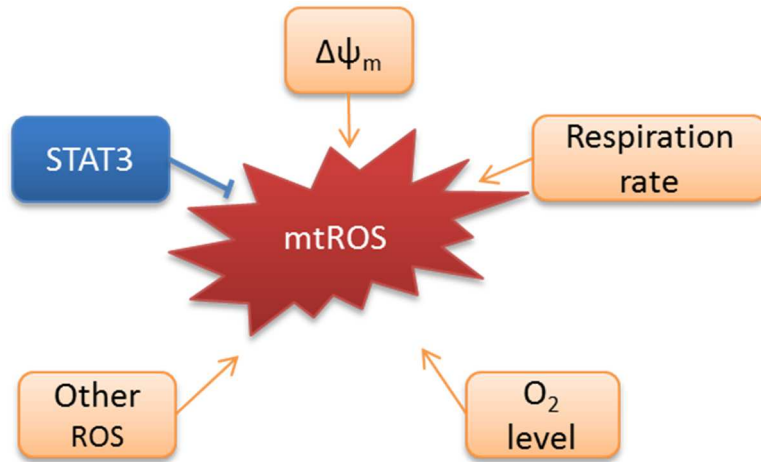


Figure 3. Regulation of mtROS production.

A number of factors including mitochondrial membrane potential ($\Delta\psi_m$), metabolic state of mitochondria, and O_2 concentration regulate the production of mtROS. Non-mitochondrial generated ROS can also augment mtROS production, a process known as “ROS-induced ROS”. Meanwhile, transcription factor STAT3 has recently been found to suppress mtROS production independent of its nuclear factor activity.

MtROS and EC Functions

Even when plenty of oxygen is presented, ECs rely heavily on glycolysis rather than mitochondrial respiration to generate ATP⁸³. Nevertheless, ECs still contain functional mitochondria, in which oxidative phosphorylation continues^{84, 85}. Thus, the primary function of mitochondria in ECs may be the regulated generation of ROS for cells signaling purpose, but not generation of ATP for energy production. If this is true, ECs could modulate mtROS production without jeopardizing their energy needs. Indeed, mtROS are involved not only in regulating a variety of important endothelial functions under basal conditions but also in activating proinflammatory pathways in response to cardiovascular risk factors in ECs⁸⁶.

Under normal physiological conditions, mtROS are capable of regulating vascular homeostasis. Firstly, it has been demonstrated that vascular endothelial growth factor (VEGF) promotes endothelial migration through mtROS in cultured human umbilical vein endothelial cells⁸⁷. Endothelial migration is critical in a variety of physiological conditions including wound healing and vascular repair. VEGF increases mitochondrial metabolism and mtROS production. Furthermore, mitochondria-targeted antioxidant prevents VEGF-induced endothelial migration. Secondly, mtROS contribute to endothelium-dependent vasodilation⁸⁸. The endothelium regulates vascular homeostasis in response to shear stress by synthesizing vasodilators such as NO. Using ESR and histochemofluorescence methods, it has been shown that shear flow increases the production of ROS in human coronary resistance arteries, which can be blocked by

mitochondrial complex I inhibitor rotenone. Moreover, complex I and complex III inhibitors, but not NADPH oxidase inhibitors, markedly blocked flow-induced dilation. Notably, ROS formation in response to flow after endothelial denudation is significantly decreased, suggesting an important role of endothelium in flow-induced mtROS formation. Thirdly, mtROS are also of importance in hypoxia-induced adaptation response in ECs. At low O₂ concentrations, mitochondria of human umbilical vein endothelial cells (HUVECs) have been shown to generate ROS for activation of enzymes such as AMP-activated protein kinase (AMPK) because: 1) AMPK activation coincides with the hypoxia condition at which ROS is produced; 2) antioxidants can rescue hypoxia-induced AMPK activation; and 3) AMPK activation does not occur in ρ^0 HUVECs devoid of mitochondria. Under the challenge of cardiovascular risk factors, however, excessive mtROS are produced in endothelial mitochondria. Vascular stressors, as diverse as oxidized lipids, high glucose, and angiotensin II, can all induce mtROS in ECs. (Table 2)

oxLDL

Substantial evidence suggests that the retention and oxidative modification of LDL and subsequently activation of ECs initiates atherosclerotic lesion formation⁸⁹. OxLDL triggers the expression of adhesion molecules and secretion of chemokines by ECs, which drive immune cell trans-EC migration and infiltration. In this sense, oxLDL has been shown to induce mtROS in ECs *in vitro*⁹⁰⁻⁹². Using confocal microscopy, it has been demonstrated that a significant proportion of oxLDL-induced cellular ROS are co-

localized to mitochondria. Moreover, ECs that are deficient in functional mitochondria show a substantial decrease in cellular ROS formation stimulated by oxLDL⁹⁰. The precise mechanisms whereby oxLDL induces excessive mtROS generation in ECs remains poorly defined. It has been suggested that oxLDL significantly reduces oxygen consumption and enzyme activity in the mitochondrial ETC⁹¹. OxLDL also increases $\Delta\psi_m$ and reduces SOD2 protein levels⁹². Moreover, c-Jun N-terminal kinases small interference RNA reduces oxLDL induced mtROS production substantially.

Glucose

Hyperglycemia is a key cardiovascular risk factor for patients with type 2 diabetes⁹³. High glucose is the first identified pathogenic stressor that induces mtROS in ECs⁹⁴. High glucose-induced DCF fluorescence in bovine aortic ECs is prevented by several factors including an inhibitor of the ETC complex, an uncoupler of oxidative phosphorylation, uncoupling protein-1 and SOD2⁹⁴. Furthermore, normalizing levels of mtROS after treatment of cells with each of these agents prevents high glucose-induced activation of protein kinase C, formation of advanced glycation end-products, sorbitol accumulation and NF κ B activation⁹⁴. Later on, other studies report similar results^{95, 96}. One study shows that inhibition of ROS production by uncoupling of the ETC significantly reduces high glucose-mediated induction of IL-8 expression in human aortic ECs⁹⁵. Another study links high glucose-dependent mtROS to increased consumption of H₂S⁹⁶. Interestingly, traditional pharmacological drugs including anti-inflammatory Sirt1 activator resveratrol, anti-inflammatory/anti-cancer drug cannabidiol, and hypolipidemic

drug simvastatin have been shown to prevent high glucose-induced mtROS⁹⁷⁻⁹⁹. The measurement of MitoSOX fluorescence shows that resveratrol attenuates high glucose-induced mtROS production in human coronary arterial ECs. The authors propose that resveratrol, via a pathway that involves the upregulation of antioxidant defense mechanism, attenuates mtROS production⁹⁷. Another paper shows that high glucose markedly increases mtROS, NF- κ B activation, upregulation of iNOS, and EC adhesion molecules ICAM-1 and VCAM-1, monocyte-endothelial adhesion in human coronary artery ECs, and transendothelial migration of monocytes. Remarkably, all the above mentioned effects induced by high glucose are attenuated by cannabidiol pretreatment⁹⁸. Similarly, Simvastatin decreases high glucose-induced mtROS in bovine retinal capillary ECs and exerts protective effects against early retinal vascular damage in diabetic rats⁹⁹. A recent study proposes that acute exposure to low glucose also increases mtROS production in human umbilical vein ECs¹⁰⁰. Interestingly, anti-diabetic drug Metformin can reverse low glucose-induced endothelial dysfunction through inhibiting excessive mtROS production.

Angiotensin II

Ang II is another pathogenic stressor that mediates endothelial dysfunction and promotes vascular inflammation and atherogenesis¹⁰¹. Ang II treatment of bovine aortic ECs is shown to significantly increase mtROS production detected by ESR. This effect is associated with decreased endothelial NO availability⁷⁴. Later on, the same group confirms this result using MitoSOX fluorescent probe. Interestingly, supplementation of

human aorta ECs with the mitochondria-targeted antioxidant mitoTEMPO abolishes the MitoSOX signal after Ang II stimulation⁷⁸. In addition, mitoTEMPO also prevents the loss of endothelial NO caused by Ang II both in cultured ECs and in mice. Furthermore, treatment of hypertensive mice with mitoTEMPO after onset of Ang II-induced hypertension significantly reduces blood pressure and substantially improves endothelium-dependent vasodilation.

Table 2. Identified pathologic stressors that induce mtROS in EC.

Cell type	Treatment	Dose	Time	PMID
Bovine aortic ECs	Oxidized LDL	200 µg/ml	30 min	15805232
Bovine aortic ECs	Electrophilic lipids	4 µM	4 h	16387790
Human umbilical vein ECs	LPC	5 µmol/L	60 min	16651638
Porcine aortic ECs	Glycated LDL	100 µg/ml	2 h	20036735
Bovine aortic ECs	Glucose	30 mM	2 h	10783895
Human aorta ECs	Glucose	25 mM	7 d	12600878
bEnd3 microvascular ECs	Glucose	40 mM	7 d	21808008
Human umbilical vein ECs	Low Glucose	≤ 80 mg/dL	5 min	22207730
Bovine aortic ECs	Angiotensin II	200 nmol/L	4 h	18096818
Human aortic ECs	Angiotensin II	200 nmol/L	4 h	20448215
Human aortic ECs	Homocysteine	150 µM	24 h	21672628
Human umbilical vein ECs	Hypoxia	14 mmHg	30 min	11950692
Human umbilical vein ECs	Hypoxia	0 mmHg	24 h	12165534
Porcine aortic ECs	Hypoxia	0 mmHg	1 h	12690038
Murine pulmonary ECs	Thrombin	1 mU/mL	100 s	17724077
Human umbilical vein ECs	PAR1-AP	50 µmol/L	1 h	18983479
Human umbilical vein ECs	TNF-α	1 ng/mL	1 h	11415943
Murine pulmonary ECs	TNF-α	1 ng/mL	10 min	21519143
Bovine aortic ECs	Leptin	10 ng/mL	45 min	11342529
Human coronary artery ECs	Resistin	40/80 ng/mL	24 h	20435848
Human umbilical vein ECs	VEGF	50 ng/mL	5 min	21653897

PMID: PubMed ID

MtROS and Cardiovascular Diseases

MtROS and hypertension

Hypertension is associated with increased ROS production in several key target organs, including the vasculature, the kidney, and the central nervous system, which all contribute to the dysregulation of blood pressure¹⁰². Ang II, the hormone commonly implicated in hypertension, is shown to increase ROS production in these sites. A key role of NADPH oxidase in this process has been demonstrated both *in vitro* and *in vivo*¹⁰³. However, later studies indicates that Ang II activation of NADPH oxidase further leads to mitochondrial dysfunction and increased mtROS production⁷⁴. Importantly, mice transgenic for thioredoxin (Trx2), the mitochondrial antioxidant enzyme, are shown to resist endothelial dysfunction and the development of Ang II-induced hypertension¹⁰⁴. Moreover, Ang II-induced hypertension is also significantly attenuated by either overexpressing SOD2 or treatment with mitoTEMPO⁷⁸. These studies strongly demonstrate the potential of antioxidant strategies specifically targeting mtROS as therapy in hypertension and possibly in other CVDs as well.

MtROS and atherosclerosis

Multiple lines of *in vivo* experimental data indicate that excessive mtROS within vasculature promote the development of atherosclerosis. ApoE^{-/-} mice that are deficient in SOD2, a mitochondria-specific antioxidant enzyme, exhibit accelerated atherogenesis at arterial branching points¹⁰⁵. SOD2 is also shown to protect against endothelial

dysfunction in carotid artery of ApoE^{-/-} mice⁴⁸. Notably, transgenic overexpression of Trx2, another mitochondrial antioxidant enzyme, improves endothelial function and reduces atherosclerotic lesions in ApoE^{-/-} mice in part by reducing oxidative stress and increasing NO bioavailability⁵⁷. It was recently shown that macrophage mtROS promote atherosclerosis development by promoting NF-κB-mediated inflammation in macrophages¹⁰⁶. There is still limited knowledge of the involvement of mtROS in human atherogenesis; however, epidemiologic data suggest that genetic nucleotide polymorphisms leading to reduced SOD2 function are associated with increased atherosclerotic risk¹⁰⁷. In addition, there is significantly increased mitochondrial DNA (mtDNA) damage in human atherosclerotic arterial specimens compared to that of normal human arterial tissue¹⁰⁵. Indeed, increased mtDNA damage is also a shared phenotype of multiple diseases including neurological degenerative disease¹⁰⁸ and cancer¹⁰⁹. As mtDNA contains genes that encode critical structural subunits for three of the four protein complexes of the ETC (complex I, III, and IV)¹¹⁰, mtDNA damage will lead to increases in mtROS generation and the extent of mtDNA damage is an index of the levels of mtROS.

Histone Acetylation

Histone Acetylation Favors Gene Transcription

Epigenetic regulations in the cell include DNA methylation, non-coding RNAs, and post translational modification of histone proteins such as acetylation, methylation, phosphorylation, ubiquitylation, and SUMOylation^{111,112}. DNA methylation mainly occurs on CpG dinucleotides of DNA and usually leads to transcriptional repression of gene expression. More than 10 different groups of non-coding RNAs have been discovered in the cell so far, such as microRNAs, small interfering RNA, and long non-coding RNAs¹¹³. MicroRNAs are small single stranded RNA molecules, which inhibit mRNA stability and translation from a different locus of which they are derived. Small interfering RNAs, on the other hand, are double stranded RNA molecules which induce gene silencing by cleaving mRNA and regulate the same genes that express them. At last, long non-coding RNAs are RNA molecules longer than 200 nucleotides and regulate gene expressions. However, the majority of the biological functions of nearly 200 identified LncRNA still remain largely unknown¹¹⁴.

Key post translational modifications of histone proteins include methylation and acetylation¹¹². Histone methylation can be associated with either transcriptional repression or activation and is mainly regulated by histone methyltransferases. For example, mono-, di, or tri-methylation of histone H3 lysine 4 (H3K4me, me2, me3) are active marks for transcription whereas methylation on H3K9, H3K27 are signals for transcriptional silencing¹¹⁵. Histone acetylation, on the other hand, favors gene transcription and is considered as a hallmark of transcriptionally active regions. Histone

acetylation modifications are carried out by histone acetyltransferase (HAT) and histone deacetylase (HDAC) enzymes. The addition of acetyl groups on histone tails was considered to facilitate gene transcription by neutralizing the histone charges, thus weakening histone-DNA interaction and relaxing the chromatin structure¹¹⁶.

Histone Acetylation and Atherosclerosis

Despite the ample knowledge of histone acetylation in cancer and the development of histone deacetylase (HDAC) inhibitors as anticancer drugs¹¹⁷, there is limited knowledge of the role of histone acetylation in atherosclerosis and the established knowledge on this topic is controversial. One study using ApoE^{-/-} atherosclerotic mouse model found that expression of HDAC3 was induced in the aortas during atherosclerosis development and in ECs exposed to disturbed flow *in vitro*. In addition, knockdown of HDAC3 in ApoE^{-/-} mice led to increased atherosclerotic lesion formation, suggesting a protective effect of HDAC3 in atherogenesis¹¹⁸. Along the same line, a recent study showed that macrophage-specific HDAC3 knockout in ApoE^{-/-} stabilized atherosclerotic lesions and HDAC3 was shown to be the sole HDAC upregulated in ruptured atherosclerotic lesions in humans¹¹⁹. However, another study investigated the role of HDAC9 in atherosclerosis and found that systemic and bone marrow cell deletion of HDAC9 decreased atherosclerosis in low density lipoprotein receptor knockout mice, another atherogenic mouse model, arguing a proatherogenic role of HDAC9 in atherosclerosis instead¹²⁰. This was supported by a study showing that trichostatin A (TSA) (a specific histone deacetylase inhibitor) treatment in low density lipoprotein receptor knockout mice exacerbated atherosclerosis development, indicating that histone acetylation plays a protective role in atherogenesis development¹²¹.

Histone Acetylation and EC Activation

The fact that histone acetylation favors gene transcription led the researchers to hypothesize that histone acetylation contributes to EC activation. In fact, oxLDL-induced secretion of IL-8 and monocyte-chemoattractant protein in ECs was enhanced by HDAC inhibitors¹²². oxLDL also induced histone H3 and H4 acetylation both globally and on the promoters of IL8 and MCP1 genes in ECs. The authors also showed that oxLDL reduced HDAC1 and HDAC2 expression in ECs and decreased expression of HDAC2 was found in ECS in atherosclerotic plaques of human coronary arteries. However, it is surprising to find that HDAC inhibitors (which increase histone acetylation) also served as potent suppressor of EC activation agents. Preincubation of HDAC inhibitor TSA attenuated tumor necrosis factor alpha (TNF- α)-induced monocyte adhesion through VCAM-1 inhibition both in HUVECs and *in vivo*¹²³. Similarly, TSA and four other HDAC inhibitors were also shown to inhibit tissue factor (a cell surface receptor for the serine protease factor VIIa, also termed platelet tissue factor) expression in HUVECs¹²⁴. Thus, inhibition of HDAC activities can have promoting and inhibiting effects in EC activation in different studies.

IL-35*

Anti-inflammatory Cytokines Suppress Atherosclerosis Development

CD4⁺ T helper cells (Th) play essential roles in regulating inflammation and immune responses via differentiation into various Th functional subtypes, including Th1, Th2, Th17, Th9, Th22, follicular Th, and regulatory T cells (Tregs)¹²⁵. The majority of Th cell functions are fulfilled via the secretion of various cytokines, which can play a dual role in regulating atherogenesis¹²⁶. Proinflammatory and Th1-related cytokines such as interleukin-1 (IL-1), IL-18 promote the development and progression of atherosclerosis^{127, 128}. However, Tregs-related anti-inflammatory cytokines such as IL-10 and transforming growth factor beta (TGF- β) exert clear anti-atherogenic activities^{129, 130}. It therefore stands to reason that patients with angina¹³¹ or familiar hypercholesterolemia¹³² have lower serum IL-10 levels than healthy controls. In fact, transfer of murine IL-10 in the atherogenic ApoE^{-/-} mouse model achieved 60% reduction in atherosclerotic lesion size¹³³. In addition, knockout of IL-10¹²⁹ or inhibition of TGF- β signaling¹³⁴ in ApoE^{-/-} mice resulted in 300% and 200% increase of atherosclerotic lesion formation, respectively. These findings suggest that anti-inflammatory cytokines play a critical role in the inhibition of atherosclerosis.

* This part of introduction is modified and updated from the article "IL-35 is a novel responsive anti-inflammatory cytokine—a new system of categorizing anti-inflammatory cytokines." *PloS one* 2012. The first author of this article is the author of this thesis.

Anti-inflammatory Cytokines Suppress EC Activation

IL-10 suppresses EC activation both *in vitro* and *in vivo*. In cell culture systems, IL-10 inhibits IL-1-induced expression of ICAM-1 and VCAM-1 in HUVECs¹³⁵. In addition, preincubation with IL-10 or overexpressing IL-10 using adenovirus in HAEC significantly decreases oxLDL-induced monocyte adhesion¹³⁶. These findings were supported by *in vivo* findings in mice. Systemic delivery of IL-10 using plasmid DNA completely prevented high fat diet-induced upregulation of ICAM-1 and VCAM-1 in the aortic sinus of mice¹³⁷.

The inhibitory effect of TGF- β was demonstrated using heterozygous TGF- β 1^{+/-} mice. After 12 weeks of high fat diet, higher level expressions of EC adhesion molecules ICAM-1 and VCAM-1 in vascular ECs and marked deposition of macrophage-enriched lipid lesions were detected in TGF- β 1^{+/-} mice compared with that of wild-type mice¹³⁸. These results suggest that endogenous TGF- β 1 is protective against EC activation in the vessel wall.

IL-35 is a Novel Responsive Anti-inflammatory Cytokine

IL-35 was identified as a novel anti-inflammatory cytokine in 2007. It is a dimeric protein with two subunits, IL-12A and Epstein-Barr virus induced 3 (EBI3)^{139, 140}. Secretion of IL-35 has only been confirmed in Tregs¹⁴⁰ and B cells^{141, 142}. Using experimental database mining approach that we developed¹⁴³⁻¹⁴⁶, we found that IL-35 was not constitutively expressed in human tissues¹⁴⁷. In addition, the genes encoding IL-35 (IL-12A and EBI3) were transcribed by vascular ECs, VSMCs, and monocytes after activation with proinflammatory cytokines and lipopolysaccharide¹⁴⁷. Furthermore, IL-35 has intrinsic instability, as it could be quickly degraded by AU-rich element- and microRNA-mediated mechanism¹⁴⁷. We concluded that IL-35, similar to IL-10 but opposite to TGF- β , is a responsive anti-inflammatory cytokine (Figure 4). Our new working model in categorizing anti-inflammatory cytokines provide important insight into the following two important issues: first, how anti-inflammatory cytokines share their duties: the house-keeping cytokines, such as TGF- β s, inhibit the initiation of inflammation whereas the responsive cytokines including novel cytokine IL-35 suppress full-blown inflammation; and second how these two groups of anti-inflammatory cytokines orchestrate their roles in suppressing inflammation in different stages in various tissues and systems.

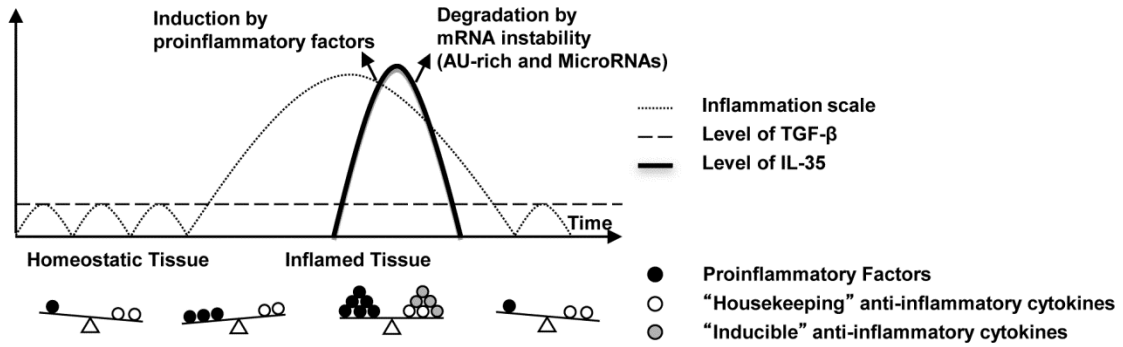


Figure 4. IL-35 is a novel responsive anti-inflammatory cytokine

Homeostatic tissues express “house-keeping” anti-inflammatory cytokines such as TGF- β to prevent it from initiation of inflammation. When tissues get inflamed, proinflammatory factors may stimulate tissues to express “responsive” anti-inflammatory cytokines such as IL-35 by specific transcription factors to counteract inflammation response. In addition, ARE binding proteins and MicroRNAs are responsible of the quick degradation of IL-35 mRNA afterwards, by which IL-35 achieves non-constitutive expression status in tissues again.

Rationale and Hypothesis of Dissertation

Atherosclerosis is a chronic inflammatory pathogenic process of the arteries that leads to CVDs including myocardial infarction, stroke and peripheral artery disease, which are the number one cause of death in the United States⁶. Atherosclerosis is initiated by the activation of EC that line the inner surface of the blood vessel wall⁵. Normally arterial EC are quiescent. When hyperlipidemia occurs, however, sub-endothelial retention and oxidation of LDL generate LPC which activates EC to upregulate the expressions of adhesion molecules and secretion of cytokines and chemokines^{7, 8}. However, the mechanisms underlying this response are not fully understood¹⁶. Previously considered as the toxic by-products of cellular metabolism, mtROS are recently found to directly contribute to both the innate and adaptive immune responses. As a novel anti-inflammatory cytokine, the role of IL-35 in EC activation is not known. Here we tested novel hypotheses that mtROS serve as signaling mediators for LPC-induced EC activation; and that IL-35 could suppress LPC-induced EC activation by inhibiting mtROS. Our hypothesis will be tested with the following specific aims:

Specific aim 1 – Determine whether and how LPC induces mtROS in HAEC

Study 1 – Determine whether LPC is induced in the aortas of ApoE^{-/-} mice during early atherogenesis

Study 2 – Determine whether LPC induces mtROS in HAEC

Study 3 – Determine the mechanisms underlying LPC-induced mtROS in HAEC

Specific aim 2 – Determine the downstream effects of LPC-induced mtROS in HAEC.

Study 1 – Determine whether mtROS mediate LPC-induced ICAM-1 upregulation

Study 2 – Determine the underlying mechanisms of LPC-induced mtROS in regulating ICAM-1 expression

Study 3 – Determine whether anti-inflammatory cytokines IL-35 and IL-10 can suppress LPC-induced EC activation by inhibiting mtROS

CHAPTER 2 - MATERIAL AND METHODS

Chemicals and Antibodies

All chemicals were from Sigma-Aldrich (St. Louis, MO) unless otherwise indicated. Three different types of lysophosphatidylcholine (16:0, 18:0, 18:1) were purchased from Avanti Polar Lipids, Inc. For the measurement of mtROS, MitoSOX Red Mitochondrial Superoxide Indicator (Life technologies) and mito-TEMPO-H Spin Probe (Enzo) were used. CPH Spin Trapping reagent (Enzo) was also used for detection of cytosolic superoxide. Fluo-4 and Rhod-2 (Life technologies) were purchased for the measurement of cytosolic and mitochondrial calcium. IRDye 700 AP-1 and NF κ B oligos were purchased from LI-COR for detecting nuclear translocation of transcription factors.

Calcium signaling inhibitor Ruthenium Red was purchased from Calbiochem. Mitochondrial ROS inhibitor MitoTEMPO was purchased from Enzo. HAT inhibitor Curcumin was purchased from Sigma. Anti-inflammatory cytokines IL-35 and IL-10 were purchased from Enzo and R&D, respectively. The primers (5'-3') used for the real-time PCR are: human ICAM1: TCTACGCTGACAATGAATCCTG and AGGGCCACTCAAATGAATCTC, human ACTB: ACCTTCTACAATGAGCTGCG and CCTGGATAGCAACGTACATGG. Anti-ICAM-1 antibody (#4915) was purchased from Cell Signaling and Anti-acetyl-Histone H3 (Lys14) antibody (#MABE351) was purchased from Millipore.

Animals

All animal experiments were performed in accordance with the Institutional Animal Care and Use Committee (IACUC) Guidelines and Authorization for the use of Laboratory Animals and approved by the Experimental Animal Committee of Temple University School of Medicine.

All mice used were on a C57BL/6 background. ApoE mutant mice or commonly known as ApoE^{-/-} mice (strain name: B6.129P2-Apoetm1Unc/J) and wild-type (WT) mice were purchased from The Jackson Laboratory (Bar Harbor, ME). Both WT and ApoE^{-/-} mice were weaned at 4 weeks of age and maintained chow diet for another 4 weeks, at which time (8 weeks-old) they were given 0.2% (w/w) cholesterol and 21.2% (w/w) fat high fat diet (TD.88137, Harlan) for 3 weeks. At 11 weeks-old, mice were sacrificed and aortas were collected for metabolomics study.

Mouse Genotype

Mouse genotype was confirmed with PCR followed by agarose gel separation of the products. Mouse tail tissue was collected and digested with 600µl of tissue lysis buffer (10mM tris (pH 8.0), 100mM NaCl, 10mM EDTA, pH 8.0, and 0.5% SDS) containing 0.4mg/ml proteinase K at 55°C overnight. Tissue lysate was centrifuged at 13,000rpm (Fisher Scientific Accuspin Micro R Centrifuge) for 20 minutes. Supernatant containing genomic DNA was collected and DNA was precipitated in 100% ethyl alcohol and dissolved in distilled deionized water at 37°C overnight.

Mouse genomic DNA was amplified with 3 specific ApoE primers by PCR: 180 (5'-GCCTAGCCGAGGGAGAGCCG-3'), 181 (5'-TGTGACTTGGGAGCTCTGCAGC-3'), and 182 (5'-GCCGCCCCGACTGCATCT-3'). The PCR cycle was 94°C for 30 seconds (sec), 68°C for 40 sec, 72°C for 1 minute (min), and repeated for 35 cycles. The PCR product was realized by gel electrophoresis with a 2% agarose gel. The DNA fragment for ApoE^{-/-} mice was 245 base pairs (bp), and the DNA fragment for WT mice was 155bp in length.

Metabolomics Analysis

Aortas were collected from mice after 3 weeks of high fat diet. Global, unbiased metabolic profiling was performed by Metabolon¹⁴⁸. Briefly, after the extraction of metabolites from tissues, the extracts were analyzed by ultra-high performance liquid chromatography-tandem mass spectrometry (UPLC-MS/MS; positive mode), UPLC-MS/MS (negative mode) and gas chromatography-mass spectrometry (GC-MS). Compounds were identified by library search and statistical analysis was performed.

Cell Culture

Human aortic endothelial cells (HAECs) (Lonza, CC2535) were cultured in medium M199 (Hyclone laboratories, Logan, UT) supplemented with 15% fetal bovine serum (FBS; HyClone), endothelial cell growth supplement (ECGS, 50µg /mL; BD Biosciences), heparin (50µg/mL), and 1% penicillin, streptomycin, and amphotericin

(PSA; Invitrogen, Carlsbad, CA). HAECs were grown on 0.2% gelatin-coated flasks, plates, or dishes and they were used between passages 8 to 9.

Fluorescence Activated Cell Sorting (FACS)

After staining with MitoSOX (5 μ M), HAECs were incubated at 37°C incubator for 10mins and washed with PBS twice afterwards. After treatment of drugs, cells were washed once with ice-cold PBS and 200 μ L of Trypsin-EDTA was added to detach cells. Trypsinization was terminated by adding FACS buffer (2% FBS in PBS) and collected by centrifuge. After re-suspension in 0.2 ml FACS buffer, samples were subjected to flow cytometry analysis and fluorescence emissions were measured at FL2 channel by FACSCalibur machine (BD).

Fluorescence Microscopy

After staining with MitoSOX (5 μ M), HAECs were incubated at 37°C incubator for 10mins and washed with PBS twice afterwards. After treatment of drugs, cells were washed twice with PBS and used for staining by fluorescence microscopy. Images were captured by the Zeiss AxioScope microscope.

Electron Spin Resonance (ESR)

After treatment, HAECs were washed with PBS twice and collected with cell scraper. HAECs were then centrifuged and collected in 100 μ l of deoxygenated modified pH 7.35 Krebs HEPES buffer (KHB) (99mM NaCl, 4.69mM KCl, 25mM NaHCO₃, 1.03mM KH₂PO₄, D-glucose 5.6mM, Na-HEPES 20mM, CaCl₂(x2H₂O) 2.5mM, MgSO₄

1.2mM). Cells were then vortexed briefly and aliquoted into 10 μ l suspension in Eppendorf tubes. , each aliquot of cells were added 80 μ l of modified KHB buffer (plus 25 μ M Deferoxamine and 5 μ M DETC) and 10 μ l of MitoTEMPO-H/CP-H buffer (10mM) to measure mitochondrial/cytosolic ROS. The remaining cells were centrifuged and the cell pellets were frozen for the determination of protein concentration.

Toxicology Assay

In vitro Toxicology Assay Kit, Lactic Dehydrogenase based (SIGMA-Aldrich, TOX7) was performed according to the manufacturer's suggestion. Briefly, cytoplasmic lactact dehydrogenase (LDH) released into the medium was measured based on the reduction of NAD by LDH. The resulting reduced NADH is converted to colored compound and measured by spectrophotometer plate reader. LDH activity was expressed by subtracting the 630nm absorbance value (background signal from instrument) from the 490nm absorbance.

Seahorse XF96 Analyzer

HAECs were seeded at 30K per well in 96-well plates and cultured overnight. Culturing media was changed to modified DMEM media (2mM sodium pyruvate, 25mM glucose) and placed into a 37°C non-CO₂ incubator for 1h. After preparation of drugs and XF Cell Mito Stress Test Kit (Seahorse Bioscience) into cartridge ports, the cartridge and cell culture plates were loaded in XF96 analyzer (Seahorse Bioscience). After 3 basal measurement of oxygen consumption rate, drugs of interest were added and basal

respiration were measured every 15 min for 1 hour. XF Cell Mito Stress Test Assay was performed afterwards to determine maximal respiration rate and other parameters of mitochondria.

Confocal Microscopy

HAEC cells were grown on 25-mm glass coverslips and loaded with 2 μ M Rhod-2 AM (50 min) and 5 μ M Fluo-4 AM (30 min)¹⁴⁹. After 1 min of baseline recording, LPC (10 μ M) was added, and confocal images were recorded every 3 s (510 Meta; Carl Zeiss, Thornwood, NY) at 488- and 561-nm excitation using a 63 \times oil objective to simultaneously monitor cytoplasmic and mitochondrial Ca^{2+} dynamics. Images were analyzed and quantified using custom-made software (Spectralyzer, Elmsford, NY).

Western Blot Analysis

Protein extracts were collected from HAEC. Protein concentrations were determined by the bicinchoninic acid (BCA) assay with BSA standards. Proteins were separated on SDS-polyacrylamide gels and transferred onto nitrocellulose membranes. Membranes were blocked by 5% BSA in tris buffered saline containing 0.01% Tween 20 [TBST, 50mM Tris (pH 7.5), 150mM NaCl, and 0.1% Tween 20 (v/v)]. Membranes were incubated with primary antibodies overnight at 4°C. Membranes were then washed extensively with TBST and incubated with the appropriate horseradish peroxidase-labeled secondary antibodies for 1 hour at room temperature. Afterward, membranes were incubated with enhanced chemiluminescence (ECL) substrate for horseradish

peroxidase (Pierce/Thermo, Rockford, IL) and the ECL intensity was detected by X-ray film exposure in a dark room. The X-ray films were developed by the SRX-101A medical film processor. The expression levels of proteins as indicated by the ECL intensity were measured with ImageJ software (NIH, Bethesda, MD, USA).

Real-Time PCR

Total RNA was isolated from HAECs with RNeasy Mini Kit (Qiagen) following the manufacturer's suggestion. The RNA was solubilized in 30µl nuclease-free water. RNA quality and concentration was determined by the Nanodrop 2000 (Thermo Scientific, Wilmington, DE). Two µg of total RNA was reverse transcribed to generate complementary DNA (cDNA) using the High Capacity cDNA Reverse Transcription Kit (Invitrogen).

The mRNA expression levels of genes were determined by quantitative real-time PCR (qRT-PCR) with the SYBR-green dye (Invitrogen) on the StepOnePlus PCR system (Applied Biosystems, Foster City, CA).

Human EC Biology PCR Array

RNA collected from HAEC was isolated using the RNeasy Mini Kit (Qiagen). RNA was converted to cDNA with the RT² First Strand Kit (SABiosciences) and used following the direction of the Human Endothelial Cell Biology PCR Array (SABiosciences). Data was analyzed with the SABiosciences PCR Array Data Analysis Software.

Site-Specific Histone Acetylation Screening

Residue-specific histone acetylation was quantified by multiplexed mass spectrometry using published methods^{150, 151}. Briefly, a Waters Acquity H-class UPLC (Milford, MA) coupled to a Thermo TSQ Quantum Access (Waltham, MA) triple quadrupole (QqQ) mass spectrometer was used to quantify site-specific acetylated H3 peptides. After histone extraction and purification by the Histone Purification Mini Kit (Active Motif), the extracted histones were subjected to propionylation and trypsin digestion. The digested samples were then injected to an Acquity BEH C18 column (2.1×50 mm; particle size 1.7 μm) with 0.2% formic acid (FA) aqueous solution (solution A) and 0.2% FA in acetonitrile (solution B). Peptides were eluted over 11 min at 0.6 mL/min and 60°C, and the gradient were programmed from 95% solution A and 5% solution B and down to 80% solution A and 20% solution B in 11 min. Selected reaction monitoring (SRM) were used to monitor the elution of the acetylated and propionylated H3 peptides. The resolved peaks were integrated using Xcalibur software (version 2.1, Thermo), and the relative quantitative analysis was used to determine the acetylation fraction on individual lysine residues.

Genome-wide Analysis of H3K14ac

To generate genome-wide maps of H3K14ac in HAEC, we performed chromatin immunoprecipitation followed by next-generation sequencing (CHIP-Seq) using previously published method¹⁵². In brief, after chromatin was isolated and cross-linked, the DNA in the chromatin was sheared to an average length of 300-500 bp. Genomic

DNA regions of interest were isolated using antibody against H3K14ac (Active Motif, cat.# 39599). Crosslinks were reversed afterwards and CHIP DNA was purified by phenol-chloroform extraction and ethanol precipitation. Quantitative PCR reactions were carried out in triplicate on specific house-keeping genes before next-generation sequencing (Illumina) was performed. Illumina sequencing libraries were prepared from the CHIP and Input DNAs (without IP) by the standard consecutive enzymatic steps of end-polishing, dA-addition, and adaptor ligation. After a final PCR amplification step, the resulting DNA libraries were quantified and sequenced on NexSeq 500. Sequences (75 nt reads, single end) were aligned to the human genome (hg19) using the BWA algorithm (default settings). Duplicate reads were removed and only uniquely mapped reads (mapping quality ≥ 25) were used for further analysis. Alignments were extended in silico at their 3'-ends to a length of 200 bp, which is the average genomic fragment length in the size-selected library, and assigned to 32-nt bins along the genome. The resulting histograms (genomic "signal maps") were generated. H3K14Ac enriched regions were identified using the SICER algorithm (threshold FDR $1E-10$, gap size 600 bp). Using a cutoff of FDR $1E-20$, significant changed-regions between the control sample and the LPC-treated sample were further identified. Signal maps and peak locations were used as input data to acquire detailed information on sample comparison, peak metrics, peak locations and gene annotations.

Preparation of Nuclear Extracts

HAECs were collected and homogenized in a low-salt buffer [10mM HEPES (pH 7.9), 1.5mM magnesium chloride (MgCl₂), 10mM KCl, 0.2mM PMSF, 0.5M DTT]. The cytoplasmic fraction was removed, and the isolated nuclei were resuspended in a high-salt buffer [20mM HEPES (pH 7.9), 25% glycerol, 1.5mM MgCl₂, 420mM NaCl, 0.2mM EDTA, 0.2mM PMSF, 0.5M DTT] to release soluble proteins. The nuclear protein preparation was then collected and stored at -80°C. Protein concentration was determined by the bovine serum albumin (BCA) assay (Pierce) using BSA as a standard (DTT was added after protein concentration determination).

Electrophoretic Mobility Shift Assay

Transcription factor interactions with DNA response elements were assessed using electrophoretic mobility shift assay (EMSA). AP-1 and NF-κB consensus oligonucleotides end-labeled with IR700 were purchased from LI-COR (Lincoln, Nebraska). The sequences of the probes are as follows: AP-1, 5'-CGCTTGATGACTCAGCCGGAA-3'; and NF-κB, 5'-AGTTGAGGGGACTTTCCCAGGC-3'. EMSA were carried out using an Odyssey Infrared EMSA kit (LI-COR) according to the manufacturer's instructions. 2-5 μg of nuclear extracts were added to each binding reaction. The probe and nuclear proteins were incubated for 20 min at room temperature and DNA-protein complexes were resolved on a 5% non-denaturing polyacrylamide gels afterwards. Images of gel were then obtained in an Odyssey scanner (LI-COR).

Microarray Analysis

RNA of the aorta from five male WT and ApoE^{-/-} mice that were fed a Western diet for 3 weeks starting from 8 weeks-old were isolated with the RNeasy Kit (Qiagen). RNA quantity was determined by the NanoDrop ND-2000 (Thermo Scientific). RNA samples were sent to the Fox Chase Cancer Center Genomic Facility. The RNA integrity was determined by the RNA 28S/18S ratio using the Agilent 2100 Bioanalyzer (Agilent Technologies). Then samples were labeled and hybridized to the Affymetrix Genechip Mouse Gene 2.0ST Arrays following the manufacturer's instructions. Scanned microarray images were analyzed using the Affymetrix Gene Expression Console with Robust Multi-array Average normalization algorithm.

Statistical Analysis

Data were expressed as the mean \pm standard error of the mean (SEM). For comparisons between two groups, two-tailed Student t test was used for evaluation of statistical significance. Comparison across multiple groups, one-way ANOVA was used. *, $p < 0.05$, **, $p < 0.01$, ***, $p < 0.001$.

CHAPTER 3 - RESULTS

Aortic LPC species are induced during early atherogenesis in mice

Multiple lines of evidence indicate that aortic LPC is induced during advanced atherosclerosis development. As early as 1969, it was reported that the concentration of LPC of atherosclerotic aorta from monkeys was nearly 8 times as that of controls¹⁵³. In addition, arterial LPC content from advanced coronary atherosclerosis in diabetic and hypercholesterolemic pigs showed a 300% increase in arterial LPC content²⁴. Furthermore, Different LPC species including palmitoyl-LPC (16:0), stearyl-LPC (18:0), and oleoyl-LPC (18:1) were about 2-times higher in atherosclerotic plaques associated with symptoms than in asymptomatic plaques in human, suggesting that LPC contribute to plaque vulnerability as well³³. However, the answer to the question of whether LPC, which has been indicated not only as a marker but also a major culprit of atherosclerosis development, is induced in the aortas during early atherogenesis remains unknown. To address this issue, we examined the expression of different species of LPC in the aortas of atherosclerotic mouse model ApoE^{-/-} mice. Wild-type (WT) and ApoE^{-/-} mice were fed with high fat diet for 3 weeks, before they were sacrificed and tissues were collected from mice for global, non-targeted metabolomics analysis (Figure 5A). It should be noted that in ApoE^{-/-} mice fed with 3 weeks of high fat diet, plasma cholesterol triples but very minimal plaque develops^{154, 155}. 8 different LPC species were detected in the aortas of WT and ApoE^{-/-} mice (Figure 5B). The most abundantly expressed species in both mice include LPC (16:0), LPC (18:0), and LPC (18:1). Except for LPC (18:2), all

the other LPC species are significantly induced in the aortas of ApoE^{-/-} compared with that of WT mice.

In addition to aorta, we also performed global metabolomics analysis of the expression of LPC species in the plasma, heart, and liver of WT and ApoE^{-/-} mice (Table 3), the results showed that LPC species are differentially expressed among tissues: pentadecanoyl-LPC (15:0) and heptadecanoyl-LPC (17:0) are expressed in heart, liver, and plasma but not in aorta; arachidoyl-LPC (20:0) and eicosadienoyl-LPC (20:2) are only expressed in plasma; docosapentaenoyl-LPC (22:5) is only expressed in heart; and docosahexaenoyl-LPC (22:6) is expressed in aorta and heart. In addition, the distributions of LPC species are similar among tissues except that plasma has high level of linoleoyl-LPC (18:2) expression (Figure 6). More importantly, major LPC species including LPC (16:0), LPC (18:0) are only induced in aorta (Figure 5) but not in the other tissues while LPC (18:1) is induced in aorta, plasma, and heart. Furthermore, only 3 minor LPC species including myristoyl-LPC (14:0) and pentadecanoyl-LPC (15:0) and eicosatrienoyl-LPC (20:3) are induced in liver, with all the major LPC species unchanged.

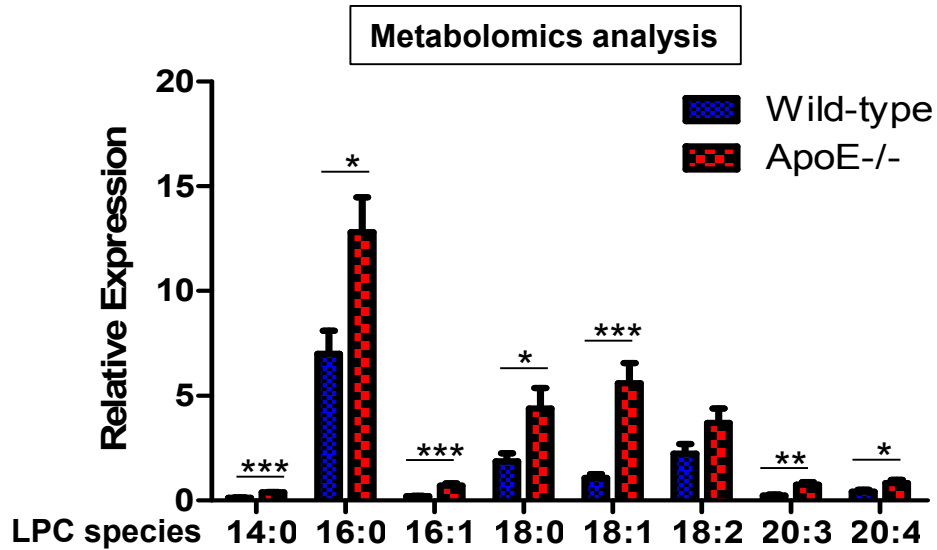
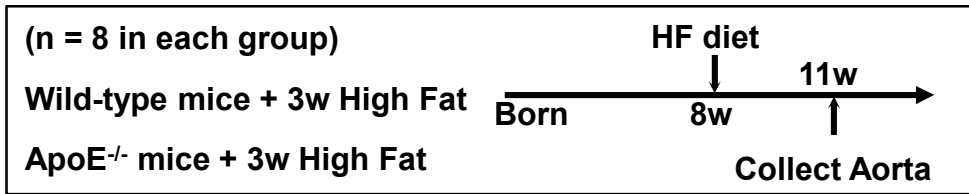


Figure 5. Aortic LPC species are induced during early atherogenesis in mice

A. Experiment design. Wild-type mice (n=8) and ApoE^{-/-} mice (n=8) were fed with high fat (HF) diet for 3 weeks (w) starting from 8 w before they were sacrificed. Aortas from were collected from the mice and metabolomics analysis was performed. B. Relative changes of aortic LPC species between WT and ApoE^{-/-} mice. Data are expressed as mean ± SEM. *, p<0.05, **, p<0.01, ***, p<0.001.

Table 3. Expression differences of LPC species in aorta, heart, liver and plasma between ApoE^{-/-} mice and WT mice.

LPC Species	Aorta		Heart		Liver		Plasma	
	FC	P	FC	P	FC	P	FC	P
14:0	3.08	0.000	3.86	0.000	1.85	0.000	3.46	0.000
15:0	--	--	2.46	0.000	1.44	0.000	4.00	0.000
16:0	1.83	0.012	1.15	0.071	0.78	0.120	0.87	0.079
16:1	3.47	0.001	1.62	0.003	1.27	0.063	2.28	0.000
17:0	--	--	1.36	0.461	0.78	0.191	2.24	0.016
18:0	2.33	0.032	0.96	0.964	1.23	0.582	1.35	0.333
18:1	5.25	0.000	1.87	0.007	1.15	0.473	2.07	0.000
18:2	1.66	0.093	0.96	0.917	0.70	0.059	1.04	0.469
20:0	--	--	--	--	--	--	1.01	0.991
20:2	--	--	--	--	--	--	1.94	0.034
20:3	3.08	0.001	4.07	0.000	2.11	0.008	1.50	0.011
20:4	2.01	0.029	3.08	0.000	1.25	0.094	1.06	0.525
22:5	--	--	2.35	0.000	--	--	--	--
22:6	--	--	--	--	0.84	0.441	0.67	0.007

FC, fold change; P, p value

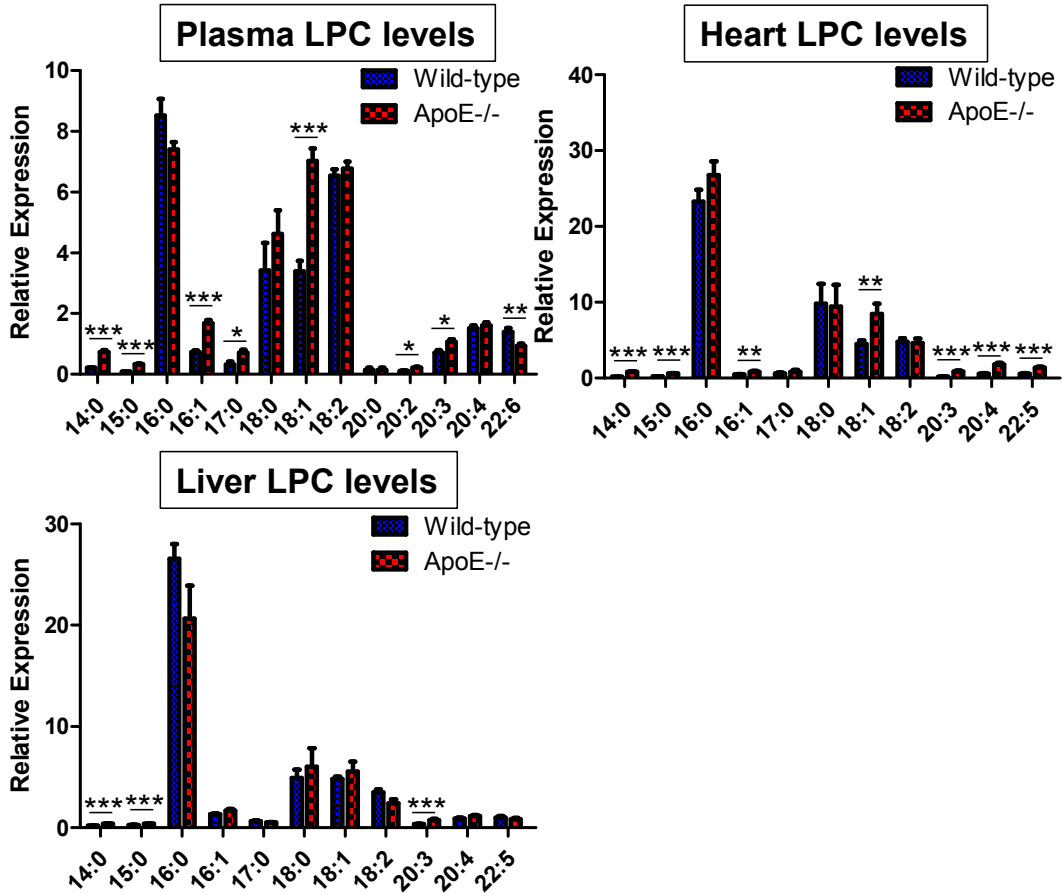


Figure 6. LPC level changes in plasma, heart, and liver between WT and ApoE^{-/-} mice.

Wild-type mice (n=8) and ApoE^{-/-} mice (n=8) were fed with high fat (HF) diet for 3 weeks (w) starting from 8 w before they were sacrificed. Plasma, heart, and liver were collected from the mice and metabolomics analyses were performed. Data are expressed as mean ± SEM. *, p<0.05, **, p<0.01, ***, p<0.001.

LPC induces mtROS in human aortic endothelial cells (HAECs)

Next, we asked whether LPC would induce mtROS in HAEC. Using flow cytometry method with mtROS-specific probe MitoSOX, we found that major LPC species including LPC (16:0), LPC (18:0), and LPC (18:1), which were induced in the aortas of ApoE^{-/-} mice during early atherogenesis, induce mtROS production by 2-fold (Figure 7A). In addition, LPC (16:0) dose-dependently increases mtROS production in HAEC (Figure 7B). Higher concentration of LPC (40μM), however, did not further induce mtROS but becomes cytotoxic as measured by LDH released into the media (Figure 8). We confirmed that MitoSOX did not incorporate with nucleus to give non-specific signals by fluorescence microscopy (Figure 7C). We also used ESR with specific spin probes MitoTEMPO-H/ CP-H to simultaneously examine LPC's effect on mtROS and cytosolic ROS (ctROS) in HAEC¹⁵⁶. The results suggested LPC similarly induced mtROS and ctROS production by 2-fold at 1 hour and lasted for at least 2 hours but decreased at 24 hours (Figure 7D). Wider time phase examination revealed that LPC induced mtROS and ctROS as early as 30 minutes and lasted for at least 6 hours and the time-phase of mtROS and ctROS inductions by LPC matched with each other tightly (Figure 9A). The specificity of the spin probes to dissect mtROS and ctROS was determined using mtROS-inducer Antimycin A (mitochondrial complex III inhibitor) and ctROS-inducer Phorbol myristate acetate (NADPH oxidase and PKC activator). The results showed that Antimycin A (5μM) induced MitoTEMPO-H ESR signal but PMA did not increase it (Figure 9B). Antimycin A and PMA both induced CP-H ESR signal.

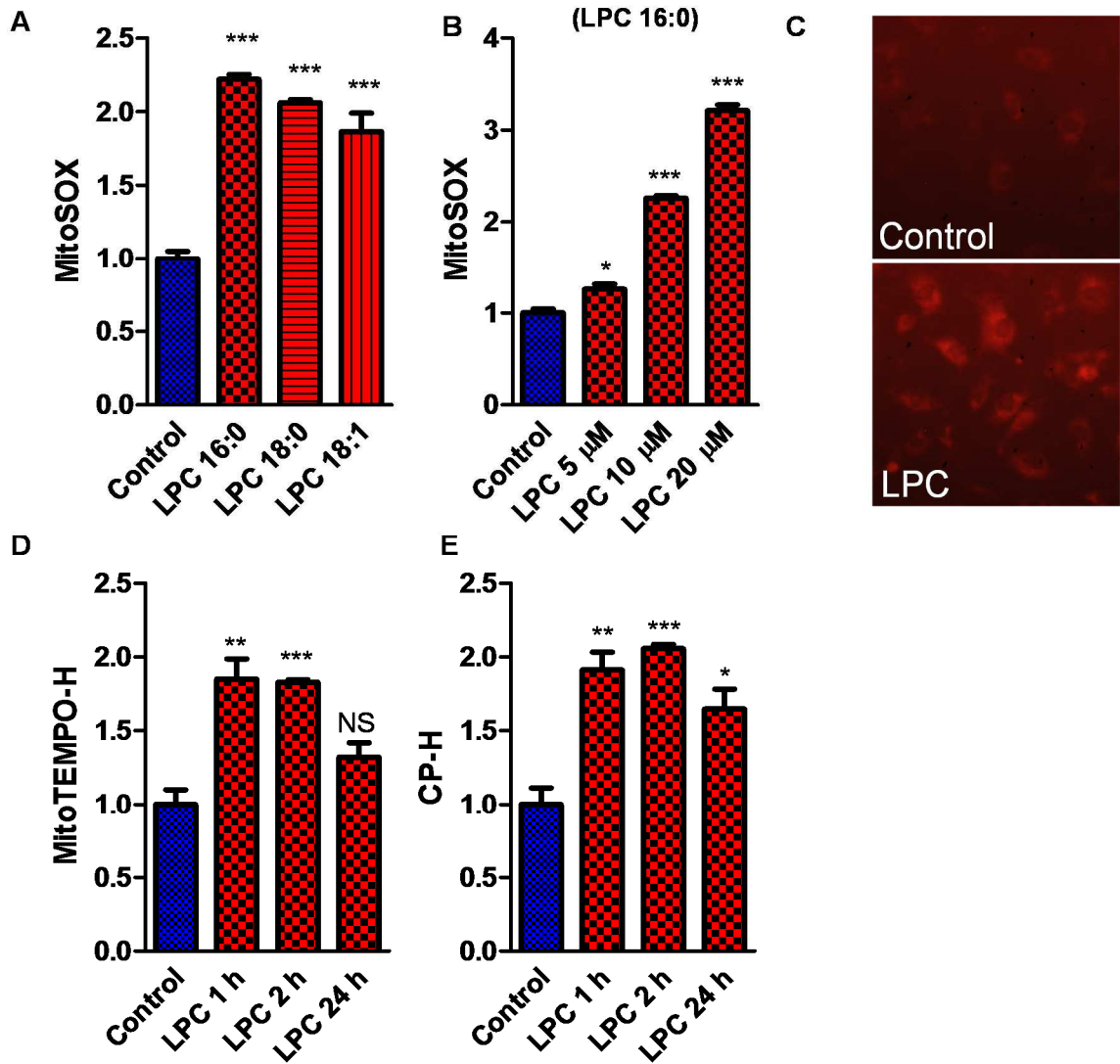


Figure 7. LPC induces mtROS in human aortic endothelial cells (HAECs).

A. After loading with MitoSOX (5 μ M) for 10 min, HAECs were treated with three major LPC species (10 μ M) including LPC (16:0), LPC (18:0), and LPC (18:1) for 1 hour and flow cytometry analysis was performed to quantify mtROS. B. Dose-dependent effects of LPC (16:0) (10 μ M, 1 hour) on mtROS in HAEC measured by MitoSOX using flow cytometry. C. After loading with MitoSOX (5 μ M) for 10 min, HAEC were treated

with LPC (16:0) (10 μ M) for 1 hour and MitoSOX staining was visualized by fluorescence microscopy. D & E. HAECs were treated with LPC (16:0) (10 μ M) for different time points and cell aliquots were incubated with either mitochondrial ROS spin probe MitoTEMPO-H (1mM, D) or cytosolic ROS spin probe CP-H (1mM, E) at 37°C for 20 minutes before electron spin resonance (ESR) analysis. Data are expressed as mean \pm SEM. *, $p < 0.05$, **, $p < 0.01$, ***, $p < 0.001$.

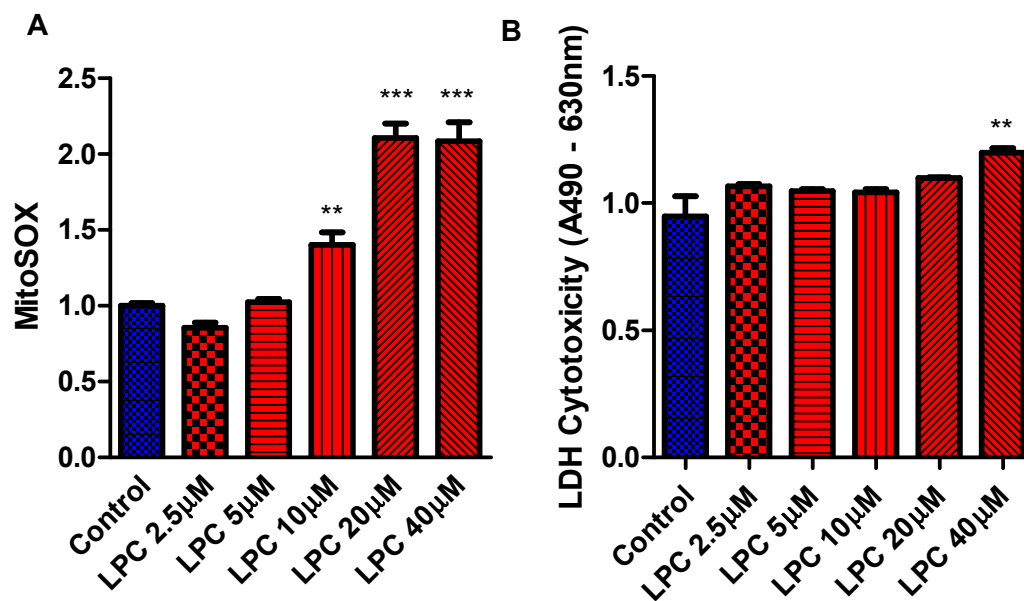


Figure 8. Higher concentration of LPC (40 μ M) does not further increase mtROS but induces cell death in HAECs.

A. After loading with MitoSOX (5 μ M) for 10 min, HAECs were treated with different doses of LPC ranging from 2.5 μ M to 40 μ M for 1 hour before flow cytometry analysis.

B. HAECs were treated with different doses of LPC for 1 hour and cell mediums were collected for the measurement of LDH release as an indicator of cytotoxicity. Data are expressed as mean \pm SEM. **, $p < 0.01$, ***, $p < 0.001$.

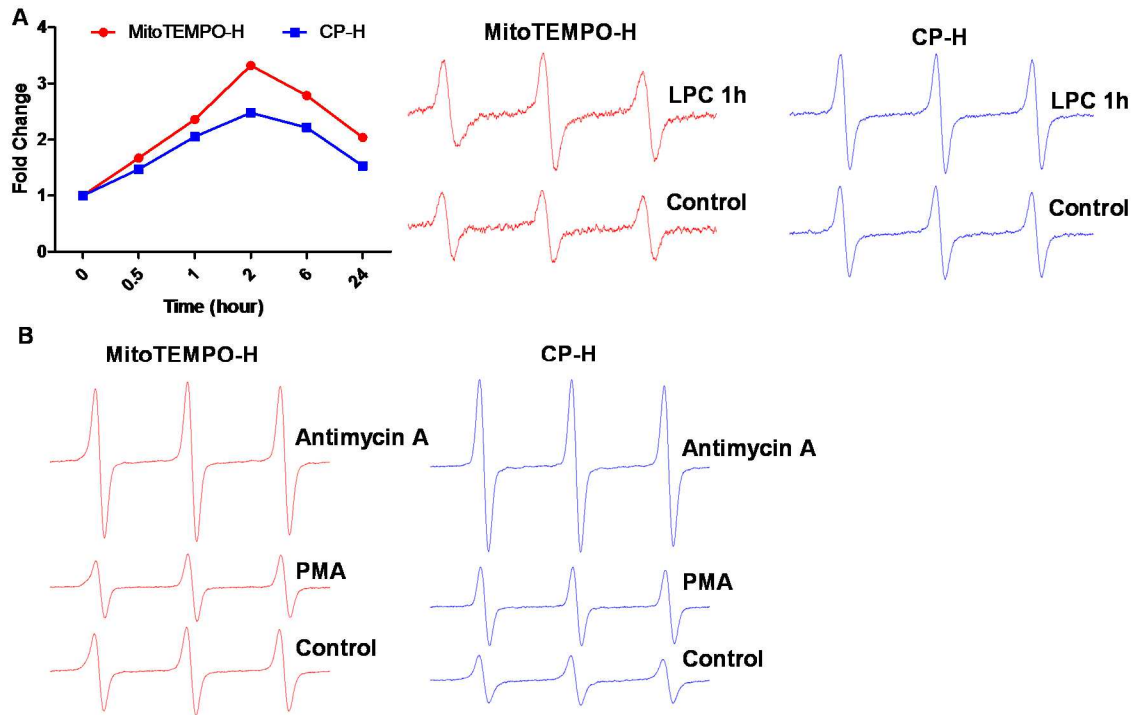


Figure 9. ESR detection of cytosolic and mitochondrial ROS in HAECs.

A. HAECs were treated with LPC (10 μ M) for different times and cell aliquots were incubated with either mitochondrial ROS spin probe MitoTEMPO-H (1mM) or cytosolic ROS spin probe CP-H (1mM) at 37°C for 20 minutes before measurement by ESR (Left). Representative ESR signals were shown in the right. C. HAECs were treated with Antimycin A (5 μ M) and PMA (5 μ M) for 1 hour and cell aliquots were incubated with MitoTEMPO-H (1mM) or CP-H (1mM) before measurement by ESR.

LPC increases mitochondrial respiration in HAEC

MtROS are produced in the ETC of mitochondria at the same time when the cell is synthesizing ATP, and higher respiration rate of mitochondria favors higher mtROS production⁴². As such, we hypothesized that LPC would increase mitochondrial respiration rate in HAEC. We tested this hypothesis using the Seahorse XF96 Analyzer, which can measure 4 different parameters of mitochondria in the cell including basal respiration, maximal respiration, ATP production, and proton leak. We first seeded different densities of HAEC ranging from 5,000 (5K) cells/well to 30K cells/well in 96-well plates to determine cell seeding density for the assay. A linear induction of oxygen consumption rate (OCR) was followed after increasing seeding densities and 30K cells/well was picked for subsequent experiments (Figure 10A). Because different cell types respond differently to $\Delta\psi_m$ uncoupler carbonilcyanide *p*-triflouromethoxyphenylhydrazone (FCCP), FCCP titration experiment was also performed, and FCCP at concentration (1 μ M) which induced maximal mitochondrial respiration was used for subsequent experiment (Figure 10B). OCR was measured every 15 minutes for 1 hour, and LPC gradually induced OCR compared with vehicle-treated cells (Figure 10C). At 1 hour, LPC significantly increased OCR by 20%, compared with 2-fold increase of mtROS in the same condition. 4 parameters of mitochondria were also measured when the XF Mito Stress Test Kit was used after 1 hour basal OCR measurement. It was found that LPC also significantly induced basal respiration, maximal respiration rate, proton leak of mitochondria, and ATP production as well (Figure 10C).

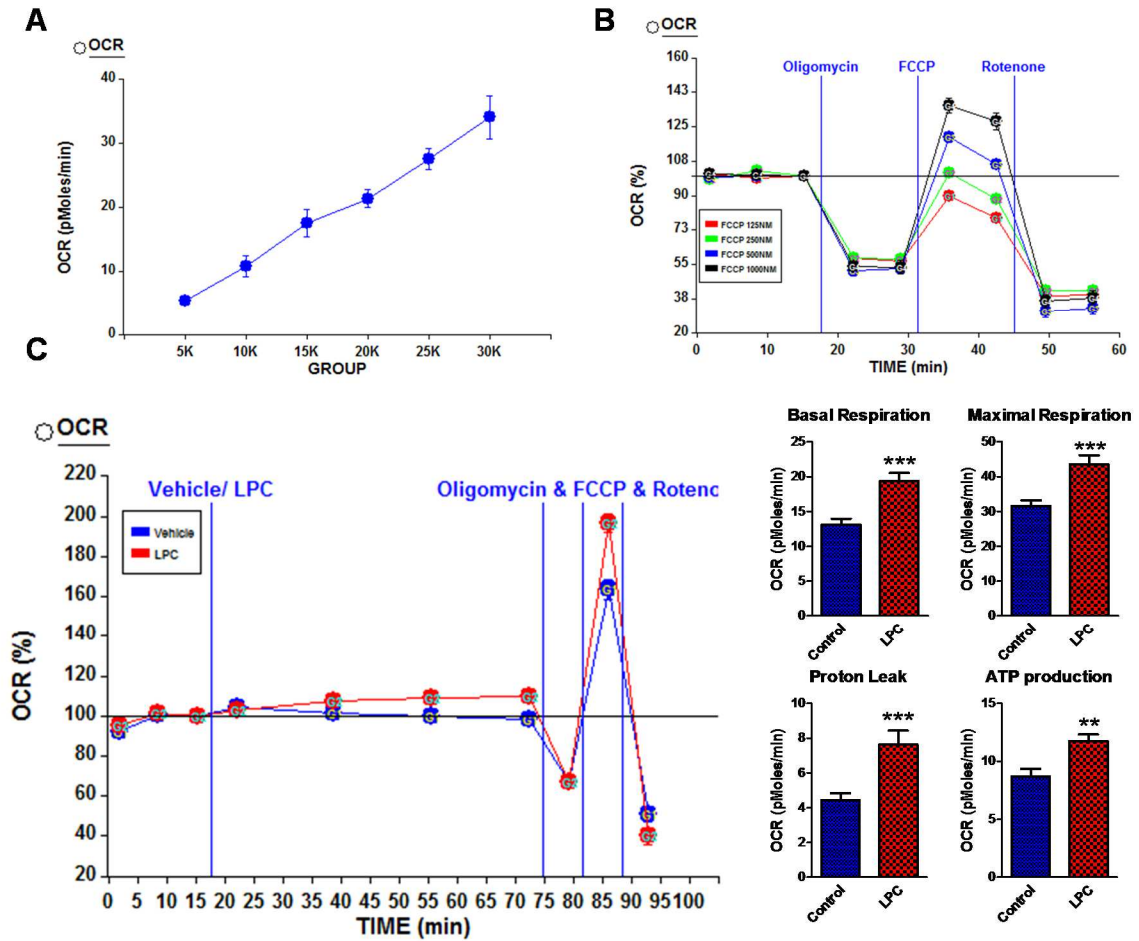


Figure 10. LPC increases mitochondrial respiration in HAEC.

A. Seeding density assay. Varying densities of HAECs from 5,000 cells /well to 30,000 cells /well were seeded into 96-well plate and oxygen consumption rate (OCR) was measured by Seahorse XF96 Analyzer afterwards. B. FCCP titration assay. After three basal measurements of OCR, XF Mito Stress Test (Seahorse Bioscience) was applied by sequential adding of Oligomycin (1 μ M), FCCP, and Rotenone (1 μ M). Different dose of FCCP (125 nM, 250 nM, 500 nM, and 1 μ M) was added in each group. C. HAECs were seeded by 30,000 cells /well into 96-well plate. After three measurements of OCR, LPC (10 μ M) or vehicle control was added to the plate and OCR was measured every 15

minutes for 1h before XF Mito Stress Test was performed by sequential adding of Oligomycin (1 μ M), FCCP (1 μ M), and Rotenone (1 μ M). Quantitation of four different parameters of mitochondria was shown in the right. Data are expressed as mean \pm SEM. **, p<0.01, ***, p<0.001.

Mitochondrial Ca²⁺ entry mediates LPC-induced respiration and mtROS

Previous studies have revealed that LPC can cause an increase in cytosolic Ca²⁺^{157, 158} and Ca²⁺ regulate mtROS production by increasing metabolic rates of mitochondria^{159, 160}. Thus, we hypothesized that LPC-induced Ca²⁺ entry into mitochondria could lead to increased metabolic rates in mitochondria and excessive mtROS production. To test this hypothesis, we first examined the effects of LPC on cytosolic and mitochondrial Ca²⁺ using confocal microscopy. The results showed that LPC dramatically induces cytosolic Ca²⁺ as measured by Fluo-4, which was quickly followed by mitochondrial Ca²⁺ induction afterwards (Figure 11A). The peak response of mitochondrial Ca²⁺ (~6 fold) is higher than that of cytosolic Ca²⁺ (~5 fold) and both signals last at least for 10 minutes. Next we used ruthenium red (RR), which is a mitochondrial calcium uniporter (MCU) inhibitor, and blocks Ca²⁺ entry into the mitochondria, to determine whether LPC-induced Ca²⁺ entry into mitochondria contributes to mtROS production. The results showed that RR significantly inhibited LPC-induced basal respiration as well as maximal respiration, measured by XF96 analyzer (Figure 11B). In addition, RR also completely abolished LPC-induced mtROS production, measured by flow cytometry using MitoSOX (Figure 11C).

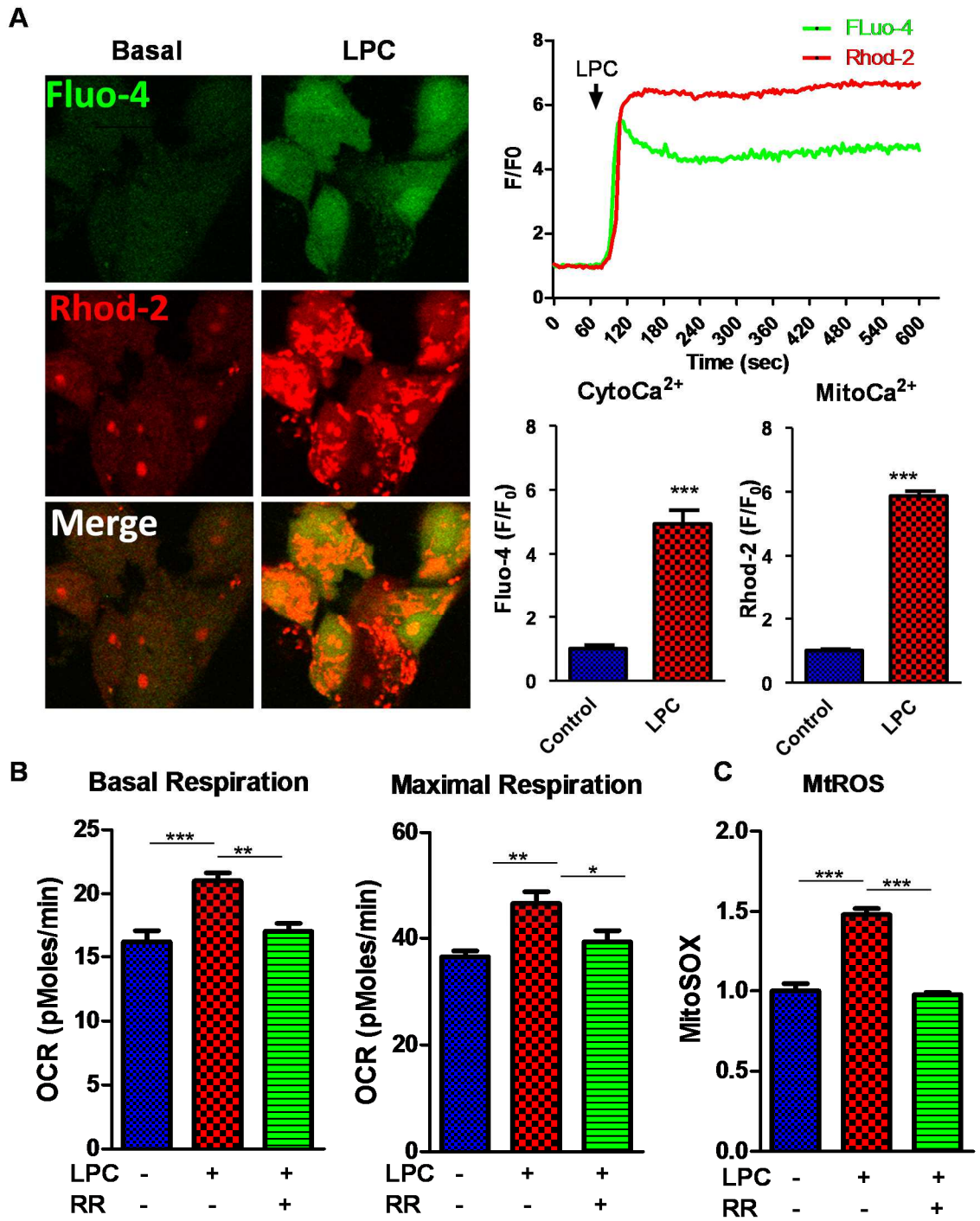


Figure 11. Ca²⁺ mediates LPC-induced respiration and mtROS in HAEC.

A. HAECs loaded with cytosolic Ca^{2+} indicator Fluo-4/AM (green) and mitochondrial Ca^{2+} indicator Rhod-2 (red) were stimulated by 10 μM LPC and analyzed by confocal microscopy. Left, Images were taken before and after the stimulation of LPC; Upper right, real-time tracing of cytosolic and mitochondrial Ca^{2+} mobilization in response to LPC; Lower right, quantitation of peak responses of cytosolic Ca^{2+} (Cyto Ca^{2+}) and mitochondrial Ca^{2+} (Mito Ca^{2+}) uptake. B. HAECs were seeded by 30,000 cells /well into 96-well plate. After three measurements of OCR, vehicle control/ LPC (10 μM)/ LPC (10 μM) plus Ruthenium Red (RR, 10 μM) were added to the plate and OCR was measured every 15 minutes for 1h before XF Mito Stress Test was performed by sequential adding of Oligomycin (1 μM), FCCP (1 μM), and Rotenone (1 μM). Quantitation of basal respiration and maximal respiration was shown. C. After loading with MitoSOX (5 μM) for 10 min, HAECs were treated with vehicle control/ LPC (10 μM)/ LPC (10 μM) plus Ruthenium Red (RR, 10 μM) for 1 hour and flow cytometry analysis was performed. Data are expressed as mean \pm SEM. *, $p < 0.05$, **, $p < 0.01$, ***, $p < 0.001$.

LPC-induced mtROS mediate ICAM-1 upregulation in HAEC

LPC has been shown to induce upregulation of EC adhesion molecule ICAM-1 in HUVEC⁸; and the induction of EC ICAM-1 by LPC in HUVEC can be blocked by general ROS inhibitor diphenyleneiodonium¹⁶. However, the source of ROS in this process remains unknown. As such, we hypothesized that LPC-induced mtROS leads to ICAM-1 upregulation in HAEC. To test this hypothesis, we applied newly-developed specific mtROS inhibitor MitoTEMPO to block mtROS induction and assayed for ICAM-1 expression using RT-PCR and Western blot with specific antibody to ICAM-1. The results showed that LPC (10 μ M) significantly induced both protein and mRNA of ICAM-1, which could be significantly suppressed by co-treatment of mtROS inhibitor MitoTEMPO (1 μ M) (Figure 12).

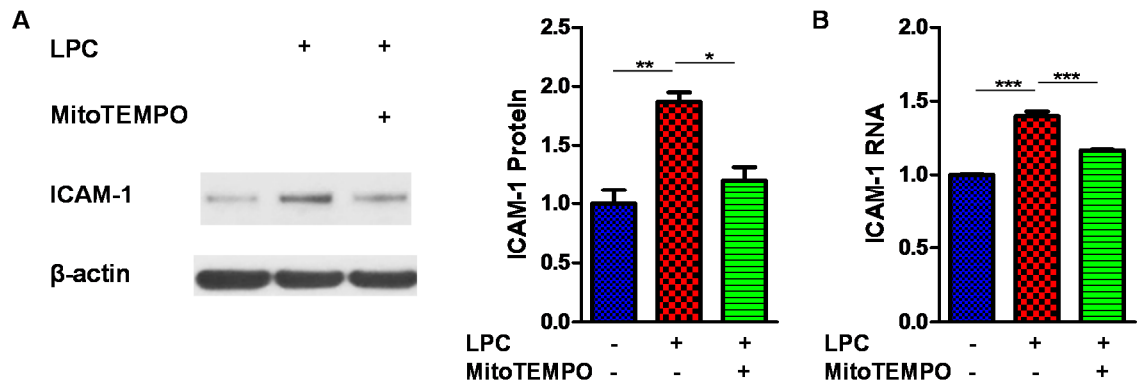


Figure 12. LPC-induced mtROS mediate ICAM-1 upregulation in HAEC.

A. HAECs were treated with LPC (10 μ M) with/without MitoTEMPO (1 μ M) for 18 hours before protein was collected. Representative Western blots were shown in the left. Quantitation of ICAM-1 protein expression normalized by β -actin was shown in the right.

B. HAECs were treated with LPC (10 μ M) with/without MitoTEMPO (1 μ M) for 18 hours before RNA was collected for real-time PCR analysis. Quantitation of ICAM-1 RNA expression normalized by β -actin was shown. Data are expressed as mean \pm SEM.

*, p < 0.05, **, p < 0.01, ***, p < 0.001.

LPC-induced mtROS contribute to EC activation

To explore additional downstream pathways that are targeted by mtROS in EC, we performed the Human EC Biology PCR Array to profile the expression of 84 genes related to EC biology, which are involved in vascular permissibility and vessel tone, angiogenesis, endothelial cell activation and endothelial cell injury. Out of 57 genes detected, we found that 34 genes were induced more than 1.2-fold by LPC after 6-hour treatment (Figure 13). More importantly, 14 out of 34 LPC-induced genes such as ICAM-1, PLAT, IL-6, and MMP2 could be blocked by co-treatment of mtROS inhibitor MitoTEMPO, with ICAM-1 being the most sensitive gene towards MitoTEMPO treatment (Figure 13).

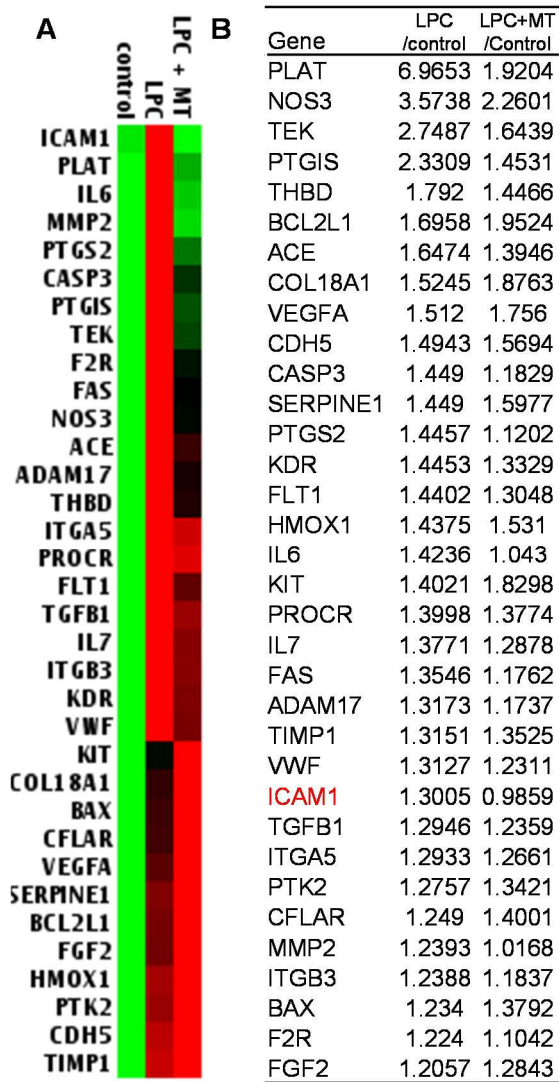


Figure 13. LPC-induced mtROS contribute to EC activation.

HAECs were treated with LPC (10 μ M) with/without MitoTEMPO (1 μ M) for 6 hours and RNA was collected for Human EC Biology PCR array (QIAGEN) analysis. A. Non-supervised hierarchical clustering of genes was used to generate heat map in the left. B. Fold changes of LPC/control and LPC plus MitoTEMPO/ control were shown in the right.

LPC induced-mtROS contribute to histone H3 lysine 14 (H3K14) acetylation

To examine how LPC-induced mtROS lead to EC biology changes, we applied site-specific histone acetylation screening by high-performance liquid chromatography coupled with mass spectrometer (HPLC-MS) method^{150, 151}. We hypothesized that LPC-induced mtROS could upregulate ICAM-1 mRNA by inducing histone H3 acetylation, facilitating transcription factor binding and gene transcription. We screened for 8 different lysine acetylation positions on histone H3 including lysine 9 (K9), K14, K18, K23, K27, K36, K37 and K64 simultaneously. The results showed that LPC specifically induces H3K14 acetylation in HAECs in a dose- and time- dependent manner (Figure 14A) and LPC (10 μ M) for 2h treatment significantly induces H3K14 and to a lesser degree H3K23 acetylation (Figure 14B). The levels of H3K9 and H3K18 stayed the same after LPC treatment, and the levels of K27, K36, K37, and K64 did not reach detection limits and were not plotted. Next, we used newly-developed specific H3K14ac monoclonal antibody that could discriminate acetylated and non-acetylated H3K14ac peptide¹⁶¹ to perform Western blots to confirm the results from HPLC-MS method. The results suggested that LPC (10 μ M) for 2h significantly induces H3K14ac by 2-fold (Figure 14C). ESR was also applied to the same sample aliquots and we found that the induction of mtROS was associated with the increase of H3K14ac (Figure 14C). Furthermore, mtROS inhibitor MitoTEMPO could inhibit LPC-induced H3K14ac (Figure 14D).

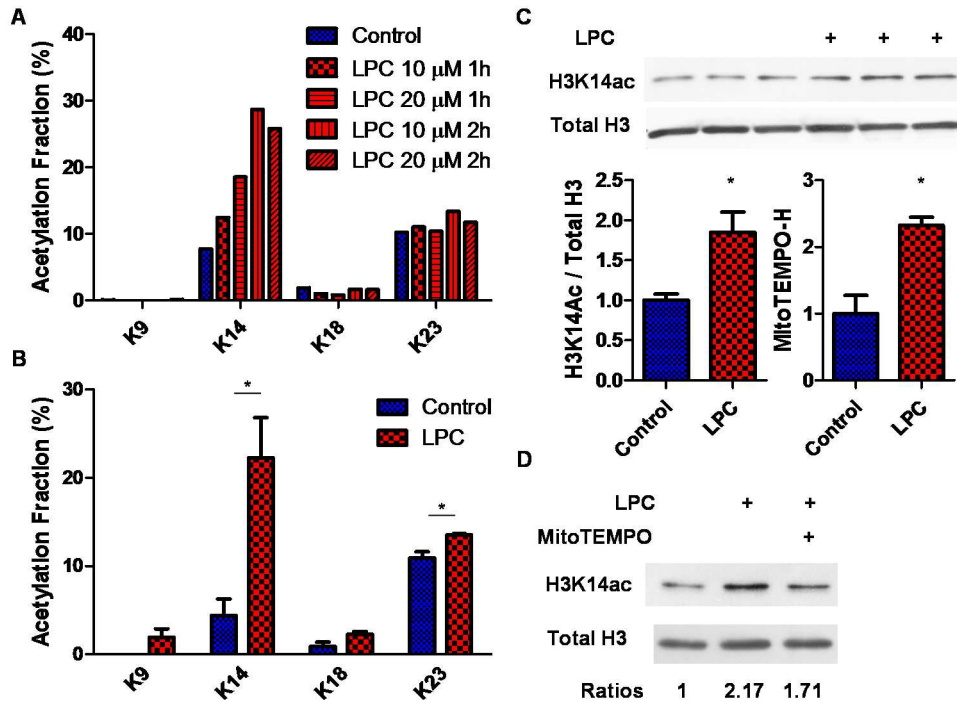


Figure 14. LPC-induced mtROS contribute to H3K14 acetylation.

A. After treatment of HAECs with LPC for different doses (10 μ M /20 μ M) and different time points (1 hour/2 hour), histones were purified using histone purification kit (Active Motif). After propionylation and trypsin digestion, the acetylation fractions on individual lysine residues on histone H3 were measured by HPLC-MS method. B. Statistical analysis of the acetylation fractions on lysine residues of H3 between control and LPC treatment group (10 μ M, 2 hours). C. HAECs were treated with LPC (10 μ M) for 2 hours and protein was collected for Western blot analysis (up and lower left). Aliquots from the same samples were also used to measure mtROS by ESR (lower right). D. HAECs were treated with LPC (10 μ M) or LPC (10 μ M) plus MitoTEMPO-H (1 μ M) for 2 hours and protein was collected for Western blot analysis. Data are expressed as mean \pm SEM. *, p<0.05.

LPC-induced H3K14ac contribute to ICAM-1 upregulation

To link LPC-induced H3K14ac to ICAM-1 upregulation, we performed genome-wide analysis for significantly increased H3K14ac bound DNA regions across human genome in HAEC by CHIP-sequencing (CHIP-seq). We hypothesized that LPC would induce H3K14ac binding in the promoter region of ICAM-1. We had three groups of cells in the immunoprecipitation experiment with anti-acetylated histone 3 lysine 14: vehicle-treated HAEC, LPC (10 μ M, 2 hour)-treated HAEC, and input (HAEC without immunoprecipitation). Each group of cells was pooled from 5 individual assay dishes to avoid potential intra-group differences between dishes. We found that when compared with input group, vehicle-treated HAEC has a significant H3K14ac-enriched region in the promoter region of ICAM-1 (SICER algorithm, threshold FDR 1E-10, gap size 600bp) (Blue bars in Figure 15A). When compared LPC-treated HAEC with vehicle-treated HAEC, LPC-treated HAEC has a significant higher H3K14ac-enriched region which is both wider and higher in the promoter region of ICAM-1 (threshold FDR 1E-20) (Red bars in Figure 15A). In addition, when HAT inhibitor curcumin (which blocks histone acetylation) was applied, the induction of ICAM-1 by LPC was abolished (Figure 15B).

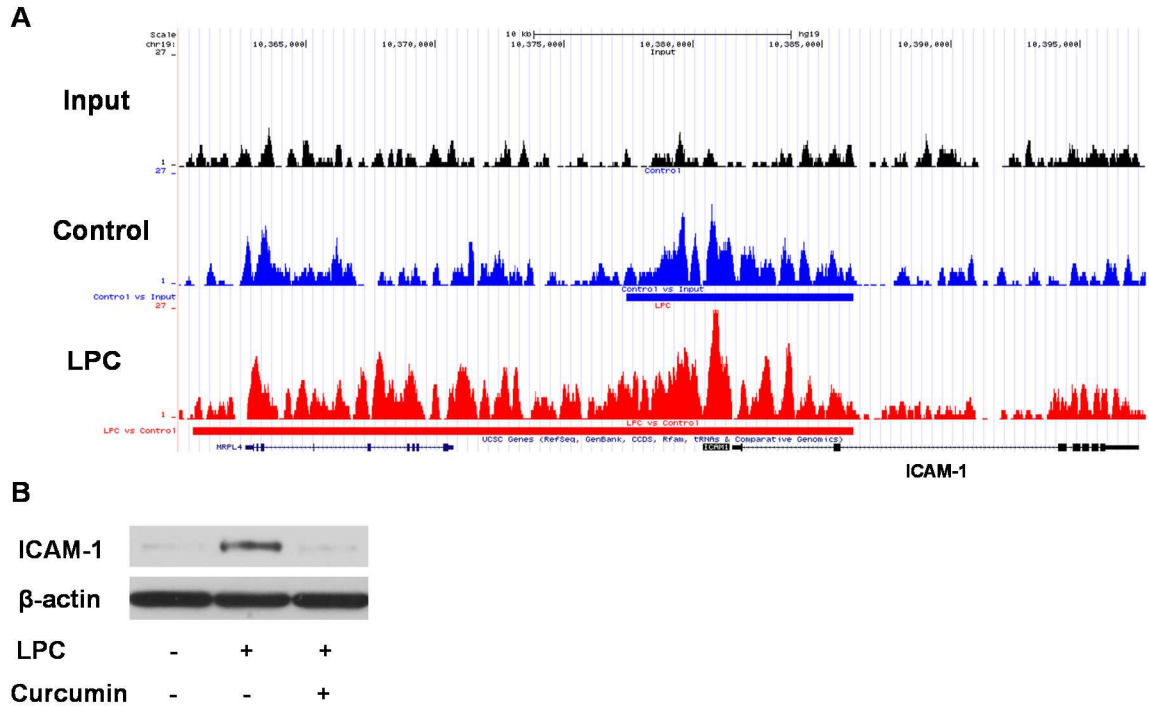


Figure 15. LPC-induced H3K14ac contribute to ICAM-1 upregulation.

A. Chip-Seq of H3K14ac in HAEC. After treatment of vehicle or LPC (10 μ M) for 2 hours, chromatin was collected, cross-linked, and sheared. Immunoprecipitation of H3K14ac was performed afterwards and the resulting co-immunoprecipitated DNA regions were purified, sequenced, and aligned to human genome (hg19). Unprecipitated chromatin sample was used for input control. Data were visualized using UCSC genome browser. Blue bars indicate significant difference between control and input, red bars indicate significant difference between LPC and control. Pooled samples in each group (n=5). B. HAECs were pre-incubated with Curcumin (10 μ M) for 1 hour and treated with LPC (10 μ M) for 2 hours and protein was collected for Western blot analysis.

LPC-induced H3K14ac contribute to EC biology changes

To explore additional genes which are regulated by LPC-induced H3K14ac, we analyzed genome-wide binding of H3K14ac in HAEC with or without LPC treatment. Using the SICER algorithm at a cutoff of $FDR 1E-10$ and a Gap parameter of 600 bp (which merges peaks located within 600 bp of each other into a single “island”), the number of H3K14ac peaks was 24,346 for the vehicle-treated sample and 31,014 for the LPC-treated sample. To identify the regions with the most significant changes in H3K14ac bound DNA enrichments, SICER was also run by comparing LPC-treated vs. vehicle-treated sample and vice versa (SICER-df). Using a cutoff of $FDR 1E-20$, SICER-df identified 2,146 regions with significant up-regulation in the control sample (located in 1330 NCBI Genes with Intervals within -10,000 base pairs (bp)/+10,000 bp), and 6,034 regions with up-regulation in the LPC-treated sample (located in 6412 NCBI Genes with Intervals within -10,000 bp/+10,000 bp) (Table 4). In addition, vehicle-treated sample has high correlation with LPC-treated sample, with more read numbers of peaks in the LPC-treated sample (slope) (Figure 16A). Furthermore, after LPC treatment, genome-binding of H3K14ac shifts from intergenic regions and introns towards the regulatory regions for gene transcription such as enhancers and promoter regions (Figure 16B).

Next, we cross-examined the genome-wide association of H3K14ac with the human EC biology PCR array data (Figure 13). Out of 34 genes which were induced more than 1.2-fold by LPC, 11 genes such as NOS3, PTGIS, ACE, COL18A1, and

VEGFA had increased H3K14ac binding after LPC treatment. By contrast, out of 23 genes which were induced less-than 1.2 fold or reduced by LPC, only one gene SPHK1 had increased H3K14ac binding after LPC treatment (Figure 17).

Table 4. Summary of H3K14ac Chip-Seq in HAEC.

SAMPLE	Control	LPC	LPC-decreased	LPC-increased
NUMBER OF PEAKS	24,346	31,014	2,146	6,034
DIST PROM (1-3 kb)	6,160	7,113	359	2,211
PROX PROM (0-1 kb)	7,614	8,263	391	2,270
GENEBODY	17,628	21,876	1,426	4,781
5'-UTR	7,576	8,236	382	2,155
EXON	10,120	13,745	733	4,150
INTRON	16,568	20,819	1,389	4,649
3'-UTR	2,926	5,558	188	2,523
PROX DOWNSTR (0-1 kb)	2,785	5,164	165	2,453
DIST DOWNSTR (1-3 kb)	3,062	5,383	156	2,429
DIST INTERGENIC	8,580	12,314	904	2,743
CpGI +/-200 bp	8,254	10,832	285	3,391
SIMPLE REPEATS	16,667	22,726	1,597	5,558

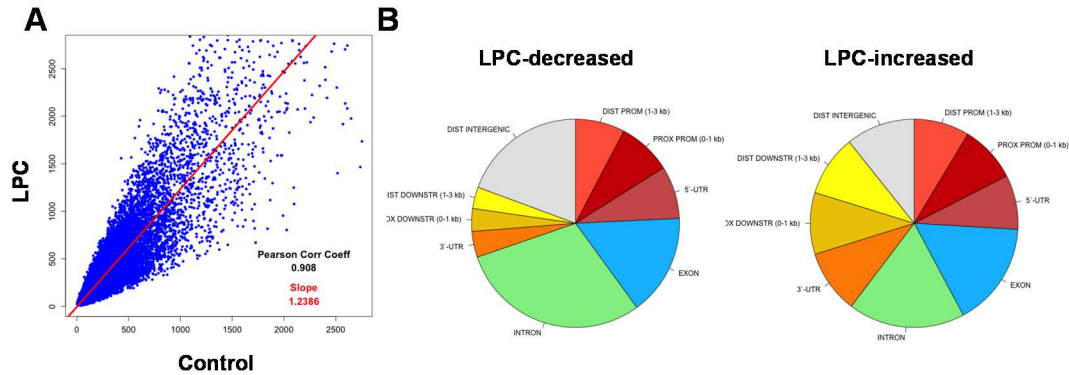


Figure 16. LPC increases H3K14ac peak lengths and shifts H3K14ac binding locations in the genome.

A. After treatment of vehicle or LPC (10 μ M) for 2 hours, chromatin was collected, cross-linked, and sheared. Immunoprecipitation of H3K14ac was performed afterwards and the resulting co-immunoprecipitated DNA regions were purified, sequenced, and aligned to human genome (hg19). Unprecipitated chromatin sample was used for input control. Scatter plot shows the tags (read numbers in peaks) between vehicle-treated group and LPC-treated group. B. Genomic locations of LPC-decreased and LPC-increased H3K14ac signals. Pooled samples in each group (n=5).

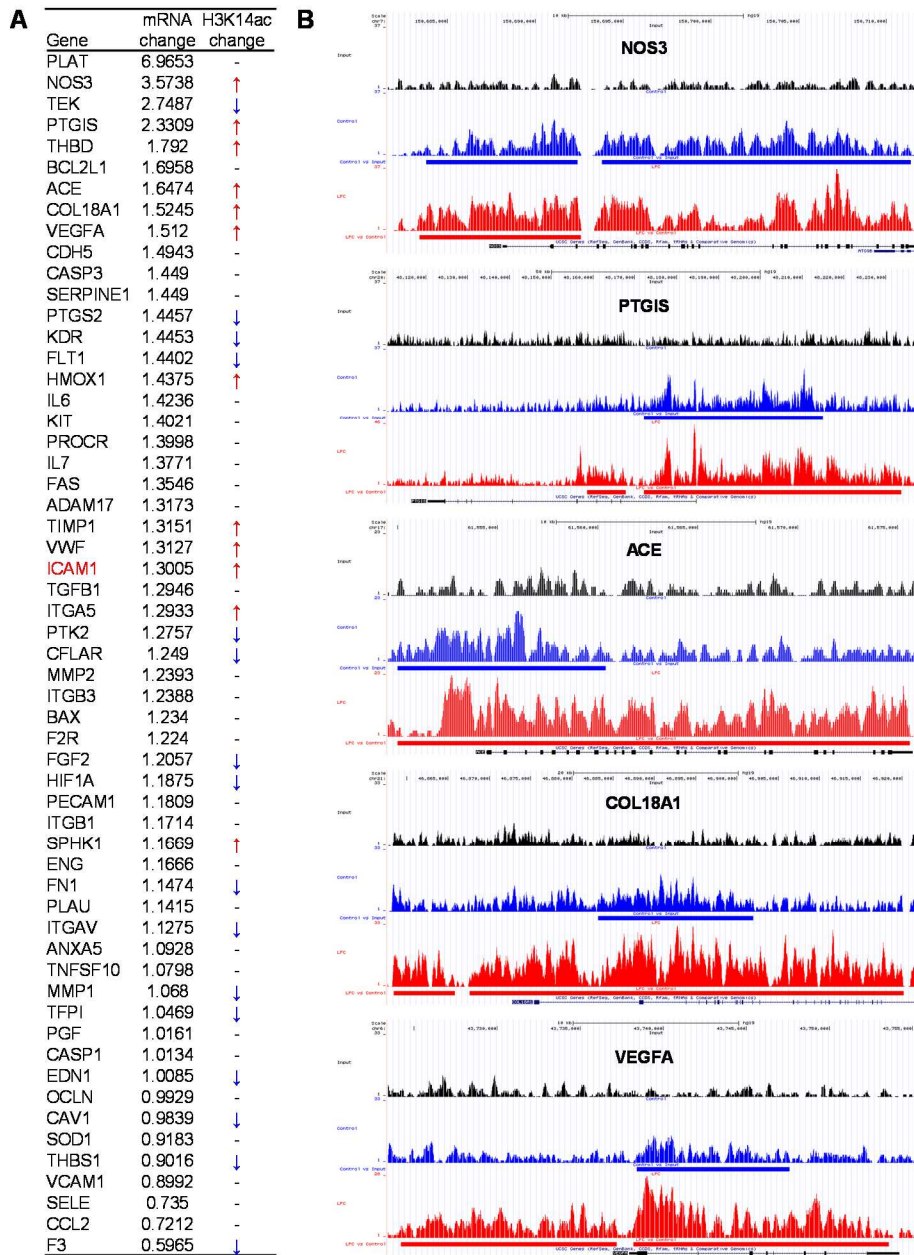


Figure 17. LPC-induced H3K14ac contribute to EC biology changes.

After treatment of vehicle or LPC (10 μ M) for 2 hours, chromatin was collected, cross-linked, and sheared. Immunoprecipitation of H3K14ac was performed afterwards and the resulting co-immunoprecipitated DNA regions were purified, sequenced, and aligned to

human genome (hg19). Unprecipitated chromatin sample was used for input control. A. Correlation between the human biology PCR array (Figure 13) and the CHIP-Seq data (Figure 15). B. Data were visualized using UCSC genome browser. Blue bars indicate significant difference between control and input. Red bars indicate significant difference between LPC and control. Pooled samples in each group (n=5).

LPC-induced mtROS and histone acetylation contribute to AP-1 nuclear translocation

Putative transcription factor binding sites of NFκB and AP-1 have been identified in the promoter region of ICAM-1¹⁶². In addition, LPC was shown to increase nuclear translocation of NFκB and AP-1 in HUVEC^{37, 38}. Thus, we hypothesized that LPC-induced mtROS and H3K14ac mediate nuclear bindings of pro-inflammatory transcription factors to the target gene promoters, which contributes to ICAM-1 upregulation. Using electrophoretic mobility shift assay (EMSA), we showed that LPC induced nuclear translocation of AP-1 and NFκB to a lesser degree as published before. Importantly, MitoTEMPO almost completely abolished LPC-induced AP-1 nuclear binding but did not affect NFκB nuclear translocation (Figure 18A). Moreover, HAT inhibitor Curcumin which blocks histone acetylation not only blocked LPC-induced AP-1 nuclear binding but also reversed basal AP-1 nuclear activity (Figure 18B).

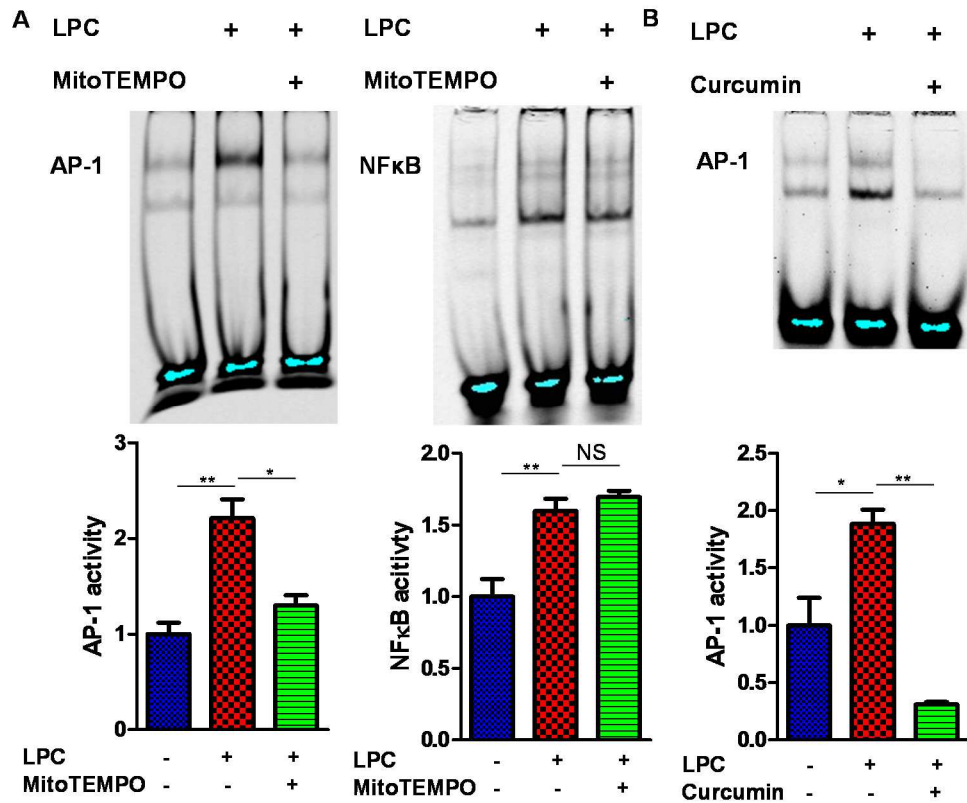


Figure 18. LPC-induced mtROS and histone acetylation contribute to AP-1 binding.

Electrophoretic mobility shift assay (EMSA) was performed using Odyssey Infrared EMSA Kit (LI-COR). A. HAECs were treated with vehicle or LPC (10 μ M) for 1 hour with or without MitoTEMPO (1 μ M) pre-incubation for 1 hour, nuclear proteins were collected afterwards. 2 μ g nuclear proteins were used for AP-1 EMSA and 5 μ g nuclear proteins were used for NF κ B EMSA. B. HAECs were treated with vehicle or LPC (10 μ M) for 1 hour with or without Curcumin (10 μ M) pre-incubation for 1 hour, 2 μ g nuclear protein were used for AP-1 EMSA. Data are expressed as mean \pm SEM. *, $p < 0.05$, **, $p < 0.01$.

Anti-inflammatory cytokines IL-35 and IL-10 suppress LPC-induced ICAM-1 upregulation by inhibiting mtROS-H3K14ac-AP-1 pathway

Lastly, we hypothesized that IL-35, as a newly identified anti-inflammatory cytokine, could inhibit ICAM-1 upregulation by inhibiting mtROS-H3K14ac-AP-1 pathway. We compared the effect of IL-35 with classic anti-inflammatory cytokine IL-10 together. The results showed that IL-35 and IL-10 both abolished LPC-induced upregulation of ICAM-1 in HAEC (Figure 19A). In addition, IL-35 and IL-10 both abolished LPC-induced mtROS generation in HAEC measured by flow cytometry method (Figure 19B). Moreover, IL-35 and IL-10 also suppressed LPC-induced H3K14ac (Figure 19C) and nuclear binding of AP-1 in HAEC (Figure 19D).

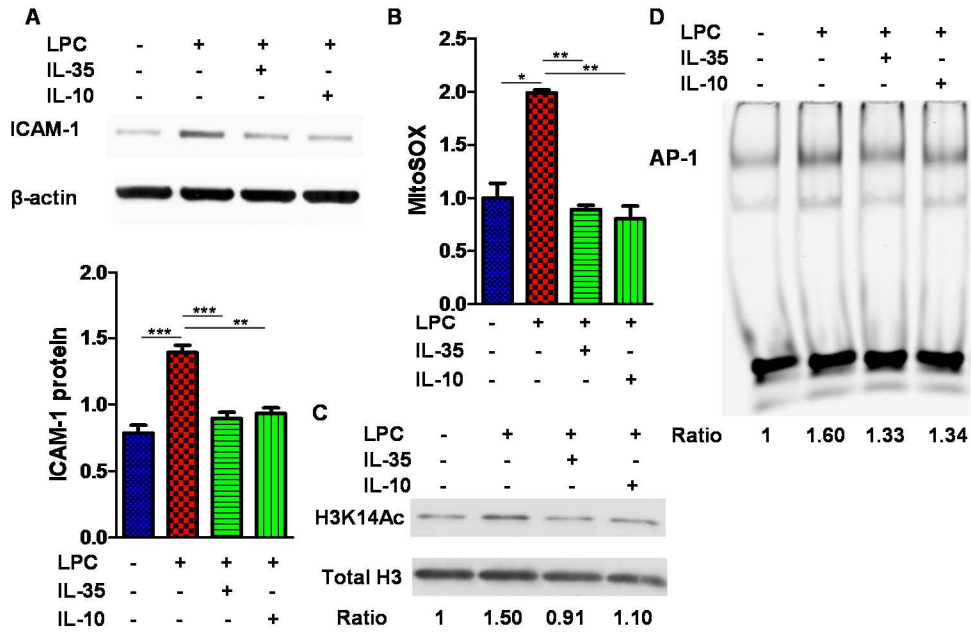


Figure 19. Anti-inflammatory cytokines IL-35 and IL-10 suppress LPC-induced ICAM-1 upregulation by inhibiting mtROS-H3K14ac-AP-1 pathway.

A. HAECs were treated with LPC (10 μ M) with/without IL-10 (10ng/mL) or IL-35 (10ng/mL) preincubation for 18 hours. Representative Western blots were shown in the upper panel. Quantitation of ICAM-1 protein expression normalized by β -actin was shown in the lower panel. B. After loading with MitoSOX (5 μ M) for 10 min, HAEC were treated with LPC (10 μ M) with or without co-treatment of IL-10 (10ng/mL) or IL-35 (10ng/mL) for 1 hour and flow cytometry analysis was performed afterwards. C&D. HAECs were treated with LPC (10 μ M) with/without IL-10 (10ng/mL) or IL-35 (10ng/mL) preincubation for 2 hours. Western blot from total proteins (C) and EMSA of AP-1 from nuclear proteins (D) were performed. Data are expressed as mean \pm SEM. *, $p < 0.05$, **, $p < 0.01$, ***, $p < 0.001$.

IL-35 suppresses LPC-induced EC activation

To explore additional genes that are inhibited by IL-35, we performed PCR Array in HAECs. Out of 84 EC biology-related genes, we found that 19 genes were induced more than 1.2-fold by LPC after 18-hour treatment (Figure 20A). Interestingly, EC activation markers including E-selectin (SELE), ICAM-1, and VCAM-1 were among the top induced genes by 18-hour LPC treatment (Figure 20B). In addition, 9 genes including PLAT, ICAM-1, TIMP1, SERPINE1, VEGFA, IL-7, TEK, THBD, and CDH5 were both induced more than 1.2-fold by LPC after 6-hour or 18-hour treatment. Furthermore, out of the 19 genes induced by LPC, IL-35 selectively inhibited the induction of 6 genes including PLAT, VCAM-1, IL1B, ICAM-1, VEGFA, and IL-7.

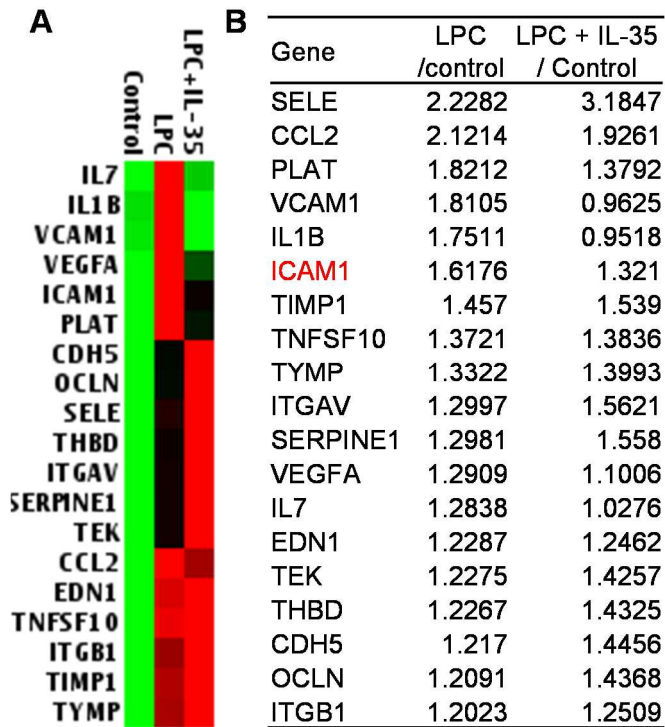


Figure 20. IL-35 suppresses LPC-induced EC activation.

HAECs were treated with LPC (10 μ M) for 6 hours with/without IL-35 (10 ng/mL) preincubation for 1 hour and RNA was collected for Human EC Biology PCR array analysis (QIAGEN). A. Non-supervised hierarchical clustering of genes was used to generate heat map. B. Fold changes of LPC/control and LPC plus IL-35/ control were shown in the right.

CHAPTER 4 - DISCUSSION

LPC-induced EC activation is considered as the initiation step of atherogenesis. Although Ca^{2+} and ROS have been indicated to be required for this process, the mechanisms underlying those cellular signal events and mechanistic links between them remain not well defined. Besides, the effect of novel anti-inflammatory cytokine IL-35 in regulating endothelial cell activation is not known. To address these issues, our current study utilized a wide spectrum of highly sophisticated state-of-the-art techniques including non-targeted metabolomics profiling to screen for metabolites changes during early atherogenesis in ApoE^{-/-} mice, FACS analysis using novel mtROS probe MitoSOX, ESR analysis using specific spin probes to detect mitochondrial and cytosol ROS simultaneously in the ECs, confocal microscopy to measure cellular mitochondrial and cytosolic Ca^{2+} , HPLC-MS -based method to measure acetylation in different lysine residues of histones, and CHIP-seq to study genome-wide association of histone acetylation in the LPC-activated ECs. We have made the following new findings: 1) Different LPC species including LPC (16:0), LPC (18:0), and LPC (18:1) were significantly induced in the aortas of mice during early atherogenesis; 2) Different LPC species including LPC (16:0), LPC (18:0), and LPC (18:1) all significantly induced mtROS after 1 hour treatment in HAECs; 3) LPC (16:0) dose-dependently and time-dependently induced mtROS after 1 hour treatment in HAECs; 4) Higher levels of LPC did not further increase mtROS production but led to significant cell death in HAEC; 5) LPC-induced mtROS happened as early as 30 minutes, which lasted for at least 6 hours. The induction of mtROS by LPC matched closely with the induction of cytosolic ROS.

6) 1 hour treatment of LPC increased both basal /maximal respiration in the mitochondria of HAEC, which are indications of increased electron transport chain activity in the mitochondria; 7) LPC significantly increased Ca^{2+} in the cytosol which was followed quickly by increased Ca^{2+} signal in the mitochondria in HAEC. Both the induction of cytosolic and mitochondrial Ca^{2+} lasted for at least 10 minutes; 8) Mitochondrial calcium uniporter inhibitor Ruthenium Red significantly abolished both LPC-induced basal or maximal respiration in the mitochondria and LPC-induced mtROS in HAEC; 9) Specific mtROS inhibitor MitoTEMPO significantly blocked LPC-induced ICAM-1 after 18 hours both in protein and mRNA level; 10) MitoTEMPO blocked LPC-induced upregulation of 14 EC biology related genes; 11) LPC dose-dependently and time-dependently increased H3K14ac but not H3K9ac, H3K23ac in HAEC. The induction of H3K14ac by 2-hour treatment of LPC was also confirmed by Western blot using novel monoclonal antibody against H3K14ac; 12) LPC-induced mtROS correlated with LPC-induced H3K14ac in the same samples and mtROS inhibitor mitoTEMPO suppressed LPC-induced H3K14ac; 13) HAEC had a significant basal H3K14ac-enriched region in the promoter of ICAM-1 compared with input sample. After LPC treatment for 2 hour, the H3K14ac-enriched region in the promoter of ICAM-1 was both significantly higher and wider than that of non-treated controls. In addition, HAT inhibitor Curcumin inhibited LPC-induced ICAM-1 upregulation; 14) 2-hour treatment of LPC significantly induced H3K14ac binding around 6412 genes and decreased H3K14ac binding around 1330 genes after genome-wide analysis of H3K14ac signals in HAEC; 15) LPC-induced H3K14ac associated with the induction of 11 gene expressions

related to EC biology; 16) MtROS inhibitor MitoTEMPO significantly blocked LPC-induced nuclear translocation of proinflammatory transcription factor AP-1 but not NF κ B after 1 hour. The induction of AP-1 nuclear binding by LPC could also be significantly blocked by HAT inhibitor Curcumin; 17) Novel anti-inflammatory cytokine IL-35 and classic anti-inflammatory cytokine IL-10 both significantly abolished LPC-induced ICAM-1 upregulation in HAEC. Mechanistically, IL-35 and IL-10 significantly blocked LPC-induced mtROS generation and suppressed LPC-induced H3K14ac and AP-1 nuclear binding in HAEC.

Atherosclerosis is a chronic inflammatory pathogenic process of the large and middle size artery wall, which leads to CVDs. CVDs are the number one cause of death in the United States. ROS have long been recognized as a major culprit in the development of atherosclerosis which has led to the enthusiastic use of antioxidants in the treatment of the disease. However, the results of randomized clinical trials of Vitamin C and Vitamin E have been disappointing. One possible explanation of such failure is our incomplete understanding in the roles of different sources of ROS in atherosclerosis. This study addressed the issue of the role of mitochondrial ROS in LPC-induced EC activation which is the initiation step of atherogenesis.

The proposed work is significant as it will greatly improve our understanding in the roles of mtROS in atherosclerosis which may lead to the development of mitochondria-targeting antioxidant in combating cardiovascular diseases. In fact, only a

small proportion of currently known antioxidants are actually accumulated in the mitochondria which might explain their failure in the treatment of the diseases.

Major LPC species are induced in the aortas of mice during early atherogenesis

To demonstrate the pathophysiological relevance of LPC, we first examined the expression profiles of LPC species in four major tissues of atherosclerotic ApoE^{-/-} mice compared with WT mice during early atherogenesis. The mice were fed with high fat diet for 3 weeks and at this time of age, very minimal lesions could be detect in the *en face* of aortas and early lesions just started to buildup in the aortic root of ApoE^{-/-} mice as we previously reported¹⁵⁴ (and unpublished data from Dr. Virtue in our lab). In addition, as defined by Ross' laboratory in ApoE^{-/-} mice¹⁵⁵, significant monocyte recruitment into ApoE^{-/-} mouse aorta does not happen until 6 weeks after HF diet. Thus, our mouse model is ideal for the examination hyperlipidemia-induced EC activation, an initiative step of early atherogenesis. We utilized a global, non-targeted metabolomics to screen for the changes of more than 500 metabolites, which has low molecular weight (50-1500Da) including LPC (~500 Da) during early atherogenesis. This type of method is particularly ideal for the analysis of LPC species since LPC is generated post-translational due to the enzymatic activity of enzyme activities. Conventional approaches including PCR and Western blot analysis thus cannot detect LPC. We examined four tissues including aorta, heart, plasma, and liver, which are key organs that participate in the pathogenic process of atherosclerosis. We found that when compared with that of WT mice, almost all the 8 LPC species detected in the aorta except for LPC (18:2) were

significantly induced in ApoE^{-/-} mice. By contrast, fewer percentage of LPC species were induced in the plasma, heart, and liver of ApoE^{-/-}, with only 3 minor LPC species induced in the liver. In addition, major LPC species including (16:0) and (18:0) were only induced in the aortas of ApoE^{-/-} mice but not in the 3 other tissues. These results pointed to a key role of LPC in the aorta of mice during early atherogenesis. Furthermore, LPC species are differentially expressed in tissues and some LPC species are only expressed in one of the four tissues examined, hinting specific biological roles of these LPC species in different tissues.

Our results correlated with previous findings, which reported increased aortic LPC expression in the aortas of atherosclerotic monkey, pig, and human^{24, 33, 153}. In addition, one of these studies also reported that LPC is strikingly induced in the aorta but not much in the plasma of atherosclerotic monkeys. However, all these studies studied in the advanced stage of atherosclerosis development, which complicate the interpretation of whether LPC is simply a marker or indeed is a causal factor in atherosclerosis. In contrast, our study examined the global changes of metabolites including LPC during early atherogenesis. The results clearly demonstrated that the induction of aortic LPC is an early event in the initiation of early atherosclerosis.

LPC induces mtROS in HAEC

Next, we studied the effects of LPC in EC activation, which initiates atherosclerosis development. Firstly, we examined the effects of LPC on mtROS in HAEC. Mitochondria contributes to early atherosclerosis development as it has been

shown that mtDNA damage not only correlated with the extent of atherosclerosis in human specimens and aortas from ApoE^{-/-} mice but also preceded atherogenesis in young ApoE^{-/-} mice. In addition, ApoE^{-/-} compound mice deficient in SOD2 (a mitochondrial antioxidant enzyme), displayed accelerated atherogenesis¹⁰⁵. Furthermore, endothelial-specific overexpression of Trx2, another mitochondrial antioxidant enzyme, improved endothelial function and reduced atherosclerosis development in ApoE^{-/-} mice⁵⁷. As such, we hypothesized that LPC could contribute to early atherosclerosis development by inducing mtROS in HAEC. We utilized 3 different methods that are complimentary to each other. We used mtROS probe MitoSOX combined with FACS analysis to study mtROS in HAEC which analyzes every single cell and gates off any debris or dead cells before providing the final data. However, measuring mtROS by detecting MitoSOX using flow cytometry has two potential drawbacks: 1) prolonged or high dose incubation of MitoSOX may incorporate nonspecifically to the nucleus to give erratic readings; 2) The reactions of MitoSOX with ROS yield two fluorescent products, one of which is superoxide specific, while the other is formed in response to general oxidative stress. HPLC methodologies are thus required to separate and identify these products^{78, 163}. We addressed the first issue by combining the use of MitoSOX with fluorescence microscopy and showed that MitoSOX did not incorporate with nucleus after 10-minute loading of 5 μ M of MitoSOX. We addressed the second issue by using ESR combined with novel mtROS spin probe MitoTEMPO-H, which specifically detects superoxide in the mitochondria. ESR also has a second advantage in that application of different spin probes allows us to localize and distinguish mtROS versus cytosolic

ROS. However, the sensitivity of ESR assay is lower than that of methods based on fluorescence. The specific principles and advantages/disadvantages of these different methods to detect mtROS have been thoroughly discussed in our review article⁴².

We found that three major LPC species including LPC (16:0), LPC (18:1), LPC (18:2), which were induced in the aortas of ApoE^{-/-} mice during early atherogenesis, all induced mtROS by 2-fold after 1 hour treatment of LPC, suggesting that the ability to induce mtROS is a common characteristic of different LPC species. We used the most abundantly expressed species LPC (16:0) in the studies afterwards, and showed that LPC at 5, 10, and 20 μ M dose-dependently increased mtROS in HAEC. However, we did not detect higher induction of mtROS by 40 μ M LPC stimulation than that of 20 μ M LPC treatment but significant cell death was observed instead. Thus, cell death induced by LPC may not be the result of increased mtROS but other pathways but other pathways may be involved. We further demonstrated that induction of mtROS by LPC is an early event, as it is induced as early as 30 minutes and persisted for at least 6 hours but decreased after 24-hour treatment. This result suggested that the induction of mtROS by LPC was not due to gene expression changes related to mitochondrial ETC or antioxidant enzymes. Instead, it should be due to the effect of cell signal mediator(s) which act promptly in the cell. Furthermore, we also demonstrated that cytosolic ROS were induced side-by-side with mtROS. Previous studies also implicated ROS generated by NADPH-oxidase in the cell also contributed to EC biology changes. To rule out the possibility that the induction of mtROS is the result of ROS generated by NADPH oxidase, we used specific NADPH-oxidase inhibitor VAS-2870 and found that inhibition

of NADPH oxidase did not suppress LPC-induced mtROS production but rather increased it (Data not shown). Thus, LPC-induced mtROS are not the result of NADPH oxidase activity.

Our result is supported by a previous study reporting similar findings¹⁵⁸. It was found that LPC induces mtROS in HUVECs using MitoSOX combined with fluorescence microscopy. In addition, they reported partial co-localization between mitochondria and ROS using ROS indicator DCFH-DA by confocal microscopy. Our study expanded on these findings and showed that the induction of mtROS is a common feature of LPC species family. We also examined the time-dependent and dose-dependent effects of LPC.

LPC-induced mtROS is mediated by Ca²⁺-regulated respiration increase

MtROS are generated in the ETC of mitochondria during mitochondrial respiration as a result of leakage of electrons from ETC complexes. Higher rates of mitochondrial respiration favor higher production of mtROS. For this reason, we measured mitochondrial respiration rate in HAEC using Seahorse XF96 Analyzer. The Seahorse XF96 Analyzer measures OCR in the cells. When different mitochondrial inhibitors and uncouplers are applied, four parameters of the mitochondria including basal respiration, maximal respiration, ATP production, and proton leak can be measured. Each cell type has different basal respiration rate and responds differently to the chemical uncoupler FCCP, so we performed pre-experiment to determine the optimal cell seeding density and titrate the concentration of FCCP. Our results demonstrated that OCR

increased linearly as cell seeding density increased and that FCCP dose-dependently increased the maximal respiration in HAEC. We picked the cell seeding density (30K) that gave the highest basal OCR and the FCCP concentration that induced maximal respiration for our studies afterwards. We found that LPC gradually increased OCR, and that higher dose of LPC accelerated this process (data not shown). At 1 hour, LPC significantly increased OCR by 20% while LPC increased mtROS by 2-fold at the same time. Thus, a higher percentage of oxygen consumption is converted to mtROS after LPC treatment. In addition, other parameters including maximal respiration, ATP production, and proton leakage were also significantly induced after 1 hour treatment. These results suggested that LPC accelerated the overall activity of ETC, which led to higher mtROS production in HAEC.

Ca^{2+} is an accelerator of ETC activity as it allosterically activates several key enzymes involved in the TCA cycle including isocitrate dehydrogenase, α -ketoglutarate dehydrogenase, and pyruvate dehydrogenase. Ca^{2+} also stimulates the ATP synthase which facilitate the transfer of electrons in the ETC. The net effect of TCA cycle activation by Ca^{2+} is a boost of supply of reducing equivalents NADH and FADH which donate electrons to ETC and cause higher mitochondrial respiration¹⁵⁹. Thus, we hypothesized that LPC would induce Ca^{2+} entry into mitochondria, which mediates the acceleration of mitochondrial respiration and mtROS production. To address this hypothesis, we measured cytosolic and mitochondrial Ca^{2+} simultaneously using confocal microscopy. As published before^{149, 160}, our method using confocal microscopy image clearly demonstrate the separation of cytosolic and mitochondrial Ca^{2+} stainings in the

cell. We found that LPC quickly induced the induction of cytosolic Ca^{2+} , which is promptly followed by the induction of mitochondrial Ca^{2+} , both of which persisted at least 10 minutes. Furthermore, we found that MCU inhibitor Ruthenium Red completely abolished LPC-induced basal/maximal respiration and mtROS induction in HAEC. These data suggested that LPC firstly induces cytosolic Ca^{2+} , which subsequently enters into mitochondria through MCU and mediate the induction of mitochondrial respiration, leading to mtROS increase at last.

Previous studies reported similar findings between Ca^{2+} signaling and mtROS in ECs^{158, 160}. It was found that thrombin-induced mtROS is channeled by Ca^{2+} evoked by G protein receptor-coupled signaling. Controversies still exist on what is the real LPC receptor in the cell, but different studies agreed on that LPC stimulates cytosolic Ca^{2+} in different cell types²⁷. Indeed, our study linking Ca^{2+} and mtROS is reinforced by one previous study, which reported similar findings that LPC-induced ROS in HUVEC is channeled through cytosolic Ca^{2+} induction. They have shown that LPC-induced cytosolic Ca^{2+} is from an extracellular source; and that different Ca^{2+} inhibitors including Ruthenium Red, EGTA, and BAPTA all significantly suppressed LPC-induced ROS in HUVEC. Our study expanded on these study and showed that mitochondrial Ca^{2+} followed quickly after cytosolic Ca^{2+} by LPC treatment and found that LPC-induced mtROS is channeled through Ca^{2+} entry into mitochondria. We further proved that LPC-induced Ca^{2+} acts to induce mtROS by increasing mitochondrial respiration rates in HAEC.

LPC-induced mtROS leads to ICAM-1 upregulation by H3K14ac-AP-1 pathway

Next, we examined the downstream effects of LPC-induced mtROS. Using EC biology array, we screened for the changes of 84 genes related to EC biology after LPC-treatment in HAEC. We found that among the 34 genes that were induced by LPC, ICAM-1 expression was decreased the most after the co-treatment of mtROS inhibitor MitoTEMPO. We further confirmed that MitoTEMPO significantly blocked LPC-induced ICAM-1 expression at both protein and mRNA levels, which suggested that LPC-induced mtROS lead to ICAM-1 induction at the transcription levels.

Next, we examined the underlying mechanisms of how LPC-induced mtROS transcriptionally increase ICAM-1 expression. It was recently discovered that mtROS contribute to inflammatory cytokine production by activation of inflammasomes (IL-1 β production)³⁹, mitogen-activated protein kinases pathway (MAPK) (IL-6 production)⁴⁰ and nuclear factor of activated T cells (NFAT) (IL-2 production)⁴¹. We generated a novel hypothesis that LPC-induced mtROS might transcriptionally upregulate ICAM-1 and other EC biology -related genes by reorganizing the chromatin architecture in EC. To address this novel hypothesis, we firstly utilized HPLC-MS-based method to screen for site-specific histone acetylation changes in HAEC after LPC-treatment and found that LPC selectively induced H3K14ac in HAEC. Histone acetylation is regulated by different enzymes, which work either by themselves or cooperatively to acetylate specific site(s) on histones. However, such “histone codes” still remain not fully understood and

we speculate that LPC acts to regulate H3K14ac by regulating the activity of either certain HAT or HDAC enzyme(s). Regardless, we found that LPC significantly induced both H3K14ac and mtROS in the same sample aliquots and also found that mtROS inhibitor MitoTEMPO inhibited LPC-induced H3K14ac. Thus, LPC-induced mtROS contribute to H3K14ac.

To examine whether LPC-induced H3K14ac contribute to EC biology changes and ICAM-1 upregulation, we performed genome-wide association of H3K14ac in HAEC by CHIP-Seq. CHIP-Seq is a recently developed method based on next generation sequencing, which is ideal to examine the binding of transcription factors or histone modifications in a genome-wide level. To our knowledge, we are the first group to examine histone acetylation changes during EC activation although this has been examined intensively during T cell activation. We found that after 2-hour LPC treatment, around 6000 genes had significant increased H3K14ac binding events around them and around 1000 genes had significant decreased H3K14ac binding events around them. In addition, we found that 11 genes out of the 34 LPC-induced genes related to EC biology including ICAM-1 had significant increased H3K14ac binding events around these genes. We also showed that HAT inhibitor Curcumin pretreatment completely wiped out the induction of ICAM-1 by LPC. Since specific H3K14ac inhibitor is not available right now, the use of nonspecific HAT inhibitor Curcumin serves as a proof of principle to demonstrate that histone acetylation event is required for LPC-induced ICAM-1 expression. Next, we hypothesized that LPC-induced H3K14ac allows for specific transcription factor to bind on the opened promoter region and regulate the expression of

ICAM-1. We performed EMSA to study the nuclear binding of NFκB and AP-1 which are putative proinflammatory transcription factors that regulate ICAM-1 expression. We found that LPC significantly induced AP-1 and to a lesser extent NFκB nuclear translocation. In addition, mtROS inhibitor MitoTEMPO significantly inhibited LPC-induced AP-1 upregulation. Furthermore, HAT inhibitor Curcumin also significantly blocked LPC-induced AP-1 upregulation. These results indicated that LPC-induced mtROS and H3K14ac contribute to the nuclear binding of AP-1 on the promoter of ICAM-1.

Previous studies showed that LPC induced ICAM-1 upregulation and monocyte adhesion in HUVEC⁸. The induction of EC adhesion molecules by LPC can be blocked by general ROS inhibitor diphenyleneiodonium³⁴ (DPI) and intracellular calcium inhibitor BAPTA¹⁶. One study also found that LPC-induced mtROS contribute to MAPK signal pathway, which is the upper signaling of AP-1¹⁵⁸. Our study connected these separate dots and suggested that mtROS mediate LPC-induced ICAM-1 upregulation by firstly increasing H3K14ac, which facilitates the opening of chromatin regions in the promoter of ICAM-1 and binding of AP-1 to transcriptionally induce the upregulation of ICAM-1.

IL-35 and IL-10 suppress LPC-induced ICAM-1 by inhibiting mtROS

Lastly, we examined the effects of novel anti-inflammatory cytokines IL-35 and IL-10 on LPC-induced EC activation. Classic anti-inflammatory cytokines including IL-10 and TGF-β has been shown to inhibit EC activation and atherosclerosis development.

However, the effect of newly discovered cytokine IL-35 in EC activation remains unknown. Thus, we examined the effects of IL-35 in LPC-induced EC activation. We found that IL-35 and IL-10 both significantly inhibited the expression of ICAM-1 by inhibiting mtROS production, as they also significantly abolished LPC-induced mtROS in HAEC. In addition, IL-35 and IL-10 also suppressed the induction of H3K14ac and AP-1 nuclear binding. We concluded that these two cytokines inhibited LPC-induced ICAM-1 by inhibiting mtROS-H3K14ac-AP-1 pathway. The striking similarity between the two cytokines could be explained by their shared signaling pathways. Although IL-35 and IL-10 engage with different set of receptors, they can both activate STAT3, which has recently been found to modulate mtROS through mechanisms independent of its nuclear factor activity, but dependent on its ability to localize into mitochondria and modulate the activity of the ETC⁷³. However, the molecular mechanism, by which STAT3 modulates ETC activity, is not currently well understood. We further explored the additional effects of IL-35 in LPC-induced EC biology changes. We found that IL-35 selectively inhibited the induction of 6 genes including PLAT, VCAM-1, interleukin 1 β (IL1B), ICAM-1, VEGFA, and IL-7.

Our results for the first time demonstrated that two endogenous cytokines IL-35 and IL-10 can suppress EC activation by inhibiting mtROS. As mtROS has recently been shown to contribute to inflammatory cytokine production and innate immune responses in macrophages and T cells³⁹⁻⁴¹, it would be interesting to examine whether these two cytokines could similarly inhibit mtROS in these immune cells.

Summary and Future Directions

To summarize, our study demonstrated that LPC is induced in the aortas of mice during early atherogenesis. In addition, LPC induces mtROS, which is mediated by Ca^{2+} -stimulation of mitochondrial respiration increase. LPC-induced mtROS further led to ICAM-1 upregulation by increasing H3K14ac, thus facilitating the nuclear translocation of AP-1 and ICAM-1 transcription. Furthermore, anti-inflammatory cytokines IL-35 and IL-10 can suppress LPC-induced EC activation by inhibiting mtROS-H3K14ac-AP-1 pathway (Figure 21).

There are several future directions to pursue. Firstly, it could be examined that whether mtROS mediate hyperlipidemia-induced EC activation *in vivo* using ApoE^{-/-} mice. Specifically, it could be determined that whether hyperlipidemia induces excessive mtROS in comparison with cytosolic ROS in the aortas of ApoE^{-/-} mice using ESR method. In addition, it could be studied that whether hyperlipidemia induces excessive mtROS in aortic EC using confocal microscopy method. Furthermore, it could be determined whether mtROS scavenger MitoTEMPO can suppress EC activation and lesion formation in ApoE^{-/-} mice. Secondly, the molecular mechanism linking LPC-induced mtROS and H3K14ac could be examined by determining whether LPC-induced mtROS regulate certain histone modification enzymes. Thirdly, the underlying mechanism of IL-35 suppression of mtROS could be examined by investigating whether IL-35 induces STAT3 in HAEC; and whether STAT3 “talks” to the mitochondria to suppress mtROS production.

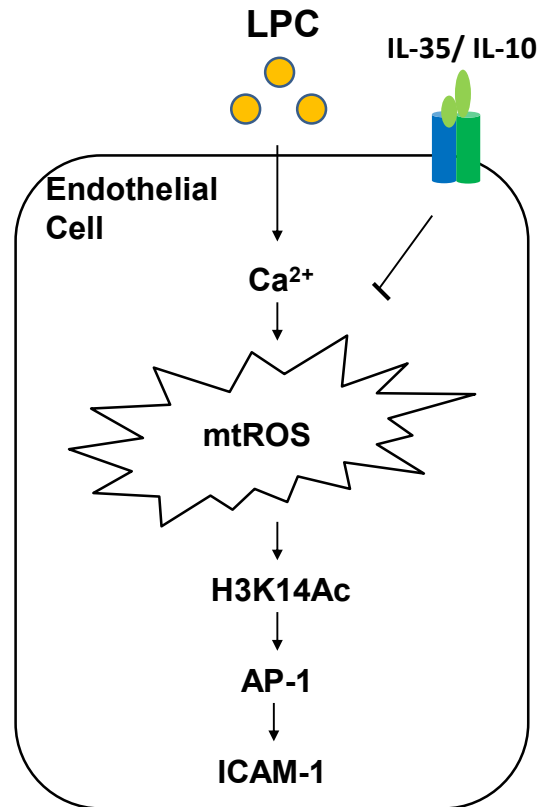


Figure 21. Working Model

LPC induces mtROS production through Ca^{2+} -regulated respiration increase in HAEC. LPC-induced mtROS mediate ICAM-1 upregulation by H3K14ac-AP-1 pathway. Anti-inflammatory cytokines IL-35 and IL-10 can suppress LPC-induced ICAM-1 upregulation by inhibiting mtROS.

REFERENCES CITED

1. Mozaffarian D, Benjamin EJ, Go AS, Arnett DK, Blaha MJ, Cushman M, de Ferranti S, Despres JP, Fullerton HJ, Howard VJ, Huffman MD, Judd SE, Kissela BM, Lackland DT, Lichtman JH, Lisabeth LD, Liu S, Mackey RH, Matchar DB, McGuire DK, Mohler ER, 3rd, Moy CS, Muntner P, Mussolino ME, Nasir K, Neumar RW, Nichol G, Palaniappan L, Pandey DK, Reeves MJ, Rodriguez CJ, Sorlie PD, Stein J, Towfighi A, Turan TN, Virani SS, Willey JZ, Woo D, Yeh RW, Turner MB. Heart disease and stroke statistics-2015 update: A report from the american heart association. *Circulation*. 2015;131:e29-e322
2. WHO. Global status report on noncommunicable diseases 2010. 2011
3. Nakashima Y, Chen YX, Kinukawa N, Sueishi K. Distributions of diffuse intimal thickening in human arteries: Preferential expression in atherosclerosis-prone arteries from an early age. *Virchows Arch*. 2002;441:279-288
4. Strong JP, Malcom GT, McMahan CA, Tracy RE, Newman WP, 3rd, Herderick EE, Cornhill JF. Prevalence and extent of atherosclerosis in adolescents and young adults: Implications for prevention from the pathobiological determinants of atherosclerosis in youth study. *Jama*. 1999;281:727-735
5. Libby P, Ridker PM, Hansson GK. Progress and challenges in translating the biology of atherosclerosis. *Nature*. 2011;473:317-325
6. Ross R. Atherosclerosis--an inflammatory disease. *The New England journal of medicine*. 1999;340:115-126
7. Hansson GK, Hermansson A. The immune system in atherosclerosis. *Nature immunology*. 2011;12:204-212
8. Kume N, Cybulsky MI, Gimbrone MA, Jr. Lysophosphatidylcholine, a component of atherogenic lipoproteins, induces mononuclear leukocyte adhesion molecules in cultured human and rabbit arterial endothelial cells. *The Journal of clinical investigation*. 1992;90:1138-1144
9. Smith JD, Trogan E, Ginsberg M, Grigaux C, Tian J, Miyata M. Decreased atherosclerosis in mice deficient in both macrophage colony-stimulating factor

(op) and apolipoprotein e. *Proceedings of the National Academy of Sciences of the United States of America*. 1995;92:8264-8268

10. Pastrana JL, Sha X, Virtue A, Mai J, Cueto R, Lee IA, Wang H, Yang XF. Regulatory t cells and atherosclerosis. *Journal of clinical & experimental cardiology*. 2012;2012:2
11. Mai J, Wang H, Yang XF. Th 17 cells interplay with foxp3+ tregs in regulation of inflammation and autoimmunity. *Front Biosci (Landmark Ed)*. 2010;15:986-1006
12. Watson AD, Leitinger N, Navab M, Faull KF, Horkko S, Witztum JL, Palinski W, Schwenke D, Salomon RG, Sha W, Subbanagounder G, Fogelman AM, Berliner JA. Structural identification by mass spectrometry of oxidized phospholipids in minimally oxidized low density lipoprotein that induce monocyte/endothelial interactions and evidence for their presence in vivo. *The Journal of biological chemistry*. 1997;272:13597-13607
13. Lee H, Shi W, Tontonoz P, Wang S, Subbanagounder G, Hedrick CC, Hama S, Borromeo C, Evans RM, Berliner JA, Nagy L. Role for peroxisome proliferator-activated receptor alpha in oxidized phospholipid-induced synthesis of monocyte chemotactic protein-1 and interleukin-8 by endothelial cells. *Circulation research*. 2000;87:516-521
14. Gharavi NM, Alva JA, Mouillesseaux KP, Lai C, Yeh M, Yeung W, Johnson J, Szeto WL, Hong L, Fishbein M, Wei L, Pfeffer LM, Berliner JA. Role of the jak/stat pathway in the regulation of interleukin-8 transcription by oxidized phospholipids in vitro and in atherosclerosis in vivo. *The Journal of biological chemistry*. 2007;282:31460-31468
15. Gargalovic PS, Gharavi NM, Clark MJ, Pagnon J, Yang WP, He A, Truong A, Baruch-Oren T, Berliner JA, Kirchgessner TG, Lusis AJ. The unfolded protein response is an important regulator of inflammatory genes in endothelial cells. *Arteriosclerosis, thrombosis, and vascular biology*. 2006;26:2490-2496
16. Erdogan A, Schaefer MB, Kuhlmann CR, Most A, Hartmann M, Mayer K, Renner FC, Schaefer C, Abdallah Y, Hoelschermann H, Schaefer CA. Activation of ca²⁺-activated potassium channels is involved in lysophosphatidylcholine-induced monocyte adhesion to endothelial cells. *Atherosclerosis*. 2007;190:100-105

17. Zhou Z, Subramanian P, Sevilmis G, Globke B, Soehnlein O, Karshovska E, Megens R, Heyll K, Chun J, Saulnier-Blache JS, Reinholz M, van Zandvoort M, Weber C, Schober A. Lipoprotein-derived lysophosphatidic acid promotes atherosclerosis by releasing cxcl1 from the endothelium. *Cell metabolism*. 2011;13:592-600
18. Mai J, Virtue A, Shen J, Wang H, Yang XF. An evolving new paradigm: Endothelial cells--conditional innate immune cells. *Journal of hematology & oncology*. 2013;6:61
19. Burke JE, Dennis EA. Phospholipase a2 structure/function, mechanism, and signaling. *Journal of lipid research*. 2009;50 Suppl:S237-242
20. Schmitz G, Ruebsaamen K. Metabolism and atherogenic disease association of lysophosphatidylcholine. *Atherosclerosis*. 2010;208:10-18
21. Boekholdt SM, Keller TT, Wareham NJ, Luben R, Bingham SA, Day NE, Sandhu MS, Jukema JW, Kastelein JJ, Hack CE, Khaw KT. Serum levels of type ii secretory phospholipase a2 and the risk of future coronary artery disease in apparently healthy men and women: The epic-norfolk prospective population study. *Arteriosclerosis, thrombosis, and vascular biology*. 2005;25:839-846
22. Rosengren B, Peilot H, Umaerus M, Jonsson-Rylander AC, Mattsson-Hulten L, Hallberg C, Cronet P, Rodriguez-Lee M, Hurt-Camejo E. Secretory phospholipase a2 group v: Lesion distribution, activation by arterial proteoglycans, and induction in aorta by a western diet. *Arteriosclerosis, thrombosis, and vascular biology*. 2006;26:1579-1585
23. Matsumoto T, Kobayashi T, Kamata K. Role of lysophosphatidylcholine (lpc) in atherosclerosis. *Current medicinal chemistry*. 2007;14:3209-3220
24. Wilensky RL, Shi Y, Mohler ER, 3rd, Hamamdzic D, Burgert ME, Li J, Postle A, Fenning RS, Bollinger JG, Hoffman BE, Pelchovitz DJ, Yang J, Mirabile RC, Webb CL, Zhang L, Zhang P, Gelb MH, Walker MC, Zalewski A, Macphee CH. Inhibition of lipoprotein-associated phospholipase a2 reduces complex coronary atherosclerotic plaque development. *Nature medicine*. 2008;14:1059-1066

25. Witte ON, Kabarowski JH, Xu Y, Le LQ, Zhu K. Retraction. *Science*. 2005;307:206
26. Sphingosylphosphorylcholine and lysophosphatidylcholine are ligands for the G protein-coupled receptor GPR4. *The Journal of biological chemistry*. 2005;280:43280
27. Sevastou I, Kaffe E, Mouratis MA, Aidinis V. Lysoglycerophospholipids in chronic inflammatory disorders: The PLA₂/LPC and ATX/LPA axes. *Biochimica et biophysica acta*. 2013;1831:42-60
28. Steinbrecher UP, Parthasarathy S, Leake DS, Witztum JL, Steinberg D. Modification of low density lipoprotein by endothelial cells involves lipid peroxidation and degradation of low density lipoprotein phospholipids. *Proceedings of the National Academy of Sciences of the United States of America*. 1984;81:3883-3887
29. Quinn MT, Parthasarathy S, Steinberg D. Lysophosphatidylcholine: A chemotactic factor for human monocytes and its potential role in atherogenesis. *Proceedings of the National Academy of Sciences of the United States of America*. 1988;85:2805-2809
30. Yla-Herttuala S, Palinski W, Rosenfeld ME, Parthasarathy S, Carew TE, Butler S, Witztum JL, Steinberg D. Evidence for the presence of oxidatively modified low density lipoprotein in atherosclerotic lesions of rabbit and man. *The Journal of clinical investigation*. 1989;84:1086-1095
31. Scalia R, Murohara T, Campbell B, Kaji A, Lefler AM. Lysophosphatidylcholine stimulates leukocyte rolling and adherence in rat mesenteric microvasculature. *The American journal of physiology*. 1997;272:H2584-2590
32. Lavi S, McConnell JP, Rihal CS, Prasad A, Mathew V, Lerman LO, Lerman A. Local production of lipoprotein-associated phospholipase A₂ and lysophosphatidylcholine in the coronary circulation: Association with early coronary atherosclerosis and endothelial dysfunction in humans. *Circulation*. 2007;115:2715-2721

33. Goncalves I, Edsfeldt A, Ko NY, Grufman H, Berg K, Bjorkbacka H, Nitulescu M, Persson A, Nilsson M, Prehn C, Adamski J, Nilsson J. Evidence supporting a key role of lp-pla2-generated lysophosphatidylcholine in human atherosclerotic plaque inflammation. *Arteriosclerosis, thrombosis, and vascular biology*. 2012;32:1505-1512
34. Li Y, Trush MA. Diphenyleneiodonium, an nad(p)h oxidase inhibitor, also potently inhibits mitochondrial reactive oxygen species production. *Biochemical and biophysical research communications*. 1998;253:295-299
35. Ochi H, Kume N, Nishi E, Kita T. Elevated levels of camp inhibit protein kinase c--independent mechanisms of endothelial platelet-derived growth factor-b chain and intercellular adhesion molecule-1 gene induction by lysophosphatidylcholine. *Circulation research*. 1995;77:530-535
36. Sugiyama S, Kugiyama K, Ohgushi M, Fujimoto K, Yasue H. Lysophosphatidylcholine in oxidized low-density lipoprotein increases endothelial susceptibility to polymorphonuclear leukocyte-induced endothelial dysfunction in porcine coronary arteries. Role of protein kinase c. *Circulation research*. 1994;74:565-575
37. Sugiyama S, Kugiyama K, Ogata N, Doi H, Ota Y, Ohgushi M, Matsumura T, Oka H, Yasue H. Biphasic regulation of transcription factor nuclear factor-kappab activity in human endothelial cells by lysophosphatidylcholine through protein kinase c-mediated pathway. *Arteriosclerosis, thrombosis, and vascular biology*. 1998;18:568-576
38. Zhu Y, Lin JH, Liao HL, Verna L, Stemerman MB. Activation of icam-1 promoter by lysophosphatidylcholine: Possible involvement of protein tyrosine kinases. *Biochimica et biophysica acta*. 1997;1345:93-98
39. Zhou R, Yazdi AS, Menu P, Tschopp J. A role for mitochondria in nlrp3 inflammasome activation. *Nature*. 2010;469:221-225
40. Bulua AC, Simon A, Maddipati R, Pelletier M, Park H, Kim KY, Sack MN, Kastner DL, Siegel RM. Mitochondrial reactive oxygen species promote production of proinflammatory cytokines and are elevated in tnfr1-associated periodic syndrome (traps). *The Journal of experimental medicine*. 2011;208:519-533

41. Sena LA, Li S, Jairaman A, Prakriya M, Ezponda T, Hildeman DA, Wang CR, Schumacker PT, Licht JD, Perlman H, Bryce PJ, Chandel NS. Mitochondria are required for antigen-specific t cell activation through reactive oxygen species signaling. *Immunity*. 2013;38:225-236
42. Li X, Fang P, Mai J, Choi ET, Wang H, Yang XF. Targeting mitochondrial reactive oxygen species as novel therapy for inflammatory diseases and cancers. *Journal of hematology & oncology*. 2013;6:19
43. Madamanchi NR, Runge MS. Mitochondrial dysfunction in atherosclerosis. *Circulation research*. 2007;100:460-473
44. Han D, Canali R, Rettori D, Kaplowitz N. Effect of glutathione depletion on sites and topology of superoxide and hydrogen peroxide production in mitochondria. *Molecular pharmacology*. 2003;64:1136-1144
45. Cadenas E, Davies KJ. Mitochondrial free radical generation, oxidative stress, and aging. *Free radical biology & medicine*. 2000;29:222-230
46. Okado-Matsumoto A, Fridovich I. Subcellular distribution of superoxide dismutases (sod) in rat liver: Cu,zn-sod in mitochondria. *The Journal of biological chemistry*. 2001;276:38388-38393
47. Li Y, Huang TT, Carlson EJ, Melov S, Ursell PC, Olson JL, Noble LJ, Yoshimura MP, Berger C, Chan PH, Wallace DC, Epstein CJ. Dilated cardiomyopathy and neonatal lethality in mutant mice lacking manganese superoxide dismutase. *Nature genetics*. 1995;11:376-381
48. Ohashi M, Runge MS, Faraci FM, Heistad DD. Mnsod deficiency increases endothelial dysfunction in apoe-deficient mice. *Arteriosclerosis, thrombosis, and vascular biology*. 2006;26:2331-2336
49. Radi R, Turrens JF, Chang LY, Bush KM, Crapo JD, Freeman BA. Detection of catalase in rat heart mitochondria. *The Journal of biological chemistry*. 1991;266:22028-22034

50. Yang H, Roberts LJ, Shi MJ, Zhou LC, Ballard BR, Richardson A, Guo ZM. Retardation of atherosclerosis by overexpression of catalase or both cu/znsuperoxide dismutase and catalase in mice lacking apolipoprotein e. *Circ Res*. 2004;95:1075-1081
51. Schriener SE, Linford NJ, Martin GM, Treuting P, Ogburn CE, Emond M, Coskun PE, Ladiges W, Wolf N, Van Remmen H, Wallace DC, Rabinovitch PS. Extension of murine life span by overexpression of catalase targeted to mitochondria. *Science*. 2005;308:1909-1911
52. Handy DE, Loscalzo J. Redox regulation of mitochondrial function. *Antioxidants & redox signaling*. 2012;16:1323-1367
53. Torzewski M, Ochsenhirt V, Kleschyov AL, Oelze M, Daiber A, Li H, Rossmann H, Tsimikas S, Reifenberg K, Cheng F, Lehr HA, Blankenberg S, Forstermann U, Munzel T, Lackner KJ. Deficiency of glutathione peroxidase-1 accelerates the progression of atherosclerosis in apolipoprotein e-deficient mice. *Arterioscler Thromb Vasc Biol*. 2007;27:850-857
54. Rhee SG, Chae HZ, Kim K. Peroxiredoxins: A historical overview and speculative preview of novel mechanisms and emerging concepts in cell signaling. *Free radical biology & medicine*. 2005;38:1543-1552
55. Winterbourn CC. Reconciling the chemistry and biology of reactive oxygen species. *Nature chemical biology*. 2008;4:278-286
56. Matsushima S, Ide T, Yamato M, Matsusaka H, Hattori F, Ikeuchi M, Kubota T, Sunagawa K, Hasegawa Y, Kurihara T, Oikawa S, Kinugawa S, Tsutsui H. Overexpression of mitochondrial peroxiredoxin-3 prevents left ventricular remodeling and failure after myocardial infarction in mice. *Circulation*. 2006;113:1779-1786
57. Zhang H, Luo Y, Zhang W, He Y, Dai S, Zhang R, Huang Y, Bernatchez P, Giordano FJ, Shadel G, Sessa WC, Min W. Endothelial-specific expression of mitochondrial thioredoxin improves endothelial cell function and reduces atherosclerotic lesions. *The American journal of pathology*. 2007;170:1108-1120

58. He M, Cai J, Go YM, Johnson JM, Martin WD, Hansen JM, Jones DP. Identification of thioredoxin-2 as a regulator of the mitochondrial permeability transition. *Toxicol Sci.* 2008;105:44-50
59. Toime LJ, Brand MD. Uncoupling protein-3 lowers reactive oxygen species production in isolated mitochondria. *Free radical biology & medicine.* 2010;49:606-611
60. Brennan JP, Southworth R, Medina RA, Davidson SM, Duchen MR, Shattock MJ. Mitochondrial uncoupling, with low concentration fccp, induces ros-dependent cardioprotection independent of katp channel activation. *Cardiovascular research.* 2006;72:313-321
61. Lee KU, Lee IK, Han J, Song DK, Kim YM, Song HS, Kim HS, Lee WJ, Koh EH, Song KH, Han SM, Kim MS, Park IS, Park JY. Effects of recombinant adenovirus-mediated uncoupling protein 2 overexpression on endothelial function and apoptosis. *Circulation research.* 2005;96:1200-1207
62. Aon MA, Cortassa S, O'Rourke B. Redox-optimized ros balance: A unifying hypothesis. *Biochimica et biophysica acta.* 2010;1797:865-877
63. Stuehr DJ. Structure-function aspects in the nitric oxide synthases. *Annual review of pharmacology and toxicology.* 1997;37:339-359
64. Ghafourifar P, Richter C. Nitric oxide synthase activity in mitochondria. *FEBS letters.* 1997;418:291-296
65. Shiva S. Mitochondria as metabolizers and targets of nitrite. *Nitric Oxide.* 2010;22:64-74
66. Feissner RF, Skalska J, Gaum WE, Sheu SS. Crosstalk signaling between mitochondrial ca²⁺ and ros. *Front Biosci.* 2009;14:1197-1218
67. Peng TI, Jou MJ. Oxidative stress caused by mitochondrial calcium overload. *Annals of the New York Academy of Sciences.* 2010;1201:183-188

68. Turrens JF, Freeman BA, Levitt JG, Crapo JD. The effect of hyperoxia on superoxide production by lung submitochondrial particles. *Archives of biochemistry and biophysics*. 1982;217:401-410
69. Guzy RD, Hoyos B, Robin E, Chen H, Liu L, Mansfield KD, Simon MC, Hammerling U, Schumacker PT. Mitochondrial complex iii is required for hypoxia-induced ros production and cellular oxygen sensing. *Cell metabolism*. 2005;1:401-408
70. McLeod CJ, Aziz A, Hoyt RF, Jr., McCoy JP, Jr., Sack MN. Uncoupling proteins 2 and 3 function in concert to augment tolerance to cardiac ischemia. *The Journal of biological chemistry*. 2005;280:33470-33476
71. Szczepanek K, Lesnefsky EJ, Larner AC. Multi-tasking: Nuclear transcription factors with novel roles in the mitochondria. *Trends in cell biology*. 2012;22:429-437
72. Wegrzyn J, Potla R, Chwae YJ, Sepuri NB, Zhang Q, Koeck T, Derecka M, Szczepanek K, Szelag M, Gornicka A, Moh A, Moghaddas S, Chen Q, Bobbili S, Cichy J, Dulak J, Baker DP, Wolfman A, Stuehr D, Hassan MO, Fu XY, Avadhani N, Drake JI, Fawcett P, Lesnefsky EJ, Larner AC. Function of mitochondrial stat3 in cellular respiration. *Science (New York, N.Y.)*. 2009;323:793-797
73. Semenza GL. Hypoxia-inducible factor 1: Regulator of mitochondrial metabolism and mediator of ischemic preconditioning. *Biochimica et biophysica acta*. 2011;1813:1263-1268
74. Doughan AK, Harrison DG, Dikalov SI. Molecular mechanisms of angiotensin ii-mediated mitochondrial dysfunction: Linking mitochondrial oxidative damage and vascular endothelial dysfunction. *Circulation research*. 2008;102:488-496
75. Baudry N, Laemmel E, Vicaut E. In vivo reactive oxygen species production induced by ischemia in muscle arterioles of mice: Involvement of xanthine oxidase and mitochondria. *Am J Physiol Heart Circ Physiol*. 2008;294:H821-828
76. Ceylan-Isik AF, Guo KK, Carlson EC, Privratsky JR, Liao SJ, Cai L, Chen AF, Ren J. Metallothionein abrogates gtp cyclohydrolase i inhibition-induced cardiac

contractile and morphological defects: Role of mitochondrial biogenesis. *Hypertension*. 2009;53:1023-1031

77. Hanna IR, Taniyama Y, Szocs K, Rocic P, Griendling KK. Nad(p)h oxidase-derived reactive oxygen species as mediators of angiotensin ii signaling. *Antioxidants & redox signaling*. 2002;4:899-914
78. Dikalova AE, Bikineyeva AT, Budzyn K, Nazarewicz RR, McCann L, Lewis W, Harrison DG, Dikalov SI. Therapeutic targeting of mitochondrial superoxide in hypertension. *Circulation research*. 2010;107:106-116
79. Giorgio M, Migliaccio E, Orsini F, Paolucci D, Moroni M, Contursi C, Pelliccia G, Luzi L, Minucci S, Marcaccio M, Pinton P, Rizzuto R, Bernardi P, Paolucci F, Pelicci PG. Electron transfer between cytochrome c and p66shc generates reactive oxygen species that trigger mitochondrial apoptosis. *Cell*. 2005;122:221-233
80. Gertz M, Fischer F, Wolters D, Steegborn C. Activation of the lifespan regulator p66shc through reversible disulfide bond formation. *Proceedings of the National Academy of Sciences of the United States of America*. 2008;105:5705-5709
81. Shi Y, Cosentino F, Camici GG, Akhmedov A, Vanhoutte PM, Tanner FC, Luscher TF. Oxidized low-density lipoprotein activates p66shc via lectin-like oxidized low-density lipoprotein receptor-1, protein kinase c-beta, and c-jun n-terminal kinase kinase in human endothelial cells. *Arteriosclerosis, thrombosis, and vascular biology*. 2011;31:2090-2097
82. Napoli C, Martin-Padura I, de Nigris F, Giorgio M, Mansueto G, Somma P, Condorelli M, Sica G, De Rosa G, Pelicci P. Deletion of the p66shc longevity gene reduces systemic and tissue oxidative stress, vascular cell apoptosis, and early atherogenesis in mice fed a high-fat diet. *Proceedings of the National Academy of Sciences of the United States of America*. 2003;100:2112-2116
83. Quintero M, Colombo SL, Godfrey A, Moncada S. Mitochondria as signaling organelles in the vascular endothelium. *Proceedings of the National Academy of Sciences of the United States of America*. 2006;103:5379-5384

84. Blouin A, Bolender RP, Weibel ER. Distribution of organelles and membranes between hepatocytes and nonhepatocytes in the rat liver parenchyma. A stereological study. *The Journal of cell biology*. 1977;72:441-455
85. Dranka BP, Hill BG, Darley-USmar VM. Mitochondrial reserve capacity in endothelial cells: The impact of nitric oxide and reactive oxygen species. *Free radical biology & medicine*. 2010;48:905-914
86. Widlansky ME, Gutterman DD. Regulation of endothelial function by mitochondrial reactive oxygen species. *Antioxidants & redox signaling*. 2011;15:1517-1530
87. Wang Y, Zang QS, Liu Z, Wu Q, Maass D, Dulan G, Shaul PW, Melito L, Frantz DE, Kilgore JA, Williams NS, Terada LS, Nwariaku FE. Regulation of vegf-induced endothelial cell migration by mitochondrial reactive oxygen species. *American journal of physiology*. 2011;301:C695-704
88. Liu Y, Zhao H, Li H, Kalyanaraman B, Nicolosi AC, Gutterman DD. Mitochondrial sources of h₂O₂ generation play a key role in flow-mediated dilation in human coronary resistance arteries. *Circulation research*. 2003;93:573-580
89. Weber C, Noels H. Atherosclerosis: Current pathogenesis and therapeutic options. *Nature medicine*. 2011;17:1410-1422
90. Zmijewski JW, Moellering DR, Le Goffe C, Landar A, Ramachandran A, Darley-USmar VM. Oxidized ldl induces mitochondrially associated reactive oxygen/nitrogen species formation in endothelial cells. *American journal of physiology*. 2005;289:H852-861
91. Roy Chowdhury SK, Sangle GV, Xie X, Stelmack GL, Halayko AJ, Shen GX. Effects of extensively oxidized low-density lipoprotein on mitochondrial function and reactive oxygen species in porcine aortic endothelial cells. *American journal of physiology*. 2010;298:E89-98
92. Takabe W, Li R, Ai L, Yu F, Berliner JA, Hsiai TK. Oxidized low-density lipoprotein-activated c-jun nh₂-terminal kinase regulates manganese superoxide

- dismutase ubiquitination: Implication for mitochondrial redox status and apoptosis. *Arteriosclerosis, thrombosis, and vascular biology*. 2010;30:436-441
93. Haffner SJ, Cassells H. Hyperglycemia as a cardiovascular risk factor. *The American journal of medicine*. 2003;115 Suppl 8A:6S-11S
 94. Nishikawa T, Edelstein D, Du XL, Yamagishi S, Matsumura T, Kaneda Y, Yorek MA, Beebe D, Oates PJ, Hammes HP, Giardino I, Brownlee M. Normalizing mitochondrial superoxide production blocks three pathways of hyperglycaemic damage. *Nature*. 2000;404:787-790
 95. Srinivasan S, Yeh M, Danziger EC, Hatley ME, Riggan AE, Leitinger N, Berliner JA, Hedrick CC. Glucose regulates monocyte adhesion through endothelial production of interleukin-8. *Circulation research*. 2003;92:371-377
 96. Suzuki K, Olah G, Modis K, Coletta C, Kulp G, Gero D, Szoleczky P, Chang T, Zhou Z, Wu L, Wang R, Papapetropoulos A, Szabo C. Hydrogen sulfide replacement therapy protects the vascular endothelium in hyperglycemia by preserving mitochondrial function. *Proceedings of the National Academy of Sciences of the United States of America*. 2011;108:13829-13834
 97. Ungvari Z, Labinskyy N, Mukhopadhyay P, Pinto JT, Bagi Z, Ballabh P, Zhang C, Pacher P, Csiszar A. Resveratrol attenuates mitochondrial oxidative stress in coronary arterial endothelial cells. *American journal of physiology*. 2009;297:H1876-1881
 98. Rajesh M, Mukhopadhyay P, Batkai S, Hasko G, Liaudet L, Drel VR, Obrosova IG, Pacher P. Cannabidiol attenuates high glucose-induced endothelial cell inflammatory response and barrier disruption. *American journal of physiology*. 2007;293:H610-619
 99. Zheng Z, Chen H, Wang H, Ke B, Zheng B, Li Q, Li P, Su L, Gu Q, Xu X. Improvement of retinal vascular injury in diabetic rats by statins is associated with the inhibition of mitochondrial reactive oxygen species pathway mediated by peroxisome proliferator-activated receptor gamma coactivator 1alpha. *Diabetes*. 2010;59:2315-2325

100. Wang J, Alexanian A, Ying R, Kizhakekuttu TJ, Dharmashankar K, Vasquez-Vivar J, Gutterman DD, Widlansky ME. Acute exposure to low glucose rapidly induces endothelial dysfunction and mitochondrial oxidative stress: Role for amp kinase. *Arteriosclerosis, thrombosis, and vascular biology*. 2012;32:712-720
101. Arruda RM, Peotta VA, Meyrelles SS, Vasquez EC. Evaluation of vascular function in apolipoprotein e knockout mice with angiotensin-dependent renovascular hypertension. *Hypertension*. 2005;46:932-936
102. Harrison DG, Gongora MC. Oxidative stress and hypertension. *The Medical clinics of North America*. 2009;93:621-635
103. Lavoie JL, Sigmund CD. Minireview: Overview of the renin-angiotensin system--an endocrine and paracrine system. *Endocrinology*. 2003;144:2179-2183
104. Widder JD, Fraccarollo D, Galuppo P, Hansen JM, Jones DP, Ertl G, Bauersachs J. Attenuation of angiotensin ii-induced vascular dysfunction and hypertension by overexpression of thioredoxin 2. *Hypertension*. 2009;54:338-344
105. Ballinger SW, Patterson C, Knight-Lozano CA, Burow DL, Conklin CA, Hu Z, Reuf J, Horaist C, Lebovitz R, Hunter GC, McIntyre K, Runge MS. Mitochondrial integrity and function in atherogenesis. *Circulation*. 2002;106:544-549
106. Wang Y, Wang GZ, Rabinovitch P, Tabas I. Macrophage mitochondrial oxidative stress promotes atherosclerosis and nf-kb-mediated inflammation in macrophages. *Circulation research*. 2013
107. Fujimoto H, Taguchi J, Imai Y, Ayabe S, Hashimoto H, Kobayashi H, Ogasawara K, Aizawa T, Yamakado M, Nagai R, Ohno M. Manganese superoxide dismutase polymorphism affects the oxidized low-density lipoprotein-induced apoptosis of macrophages and coronary artery disease. *European heart journal*. 2008;29:1267-1274
108. Ciccone S, Maiani E, Bellusci G, Diederich M, Gonfloni S. Parkinson's disease: A complex interplay of mitochondrial DNA alterations and oxidative stress. *International journal of molecular sciences*. 2013;14:2388-2409

109. Xie H, Lev D, Gong Y, Wang S, Pollock RE, Wu X, Gu J. Reduced mitochondrial DNA copy number in peripheral blood leukocytes increases the risk of soft tissue sarcoma. *Carcinogenesis*. 2013
110. Krzywanski DM, Moellering DR, Fetterman JL, Dunham-Snary KJ, Sammy MJ, Ballinger SW. The mitochondrial paradigm for cardiovascular disease susceptibility and cellular function: A complementary concept to mendelian genetics. *Laboratory investigation; a journal of technical methods and pathology*. 2011;91:1122-1135
111. Egger G, Liang G, Aparicio A, Jones PA. Epigenetics in human disease and prospects for epigenetic therapy. *Nature*. 2004;429:457-463
112. Kouzarides T. Chromatin modifications and their function. *Cell*. 2007;128:693-705
113. Esteller M. Non-coding rnas in human disease. *Nature reviews. Genetics*. 2011;12:861-874
114. Amaral PP, Clark MB, Gascoigne DK, Dinger ME, Mattick JS. Lncrnadb: A reference database for long noncoding rnas. *Nucleic acids research*. 2011;39:D146-151
115. An integrated encyclopedia of DNA elements in the human genome. *Nature*. 2012;489:57-74
116. Lopez-Pastrana J, Shao Y, Chernaya V, Wang H, Yang XF. Epigenetic enzymes are the therapeutic targets for cd4(+)/cd25(+)/high)foxp3(+) regulatory t cells. *Translational research : the journal of laboratory and clinical medicine*. 2015;165:221-240
117. Bolden JE, Peart MJ, Johnstone RW. Anticancer activities of histone deacetylase inhibitors. *Nature reviews. Drug discovery*. 2006;5:769-784
118. Zampetaki A, Zeng L, Margariti A, Xiao Q, Li H, Zhang Z, Pepe AE, Wang G, Habi O, deFalco E, Cockerill G, Mason JC, Hu Y, Xu Q. Histone deacetylase 3 is

critical in endothelial survival and atherosclerosis development in response to disturbed flow. *Circulation*. 2010;121:132-142

119. Hoeksema MA, Gijbels MJ, Van den Bossche J, van der Velden S, Sijm A, Neele AE, Seijkens T, Stoger JL, Meiler S, Boshuizen MC, Dallinga-Thie GM, Levels JH, Boon L, Mullican SE, Spann NJ, Cleutjens JP, Glass CK, Lazar MA, de Vries CJ, Biessen EA, Daemen MJ, Lutgens E, de Winther MP. Targeting macrophage histone deacetylase 3 stabilizes atherosclerotic lesions. *EMBO molecular medicine*. 2014;6:1124-1132
120. Cao Q, Rong S, Repa JJ, St Clair R, Parks JS, Mishra N. Histone deacetylase 9 represses cholesterol efflux and alternatively activated macrophages in atherosclerosis development. *Arteriosclerosis, thrombosis, and vascular biology*. 2014;34:1871-1879
121. Choi JH, Nam KH, Kim J, Baek MW, Park JE, Park HY, Kwon HJ, Kwon OS, Kim DY, Oh GT. Trichostatin a exacerbates atherosclerosis in low density lipoprotein receptor-deficient mice. *Arteriosclerosis, thrombosis, and vascular biology*. 2005;25:2404-2409
122. Dje N'Guessan P, Riediger F, Vardarova K, Scharf S, Eitel J, Opitz B, Slevogt H, Weichert W, Hocke AC, Schmeck B, Suttorp N, Hippenstiel S. Statins control oxidized ldl-mediated histone modifications and gene expression in cultured human endothelial cells. *Arteriosclerosis, thrombosis, and vascular biology*. 2009;29:380-386
123. Inoue K, Kobayashi M, Yano K, Miura M, Izumi A, Mataka C, Doi T, Hamakubo T, Reid PC, Hume DA, Yoshida M, Aird WC, Kodama T, Minami T. Histone deacetylase inhibitor reduces monocyte adhesion to endothelium through the suppression of vascular cell adhesion molecule-1 expression. *Arteriosclerosis, thrombosis, and vascular biology*. 2006;26:2652-2659
124. Wang J, Mahmud SA, Bitterman PB, Huo Y, Slungaard A. Histone deacetylase inhibitors suppress tf-kappab-dependent agonist-driven tissue factor expression in endothelial cells and monocytes. *The Journal of biological chemistry*. 2007;282:28408-28418
125. Mai J, Wang H, Yang XF. Th 17 cells interplay with foxp3+ tregs in regulation of inflammation and autoimmunity. *Front Biosci*. 2010;15:986-1006

126. Ait-Oufella H, Taleb S, Mallat Z, Tedgui A. Recent advances on the role of cytokines in atherosclerosis. *Arteriosclerosis, thrombosis, and vascular biology*. 2011;31:969-979
127. Merhi-Soussi F, Kwak BR, Magne D, Chadjichristos C, Berti M, Pelli G, James RW, Mach F, Gabay C. Interleukin-1 plays a major role in vascular inflammation and atherosclerosis in male apolipoprotein e-knockout mice. *Cardiovascular research*. 2005;66:583-593
128. Mallat Z, Corbaz A, Scoazec A, Graber P, Alouani S, Esposito B, Humbert Y, Chvatchko Y, Tedgui A. Interleukin-18/interleukin-18 binding protein signaling modulates atherosclerotic lesion development and stability. *Circulation research*. 2001;89:E41-45
129. Caligiuri G, Rudling M, Ollivier V, Jacob MP, Michel JB, Hansson GK, Nicoletti A. Interleukin-10 deficiency increases atherosclerosis, thrombosis, and low-density lipoproteins in apolipoprotein e knockout mice. *Mol Med*. 2003;9:10-17
130. Singh NN, Ramji DP. The role of transforming growth factor-beta in atherosclerosis. *Cytokine & growth factor reviews*. 2006;17:487-499
131. Yamashita H, Shimada K, Seki E, Mokuno H, Daida H. Concentrations of interleukins, interferon, and c-reactive protein in stable and unstable angina pectoris. *The American journal of cardiology*. 2003;91:133-136
132. Narverud I, Ueland T, Nenseter MS, Retterstol K, Telle-Hansen VH, Halvorsen B, Ose L, Aukrust P, Holven KB. Children with familial hypercholesterolemia are characterized by an inflammatory imbalance between the tumor necrosis factor alpha system and interleukin-10. *Atherosclerosis*. 2011;214:163-168
133. Mallat Z, Besnard S, Duriez M, Deleuze V, Emmanuel F, Bureau MF, Soubrier F, Esposito B, Duez H, Fievet C, Staels B, Duverger N, Scherman D, Tedgui A. Protective role of interleukin-10 in atherosclerosis. *Circulation research*. 1999;85:e17-24
134. Mallat Z, Gojova A, Marchiol-Fournigault C, Esposito B, Kamate C, Merval R, Fradelizi D, Tedgui A. Inhibition of transforming growth factor-beta signaling

accelerates atherosclerosis and induces an unstable plaque phenotype in mice. *Circulation research*. 2001;89:930-934

135. Krakauer T. Il-10 inhibits the adhesion of leukocytic cells to il-1-activated human endothelial cells. *Immunology letters*. 1995;45:61-65
136. Pinderski Oslund LJ, Hedrick CC, Olvera T, Hagenbaugh A, Territo M, Berliner JA, Fyfe AI. Interleukin-10 blocks atherosclerotic events in vitro and in vivo. *Arteriosclerosis, thrombosis, and vascular biology*. 1999;19:2847-2853
137. Potteaux S, Deleuze V, Merval R, Bureau MF, Esposito B, Scherman D, Tedgui A, Mallat Z. In vivo electrotransfer of interleukin-10 cDNA prevents endothelial upregulation of activated NF- κ B and adhesion molecules following an atherogenic diet. *European cytokine network*. 2006;17:13-18
138. Grainger DJ, Mosedale DE, Metcalfe JC, Bottinger EP. Dietary fat and reduced levels of TGF β 1 act synergistically to promote activation of the vascular endothelium and formation of lipid lesions. *Journal of cell science*. 2000;113 (Pt 13):2355-2361
139. Collison LW, Vignali DA. Interleukin-35: Odd one out or part of the family? *Immunological reviews*. 2008;226:248-262
140. Collison LW, Workman CJ, Kuo TT, Boyd K, Wang Y, Vignali KM, Cross R, Sehy D, Blumberg RS, Vignali DA. The inhibitory cytokine IL-35 contributes to regulatory T-cell function. *Nature*. 2007;450:566-569
141. Wang RX, Yu CR, Dambuza IM, Mahdi RM, Dolinska MB, Sergeev YV, Wingfield PT, Kim SH, Egwuagu CE. Interleukin-35 induces regulatory B cells that suppress autoimmune disease. *Nature medicine*. 2014;20:633-641
142. Shen P, Roch T, Lampropoulou V, O'Connor RA, Stervbo U, Hilgenberg E, Ries S, Dang VD, Jaimes Y, Daridon C, Li R, Jouneau L, Boudinot P, Wilantri S, Sakwa I, Miyazaki Y, Leech MD, McPherson RC, Wirtz S, Neurath M, Hoehlig K, Meinel E, Grutzkau A, Grun JR, Horn K, Kuhl AA, Dorner T, Bar-Or A, Kaufmann SH, Anderton SM, Fillatreau S. IL-35-producing B cells are critical regulators of immunity during autoimmune and infectious diseases. *Nature*. 2014;507:366-370

143. Ng B, Yang F, Huston DP, Yan Y, Yang Y, Xiong Z, Peterson LE, Wang H, Yang XF. Increased noncanonical splicing of autoantigen transcripts provides the structural basis for expression of untolerized epitopes. *The Journal of allergy and clinical immunology*. 2004;114:1463-1470
144. Yin Y, Yan Y, Jiang X, Mai J, Chen NC, Wang H, Yang XF. Inflammasomes are differentially expressed in cardiovascular and other tissues. *International journal of immunopathology and pharmacology*. 2009;22:311-322
145. Mai J, Virtue A, Maley E, Tran T, Yin Y, Meng S, Pansuria M, Jiang X, Wang H, Yang XF. Micrnas and other mechanisms regulate interleukin-17 cytokines and receptors. *Front Biosci (Elite Ed)*. 2012;4:1478-1495
146. Virtue A, Mai J, Yin Y, Meng S, Tran T, Jiang X, Wang H, Yang XF. Structural evidence of anti-atherogenic micrnas. *Front Biosci (Landmark Ed)*. 2011;16:3133-3145
147. Li X, Mai J, Virtue A, Yin Y, Gong R, Sha X, Gutchigian S, Frisch A, Hodge I, Jiang X, Wang H, Yang XF. Il-35 is a novel responsive anti-inflammatory cytokine--a new system of categorizing anti-inflammatory cytokines. *PloS one*. 2012;7:e33628
148. Du F, Virtue A, Wang H, Yang XF. Metabolomic analyses for atherosclerosis, diabetes, and obesity. *Biomarker research*. 2013;1:17
149. Hoffman NE, Chandramoorthy HC, Shanmughapriya S, Zhang XQ, Vallem S, Doonan PJ, Malliankaraman K, Guo S, Rajan S, Elrod JW, Koch WJ, Cheung JY, Madesh M. Slc25a23 augments mitochondrial ca(2)(+) uptake, interacts with mcu, and induces oxidative stress-mediated cell death. *Molecular biology of the cell*. 2014;25:936-947
150. Kuo YM, Andrews AJ. Quantitating the specificity and selectivity of gcn5-mediated acetylation of histone h3. *PloS one*. 2013;8:e54896
151. Kuo YM, Henry RA, Andrews AJ. A quantitative multiplexed mass spectrometry assay for studying the kinetic of residue-specific histone acetylation. *Methods*. 2014;70:127-133

152. Bender S, Tang Y, Lindroth AM, Hovestadt V, Jones DT, Kool M, Zapatka M, Northcott PA, Sturm D, Wang W, Radlwimmer B, Hojfeldt JW, Truffaux N, Castel D, Schubert S, Ryzhova M, Seker-Cin H, Gronych J, Johann PD, Stark S, Meyer J, Milde T, Schuhmann M, Ebinger M, Monoranu CM, Ponnuswami A, Chen S, Jones C, Witt O, Collins VP, von Deimling A, Jabado N, Puget S, Grill J, Helin K, Korshunov A, Lichter P, Monje M, Plass C, Cho YJ, Pfister SM. Reduced h3k27me3 and DNA hypomethylation are major drivers of gene expression in k27m mutant pediatric high-grade gliomas. *Cancer cell*. 2013;24:660-672
153. Portman OW, Alexander M. Lysophosphatidylcholine concentrations and metabolism in aortic intima plus inner media: Effect of nutritionally induced atherosclerosis. *Journal of lipid research*. 1969;10:158-165
154. Yin Y, Li X, Sha X, Xi H, Li YF, Shao Y, Mai J, Virtue A, Lopez-Pastrana J, Meng S, Tilley D, Monroy MA, Choi ET, Thomas CJ, Jiang X, Wang H, Yang XF. Early hyperlipidemia promotes endothelial activation via a caspase-1-sirtuin 1 pathway. *Arteriosclerosis, thrombosis, and vascular biology*. 2015
155. Nakashima Y, Plump AS, Raines EW, Breslow JL, Ross R. Apoe-deficient mice develop lesions of all phases of atherosclerosis throughout the arterial tree. *Arteriosclerosis and thrombosis : a journal of vascular biology / American Heart Association*. 1994;14:133-140
156. Dikalov SI, Harrison DG. Methods for detection of mitochondrial and cellular reactive oxygen species. *Antioxidants & redox signaling*. 2014;20:372-382
157. Inoue N, Hirata K, Yamada M, Hamamori Y, Matsuda Y, Akita H, Yokoyama M. Lysophosphatidylcholine inhibits bradykinin-induced phosphoinositide hydrolysis and calcium transients in cultured bovine aortic endothelial cells. *Circulation research*. 1992;71:1410-1421
158. Watanabe N, Zmijewski JW, Takabe W, Umezu-Goto M, Le Goffe C, Sekine A, Landar A, Watanabe A, Aoki J, Arai H, Kodama T, Murphy MP, Kalyanaraman R, Darley-Usmar VM, Noguchi N. Activation of mitogen-activated protein kinases by lysophosphatidylcholine-induced mitochondrial reactive oxygen species generation in endothelial cells. *The American journal of pathology*. 2006;168:1737-1748

159. Brookes PS, Yoon Y, Robotham JL, Anders MW, Sheu SS. Calcium, atp, and ros: A mitochondrial love-hate triangle. *American journal of physiology. Cell physiology*. 2004;287:C817-833
160. Hawkins BJ, Solt LA, Chowdhury I, Kazi AS, Abid MR, Aird WC, May MJ, Foskett JK, Madesh M. G protein-coupled receptor ca²⁺-linked mitochondrial reactive oxygen species are essential for endothelial/leukocyte adherence. *Molecular and cellular biology*. 2007;27:7582-7593
161. Karmodiya K, Krebs AR, Oulad-Abdelghani M, Kimura H, Tora L. H3k9 and h3k14 acetylation co-occur at many gene regulatory elements, while h3k14ac marks a subset of inactive inducible promoters in mouse embryonic stem cells. *BMC genomics*. 2012;13:424
162. van de Stolpe A, van der Saag PT. Intercellular adhesion molecule-1. *J Mol Med (Berl)*. 1996;74:13-33
163. Kalyanaraman B, Darley-Usmar V, Davies KJ, Dennery PA, Forman HJ, Grisham MB, Mann GE, Moore K, Roberts LJ, 2nd, Ischiropoulos H. Measuring reactive oxygen and nitrogen species with fluorescent probes: Challenges and limitations. *Free radical biology & medicine*. 2012;52:1-6